REGULATION OF NEUTROPHIL MIGRATION TO INFLAMMATION

by

Wenqing Zhou

A Dissertation

Submitted to the Faculty of Purdue University

In Partial Fulfillment of the Requirements for the degree of

Doctor of Philosophy

Department of Biological Sciences

West Lafayette, Indiana

May 2019

THE PURDUE UNIVERSITY GRADUATE SCHOOL
STATEMENT OF COMMITTEE APPROVAL

Dr. Qing Deng, Chair
Department of Biological Sciences
Dr. Chris Staiger
Department of Botany and Plant Pathology
Dr. Andrea Kasinski
Department of Biological Sciences
Dr. Guangjun Zhang
Department of Comparative Pathobiology

Approved by:
Dr. Janice Evans
Head of the Graduate Program

To my grandma Huaying Wang, my mom Xiaofeng Zhou,
my husband Yao Liu and my daughter Grace Q. Liu

ACKNOWLEDGMENTS

I would like to thank my amazing PhD supervisor Dr. Qing Deng for her support and guidance during these past four and half years. She is a very passionate and energetic scientist. She would always be excited when a technique hurdle is resolved and encourage us to celebrate when a breakthrough is made (even a tiny one). Her passion in science greatly influences me to pursue an academic career. She keeps telling me that if someone else can do this experiment, then I can do that too. I am very grateful for her trust and the confidence on me. She has always been supportive and given me enough freedom to manage my projects. She is knowledgeable and full of wonderful ideas. She is usually my primary resource for getting my questions answered. No matter how busy she was, she never cancelled our weekly meeting. I can always get insightful advice and suggestions from weekly discussions. She is optimistic even when we have negative results and always has backup plans, which I think is very important for my PhD training and my future career. I cannot always get expected results, but, with this optimistic attitude and backup plans, I can still keep moving forward. She is the advisor not only for my PhD training, but also for my life. She cares about my projects as well as my life and my family, and shares her experience about how to balance the work and life. She makes me believe that I am able to do whatever I want to do in science. I feel so fortunate to be a student of her.

I would like to thank my committee members Dr. Chris Staiger for teaching me how important the quantification is and allowing me to use the confocal microscope with which I got very beautiful in vivo migration movie of neutrophils; Dr. Andrea Kasinski for helping me thinking critically and creatively; Dr. Guangjun Zhang for making me pay more attention to the rationale and the biological significance of each project.

I would like to thank Dr. Zhao-Qing Luo for his generous help on ordering and managing mice for us, and for letting me use the cell culture room for two months, which really saved me a lot of time. I would like to thank Dr. David Umulis for sharing the confocal microscope with us, so I can have all these high-resolution cell images. I also want to thank Dr. Daniel Suter and Dr. Yuk Fai Leung for advice on my projects during group meetings.

I would like to thank all my current lab mates Tianqi Wang, Alan Hsu and former lab mates Dr. Xiaoguang Zhu, Dr. Theodore Gurol Naef, Dr. Decheng Wang and Jacob Jefferies for their help and sharing ideas and reagents with me.

Finally, I would like to express my sincere gratitude to my family. I especially thank my husband Dr. Yao Liu for his love and tremendous support. Because of him, I came here. It is a wonderful journey for me and I think I will never regret the decision I made 5 years ago. Since he also studies biology and our labs are on the same floor, he really helped a lot. He taught me how to do western blot and basic cell culture techniques. He also helped me organize and genotype mice. To be honest, he did much more than I did to take care of my mice. Without the help from him, I would be much less efficient. He always has faith in me and my intellect and encourages me to pursue whatever I want in science and in life. I would like to dedicate my gratitude to my grandma and my mom for their unconditional love, understanding and care. I also want to thank my husband's parents for their selfless devotion and constant encouragements to my husband and to me. Last, I want to give special thanks to my little daughter for bringing so much laughter and joy into my life. No matter how hard the day was, when I saw her face, all bad things disappeared. She is the most wonderful gift for me.

TABLE OF CONTENTS

NOTE

Chapters 2, 3, 4, and 5 of the dissertation contain content of the following published units:

Wenqing Zhou, Arpita S. Pal, Alan Yi-Hui Hsu, Theodore Gurol, Xiaoguang Zhu, Sarah E. Wirbisky, Jennifer Freeman, Andrea Kasinski, Qing Deng. MicroRNA-223 suppresses the canonical NF-kB pathway in basal keratinocytes to dampen neutrophilic inflammation. 2018. *Cell Reports*. 22: 1810-1823.

Wenqing Zhou, Lingyan Cao, Jacob Jeffries, Xiaoguang Zhu, Christopher J Staiger, Qing Deng. Neutrophil-specific knockout demonstrates a role for mitochondria in regulating neutrophil motility in zebrafish. 2018. *Disease Models & Mechanism*. 11:dmm033027. *Doi: 10.1242/dmm.033027.*

Wenqing Zhou, Alan Hsu, Tianqi Wang, Jacob Jefferies, Haroon Mohammad, Xu Wang, David Umulis, Mohamed N. Seleem, Qing Deng. Mitofusin 2 regulates neutrophil adhesive migration via suppressing Rac activation. 2019. *BioRxiv*. *Doi: https://doi.org/10.1101/608091*

LIST OF FIGURES

ABSTRACT

Author: Zhou, Wenqing. PhD
Institution: Purdue University
Degree Received: May 2019
Title: Regulation of Neutrophil Migration to Inflammation
Committee Chair: Qing Deng

Neutrophils, contributing to approximately 40%-70% of white blood cells in mammals, are the most abundant type of leukocytes in human circulation. As critical effector cells in innate immunity, neutrophils form the first line of host defense against microbes and are the first immune cells recruited to an inflamed tissue. The pathogen phagocytosis, release of reactive chemicals and proteases, and formation of extracellular traps are the key weapons of neutrophils in host defense. However, neutrophils also contribute to collateral tissue damage when performing their antimicrobial functions. The destructive potential of neutrophils requires the tight regulation of their activation and recruitment. In this study, we found that miR-223 in epithelial cells controls neutrophil response to inflammation through regulating the activation of NF-κB. As fast moving cells, neutrophils rely on glycolysis for energy production. The function of mitochondria in neutrophil motility is unknown. We demonstrated that mitochondria play an indispensable role in neutrophil migration: the biogenesis of mitochondria, mitochondrial ROS and the interaction between mitochondria and ER are all involved in maintaining the movement of neutrophils.

CHAPTER 1. INTRODUCTION

Neutrophil development

The lifespan of neutrophils is short ranging from several hours to several days, which requires their constant production with an estimated rate of 10^{11} neutrophils every day in humans (Dancey et al., 1976). The production rate will increase under condition of stress. Neutrophils are generated in bone marrow from hematopoietic stem cells. Segmented nucleus and granules are hallmarks of neutrophil maturation. The life cycle of neutrophils is predominantly regulated by the cytokine granulocyte colony stimulating factor (G-CSF). In healthy mice, the level of G-CSF in plasma correlates with the number of neutrophils in circulation (Casanova-Acebes et al., 2013). Mice lacking of either G-CSF or its receptor display obvious neutropenia at steady state (Semerad et al., 2002), but mature neutrophils still exist indicating an involvement of other regulators.

More than 90% of total neutrophils are stored in the bone marrow. Under physiological stress, neutrophils are released into the blood. The balance of neutrophil retention and release is modulated by chemokines. When C-X-C-motif chemokine ligand (CXCL) 12 binds to its receptor CXCR4, neutrophils retain in the bone marrow. Whereas the release is mediated by the binding of CXCR2 to ligands (Martin et al., 2003). The switch between CXCR4 and CXCR2 binding can be regulated by other factors to orchestrate neutrophil mobilization under inflammatory conditions. For instance, G-CSF is able to inhibit the CXCR4/CXCL12 axis or induce the production of CXCL1, a ligand of CXCR2, to promote neutrophil release in acute inflammation (Kohler et al., 2011; Semerad et al., 2002).

Neutrophil apoptosis is critical for immune homeostasis. Apoptotic neutrophils are cleared by phagocytic macrophages mediated by liver X receptor (LXR) signaling (Hong et al., 2012; N et al., 2009). It has been shown that bone marrow is the major site of neutrophil clearance. About 32% of senescent neutrophils home back to the bone marrow from circulation to be eliminated in mice (Furze and Rankin, 2008).

Neutrophil migration

Neutrophils in the bloodstream are capable of rapidly infiltrating into peripheral tissues and responding to pathogenic invasion or sterile tissue inflammation. Numerous stimuli, including pathogen-associated molecular pattern (PAMP) and damage-associated molecular pattern (DAMP) molecules, can activate sentinel cells in tissues when tissue homeostasis is disturbed, to release proinflammatory mediators, such as interleukin-1β (IL-1β) and tumor necrosis factor α (TNFα), or chemoattractants. These mediators then trigger rapid neutrophil recruitment into tissues (Williams et al., 2011; Zeytun et al., 2010).

To arrive at the infected or inflamed tissue, neutrophils need to cross the endothelium layer of the vasculature. The crossing consists of several steps including rolling, firm adhesion, and transendothelium migration. Proinflammatory mediators generated during infection or inflammation activate endothelial cells resulting in expression of E-selectin and P-selectin on the surface. The binding of these selectins to PSGL-1 (P-selectin ligand 1) and L-selectin that is expressed constitutively on the surface of neutrophils, initiates the attachment of neutrophils to endothelial cells (Bruehl et al., 1997; Steegmaier et al., 1997). Neutrophils also express ESL-1 (E-selectin ligand 1) on the surface which binds to E-selectin as well, contributing to slow rolling (Hidalgo et al., 2007). Even though the selectin-associated binding is not stable and turns over quickly, it is sufficient to mediate the attachment of neutrophils to endothelial cells in the bloodstream with shear stress (Pospieszalska and Ley, 2009).

The tight adhesion of neutrophils to endothelial cells is mediated by integrins and their ligands. β2 integrins LAF-1 and Mac-1 are expressed by neutrophils on the surface, while their ligands, ICAM-1and ICAM-2 are present on the surface of endothelial cells (Bunting et al., 2002). Integrins have three distinct conformations: a bent form without ligand binding, an extended form with intermediate ability of ligand binding, and a fully opened form with tight ligand binding. Conformation change of integrins determines the affinity for their binding partners to modulate the tightness of adhesion between two cell types. The transition between slow rolling and adhesion of neutrophils on endothelial cells is predominantly determined by LFA-1 (Phillipson et al., 2006). Selectins-mediated rolling triggers the conformation change of LFA-1, facilitating intermediate binding to ICAM-1 (Kuwano et al., 2010). Full activation of LFA-1 which results in firm adhesion requires the engagement of chemokine signaling of neutrophils (Zarbock et al., 2007).

Once the tight adhesion is formed, transmigration starts. Neutrophils migrate through endothelial cells either via the paracellular route crossing junctions between endothelial cells, or the transcellular route crossing an endothelial cell body. The main players involved in transendothelial migration are β2 integrins and their ligands. Paracellular migration, the predominant route, also requires endothelial junction and adhesion molecules including JAM (junctional adhesion molecule), PECAM (platelet endothelial cell adhesion molecule), ESAM (endothelial cell-selective adhesion molecule), CD99, and VE-Cadherin (Allingham et al., 2007; van Buul et al., 2005; Woodfin et al., 2009). About 20% of neutrophils take the transcellular route, in which endothelial cells form docking structures and progress to dome structures enabling endothelial cells to envelop neutrophils in a phagocytosis-like process (Phillipson et al., 2008).

Having crossed the endothelial lining, neutrophils must penetrate the basal membrane consisting of collages and laminins. By expressing proteases and matrix metalloproteinase (MMP-8, MMP-9), neutrophils are able to break down the basal membrane and migrate forward (Kang et al., 2001). Once neutrophils are in the tissue, they follow the guidance of chemokine gradients, both host-derived and pathogen-produced, toward the site of inflammation.

Neutrophil function

Phagocytosis is the major way to clear pathogens and damaged tissues. It is mediated by the interaction between receptors and their ligands, either direct, through binding of PAMPs to PRR, or indirect, through opsonizations. Internalization of engaged receptors enables neutrophils to engulf particles and further progresses to phagosomes. Phagosome maturation is mediated by fusing with granules which contain antimicrobial molecules. Meanwhile, ROS are generated by NADPH oxidase on the phagosomal membrane, promoting the killing of pathogens (Amulic et al., 2012).

Granules are specific storage compartments that neutrophils have evolved to carry dangerous substances. There are three types of granules in neutrophils. Primary granules (also known as azurophilic granules) are the largest and first granules formed during neutrophil maturation. They possess a specific cargo myeloperoxidase (MPO) which does not exist in other granules, and other proteins including defensins, lysozyme, serine proteases (elastase, proteinase 3 and cathepsin G)

(Lacy, 2005; Nusse and Lindau, 1988). Secondary granules (or specific granules) are generated after primary granules. They are smaller and contain the glycoprotein lactoferrin and other antimicrobial compounds (Faurschou and Borregaard, 2003). The third type is gelatinase granules, the smallest and last granules formed in neutrophils. These granules are filled with metalloproteases including gelatinase and leukolysin. When neutrophils are activated, granules are able to mobilize and fuse with either phagosomes or the plasma membrane, releasing compounds into the surrounding tissue and resulting in an inhospitable environment for invading microbes (Borregaard, 2010).

Neutrophils are among the first cells that arrive at the inflamed tissue. They participate in establishing the defense line and shaping the immune response. To fulfill this, neutrophils secrete cytokines and chemokines. The most abundant cytokine produced by neutrophils is IL-8 which recruits other neutrophils reinforcing the immune response (Scapini et al., 2000). IL-1β and TNF-α are proinflammatory mediators produced by neutrophils to activate other cells to release more neutrophil chemoattractants (Sica et al., 1990). Additionally, neutrophils express monocyte chemoattractants including CCL2, CCL3, CCL20, and CCL19 (Scapini et al., 2001; Yoshimura and Takahashi, 2007). They also are capable of activating dendritic cells by releasing CCL3 (Peters et al., 2008). Furthermore, neutrophils serve as the bridge between innate immunity and adaptive immunity. They influence T cell function directly by secreting IL-12 which is critical for T cell differentiation and maturation (Romani et al., 1997). Recently, it has been reported that neutrophils act as antigen-presenting cells for T cells to modulating adaptive immunity (Abdallah et al., 2011; Davis et al., 2017).

The formation of neutrophil extracellular traps (NETs) is another key mechanism of bacterial killing in neutrophils. The process to produce NETs is called NETosis and is defined by the release of decondensed chromatin into the extracellular space by neutrophils (Brinkmann et al., 2004). With the corporation of histones, granules and antimicrobial proteins, extracellular chromatins form a fibrous structures to trap and eliminate microbes (Fuchs et al., 2007; Urban et al., 2009).

Neutrophil clearance

Neutrophils possess a tremendous amount of lethal cargos which are not only detrimental to microbes, but also destructive to host cells. Thus, neutrophil infiltration and activation must be

tightly regulated. Removal of neutrophils from inflamed tissue is crucial for resolution of inflammation and maintenance of tissue homeostasis. Failure of neutrophil clearance usually leads to chronic inflammation and autoimmune disorders, including cystic fibrosis, atherosclerosis, chronic obstructive pulmonary disease and rheumatoid arthritis (Amulic et al., 2012).

Apoptosis is a dominant way for neutrophil clearance. Once neutrophils have performed their antimicrobial function, they die via apoptosis. In addition to directly reducing the number of neutrophils in the tissue, apoptosis also induces signals to prevent further neutrophil infiltration. The clearance of apoptotic neutrophils relies on macrophages. With the engulfment of apoptotic cells, macrophages secrete anti-inflammatory cytokines including tumor growth factor TGF-β and IL-10, further promoting inflammation resolution (Kennedy and DeLeo, 2009).

Reverse migration is another way for neutrophils to leave sites of inflammation. This phenomenon was first observed in zebrafish with live imaging. In the resolution phase of wound response, neutrophils migrate away from the inflamed tissue (Mathias et al., 2006) and re-enter into the vasculature by reverse transendothelial migration (Yoo and Huttenlocher, 2011). This was further confirmed in mice. The mouse study identified that downregulation of JAMC, a junctional adhesion protein, is required for reverse transmigration (Woodfin et al., 2011). Reverse migration of neutrophils promotes the resolution of inflammation in the local inflamed sites. However, this process may lead to disseminated inflammation into other places when neutrophils re-enter circulation and cause systemic inflammation (Kolaczkowska and Kubes, 2013).

Challenge in neutrophil study

Neutrophils are terminally differentiated cells making them unculturable in vitro. Moreover, they have a very short life span and only survive for several hours ex vivo. These characteristics render genetic manipulation in neutrophils almost impossible. Neutrophil-like cell lines have been used recently in the neutrophil field including the human promyelocytic leukemia HL-60 cells and PLB-985 cells (Pedruzzi et al., 2002; Tucker et al., 1987). Even though they display neutrophil-like morphology and function, these cell lines cannot fully recapitulate the biology of neutrophils. Furthermore, in vitro assays are not likely to completely mimic the in vivo environments, which is another limitation of using cell lines. As a well-established animal model, mice are usually the first choice to characterize neutrophil biology in vivo. The genetic tools to manipulate the murine

genome including constitutively and conditionally knockout, knockdown and knockin, which are all available and well-established. However, the obvious drawbacks of this model include the low throughput and time-consuming crossing. Recently, zebrafish has emerged as a popular model in neutrophil studies. Zebrafish share a conserved innate immune system with humans (Renshaw and Trede, 2012; van der Vaart et al., 2012). Importantly, zebrafish neutrophils are very similar to human neutrophils in terms of morphology and function (Henry et al., 2013). As vertebrates, numerous embryos can be produced at once from one pair of parents and develop outside the uterus. Neutrophils start to differentiate within 24-36 hours post fertilization, so neutrophil-related assays can be performed as early as two days after fertilization. The biggest advantage of zebrafish as an animal model system is the intrinsic transparence of zebrafish larva enabling the visualization of neutrophil behavior in vivo. *Tol2* transposon mediated insertion facilitates genome editing in zebrafish (Kawakami, 2005), however, robust and efficient precise editing and conditional knockouts are still lacking, which hinders the application of this model.

Neutrophils play a pivotal role in host defense. However, the regulation of neutrophil migration and activation is still not fully understood, especially in vivo. Given that immune response requires the collaboration of different cell types and neutrophils crosstalk with other cells including both immune cells and nonimmune cells, it is more physiologically relevant to study neutrophil biology in vivo. Comprehensive description of neutrophil's function and regulation may require the information obtained from different models.

CHAPTER 2. MICRORNA-223 SUPPRESSES THE CANONICAL NF-KB PATHWAY IN BASAL KERATINOCYTES TO DAMPEN NEUTROPHILIC INFLAMMATION

Abstract

MicroRNA-223 is known as a myeloid-enriched anti-inflammatory microRNA that is dysregulated in numerous inflammatory conditions. Here we report that neutrophilic inflammation (wound response) is augmented in miR-223-deficient zebrafish, due primarily to elevated activation of the canonical NF-κB pathway. Unexpectedly, NF-κB over-activation is restricted to the basal layer of the surface epithelium, although miR-223 is detected throughout the epithelium and in phagocytes. Not only phagocytes, but also epithelial cells are involved in miR-223-mediated regulation of neutrophils' wound response and NF-κB activation. *Cul1a/b*, *Traf6* and *Tab1* are identified as direct targets of miR-223 and their levels rise in injured epithelium lacking miR-223. In addition, miR-223 is expressed in cultured human bronchial epithelial cells, where it also down-regulates NF-κB signaling. Together, this direct connection between miR-223 and the canonical NF-κB pathway provides a mechanistic understanding of the multifaceted role of miR-223 and highlights an overlooked relevance of epithelial cells in dampening neutrophil activation.

Introduction

Neutrophilic inflammation is critical for host defense and tissue repair. Neutrophils are recruited by multiple "intermediate" and "end-target" chemoattractants released by tissue resident sentinel cells upon activation by pathogen or damage-associated molecular pattern molecules (Kim and Luster, 2015; Kolaczkowska and Kubes, 2013). Activated neutrophils release oxidants, proteases, and antimicrobial proteins to eliminate pathogens or damaged cells, which also causes collateral tissue damage (Nathan, 2006). As a result, chronic or rampant neutrophilic inflammation drives the immunopathology involved in numerous human diseases, including those directly involving an immune component such as rheumatic arthritis and those that are not obviously linked such as diabetes, neurodegenerative disease and cancer (Borregaard, 2010; Nathan, 2006). Therefore, fine-tuning the magnitude and resolution of neutrophilic inflammation is critical for the host to restore homeostasis.

It is estimated that 30-80% of genes in humans are regulated by microRNAs (miRNAs) (Lu and Clark, 2012). MiRNAs are small (20-22 nucleotides) non-coding RNA molecules that typically suppress the translation and the stability of transcripts through partial complementarity (Ha and Kim, 2014; Jonas and Izaurralde, 2015). MiRNAs are fine-tuners that suppress target gene expression at modest levels, yet master regulators that suppress multiple genes in the same pathways (Gurol et al., 2016; Orellana and Kasinski, 2015). These features suggest that miRNAs may be suitable modulators for the duration and the magnitude of inflammation. Several miRNAs, including miR-223, miR-155, miR-146, and miR-125b, have a role in the differentiation and function of the innate immune system (Johnnidis et al., 2008; Lindsay, 2008; Lu and Liston, 2009). However, as a result of the complex and dynamic interactions between multi-tissues that coordinate an inflammatory response, the functions of these miRNAs in immune response are not fully understood.

MiR-223 has previously been observed primarily in the myeloid lineage, especially in neutrophils (Chen et al., 2004; Johnnidis et al., 2008), and is implicated in many inflammatory disorders, infections and cancers (Haneklaus et al., 2013). Global miRNA expression profiling revealed dysregulation of miR-223 in numerous conditions, however no consensus between the level of miR-223 and the type or progress of the diseases can be concluded (reviewed in (Haneklaus et al., 2013)). Opposing roles of miR-223 have been reported, suggesting that miR-223 plays parts of a complex regulatory network with profound impact from the surrounding tissues.

The first *in vivo* characterization of miR-223 was performed in a miR-223 loss-of-function mouse model (*miR-223*$^{-/Y}$), where an increase in granulopoiesis, as well as hyper-mature and hyper-responsive neutrophils were observed (Johnnidis et al., 2008). This strain displayed increased susceptibility to *Mycobacterial* infection, which is due to increased neutrophil accumulation in the lung (Dorhoi et al., 2013), where a cell-autonomous role of miR-223 in neutrophil recruitment was suggested. NLR Family Pyrin Domain Containing 3 (NLRP3) inflammasome activity was also regulated by miR-223 in primary murine neutrophils (Bauernfeind et al., 2012). In addition to the immune system, Harraz *et al*. revealed that miR-223, delivered by adenovirus to the brain, protected mice from an ischemic reperfusion brain injury (Harraz et al., 2012).
In addition, there is a body of literature related to the function of miR-223 in myeloid cells *in vitro*, with yet to be verified *in vivo* relevance. As one of the most abundant miRNAs in macrophages,

miR-223 responds to stimuli to control the production of IL-6 and IL-1β (Chen et al., 2012), or promotes alternative macrophage activation to inhibit diet-induced adipose tissue inflammation and insulin resistance by targeting *Pknox1*, *Rasa1* and *Nfat5* in murine macrophages (Ying et al., 2015; Zhuang et al., 2012). MiR-223 is also associated with macrophage differentiation through targeting IKKα (Li et al., 2010). Furthermore, macrophages and monocytes secrete miR-223 in microvesicles or associated high-density lipoproteins, which are delivered into non-immune cells such as endothelial cells (Ismail et al., 2013; Tabet et al., 2014). Those transferred miRNAs are functionally active, indicating the potential of miR-223 as a central mediator for intercellular cross-talk.

Aside from the immune cells, miR-223 is required for stem cell differentiation, such as the differentiation of mesenchymal stem cells into adipocytes and osteoblasts (Guan et al., 2015). In cancers, the role of miR-223 is conflicting. For example, miR-223 is upregulated in acute lymphoblastic leukemia and bladder cancers, but down regulated in chronic lymphoid leukemia and hepatocellular carcinoma (Chiaretti et al., 2010; Gottardo et al., 2007; Stamatopoulos et al., 2009; Wong et al., 2008). Elevated miR-223 supports migration and invasion in gastric cancer cells but has opposite effect in oesophageal cancer cells and human cervical cancer (Li et al., 2011a; Li et al., 2011b; Tang et al., 2015).

In this study, we took advantage of the zebrafish system, which offers a unique genetic and imaging platform to dissect the interplay of various tissues during inflammation. Moreover, zebrafish are a suitable model for studying innate immunity as they possess conserved innate immune cells and signaling molecules as human (Renshaw and Trede, 2012). We discovered an unexpected importance of NF-κB activation in epithelial cells at the center of miR-223 regulated neutrophilic inflammation, which provides insights into the multifaceted role of miR-223 in various inflammatory conditions.

Results

miR-223 deficiency delays the resolution of neutrophilic inflammation

The gene structure and mature sequence of miR-223 are conserved within vertebrates (Roberto et al., 2015). Similar to mice and human (Johnnidis et al., 2008), miR-223 expression was

significantly higher in neutrophils in zebrafish (Fig. 2-1A, B), supporting zebrafish as a suitable model for miR-223 research. We then generated a miR-223 deficient (*miR-223*$^{-/-}$) zebrafish line using the CRISPR/Cas system. An allele containing an 18-bp mismatch to the wild-type (WT), which is predicted to disrupt the hairpin structure of *pre-mir-223* was selected (Fig. 2-2A and B). A complete loss of miR-223, with no alterations of two other microRNAs expressed in neutrophils (miR-142-3p and miR-92a), was detected in the *miR-223*$^{-/-}$ fish (Fig. 2-2C). No apparent abnormalities in development, viability or life-span were noted in the *miR-223*$^{-/-}$ fish, similarly to the *miR-223*$^{-/Y}$ mice (Johnnidis et al., 2008) and a recently generated *miR-223*$^{-/-}$ zebrafish line (Kasper et al., 2017). In addition, no differences in total neutrophil numbers, spontaneous inflammation or cell death in 3 day post fertilization (dpf) embryos were noted (Fig. 2-2D, E and Fig. 2-1C, D, E, F).

Figure 2-1. miR-223 deficiency does not lead to cell death in zebrafish

Neutrophils were isolated by fluorescence-activated cell sorting from 3 dpf zebrafish embryos. (A) RT-PCR of indicated cell markers. *mpeg*: macrophage marker; *mpx*: neutrophil marker; *myoD*: muscle cell marker; *ef1a*: loading control. WE: whole embryo. NTC: non-template control. (B) RT-qPCR of miR-223 expression in neutrophils, presented as the relative expression to whole embryos normalized to U6. Two individual experiments are shown. (C) Representative images and (D) Quantification of the neutrophil numbers in the fin in WT and *miR-223*$^{-/-}$ embryos. One representative experiment of three independent repeats is shown. NS, $P > 0.05$, unpaired student t-test. (E, F) Representative images of TUNEL staining and quantification of TUNEL+ cells in the fin in WT and *miR-223*$^{-/-}$ embryos. WT embryos treated with DNase I were used as the positive control. Yellow arrows indicate TUNEL^{+} cells. Scale bars, 100 μm. NS: $P > 0.05$, unpaired student *t*-test.

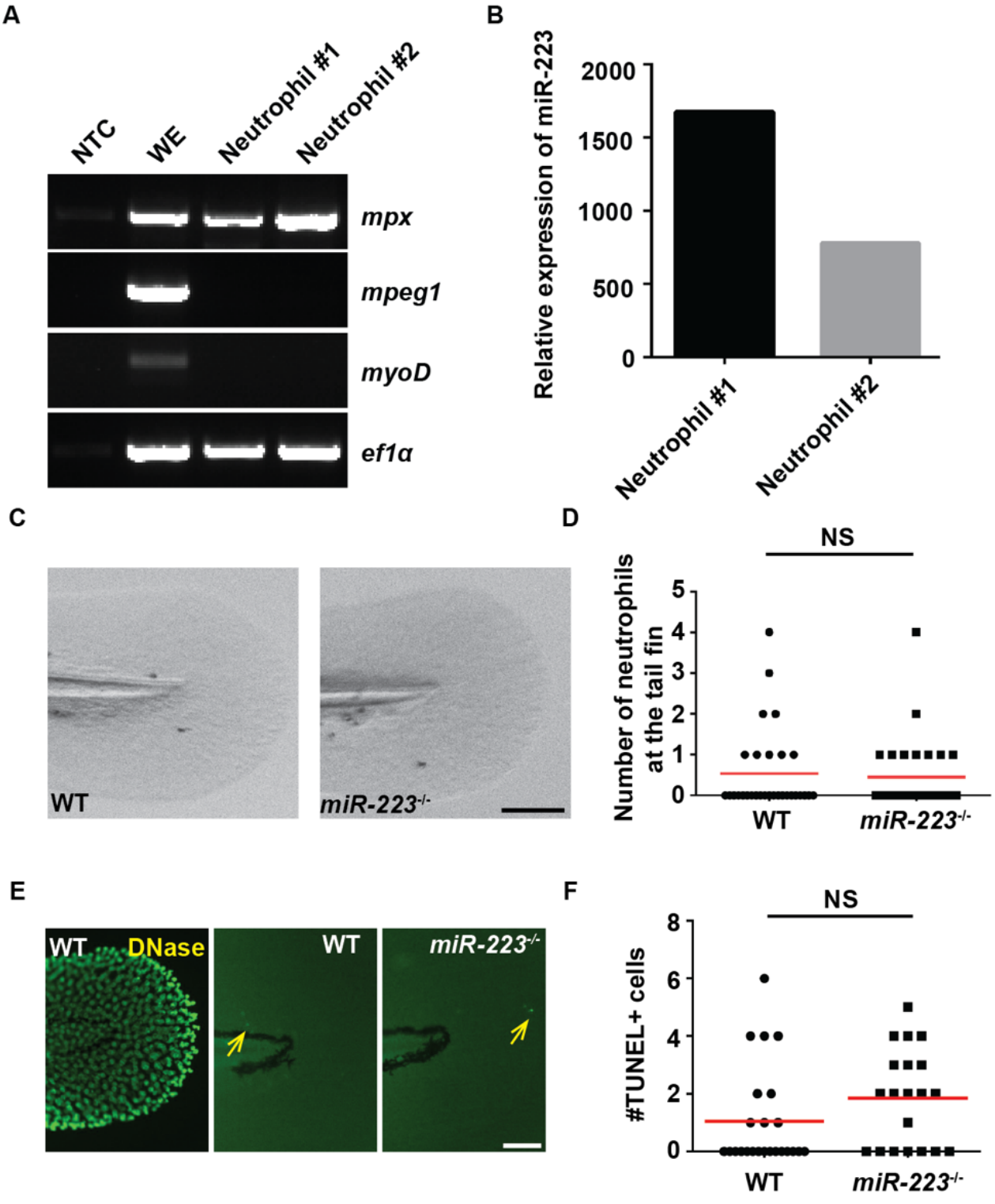
A
NTC
WE
Neutrophil #1
Neutrophil #2
mpx
mpeg1
myoD
ef1α
B
Relative expression of miR-223
2000
1500
1000
500
0
Neutrophil #1
Neutrophil #2
C
WT
miR-223-/-
D
NS
Number of neutrophils at the tail fin
5
4
3
2
1
0
WT
miR-223-/-
E
WT
DNase
WT
miR-223-/-
F
NS
#TUNEL+ cells
8
6
4
2
0
WT
miR-223-/-

Figure 2-2. miR-223 deficient embryos display augmented neutrophil response to tissue injury.

(A) Sequences of *pre-mir-223* in wild-type and miR-223 mutant embryos. Mutated nucleotides are labeled in red. (B) The hairpin structures of miR-223 in wild-type and mutant embryos predicted by Centroidfold. (C) Expression of miR-223, miR-142-3p, and miR-92a in WT and *miR-223*$^{-/-}$ embryos determined by RT-qPCR. (D, E) Representative images and quantification of total neutrophil numbers in WT and *miR-223*$^{-/-}$ embryos. (F, G) Representative images and quantification of neutrophil recruitment to tail transection sites in WT and *miR-223*$^{-/-}$ embryos at 1 hpw and 6 hpw. The number of neutrophils in the boxed region were quantified. Scale bars, 100 μm. Data are representative of three independent experiments (E, G) or are pooled from three independent experiments (C; mean ± s.d.). *** $P < 0.001$ and **** $P < 0.0001$, unpaired student *t*-test.

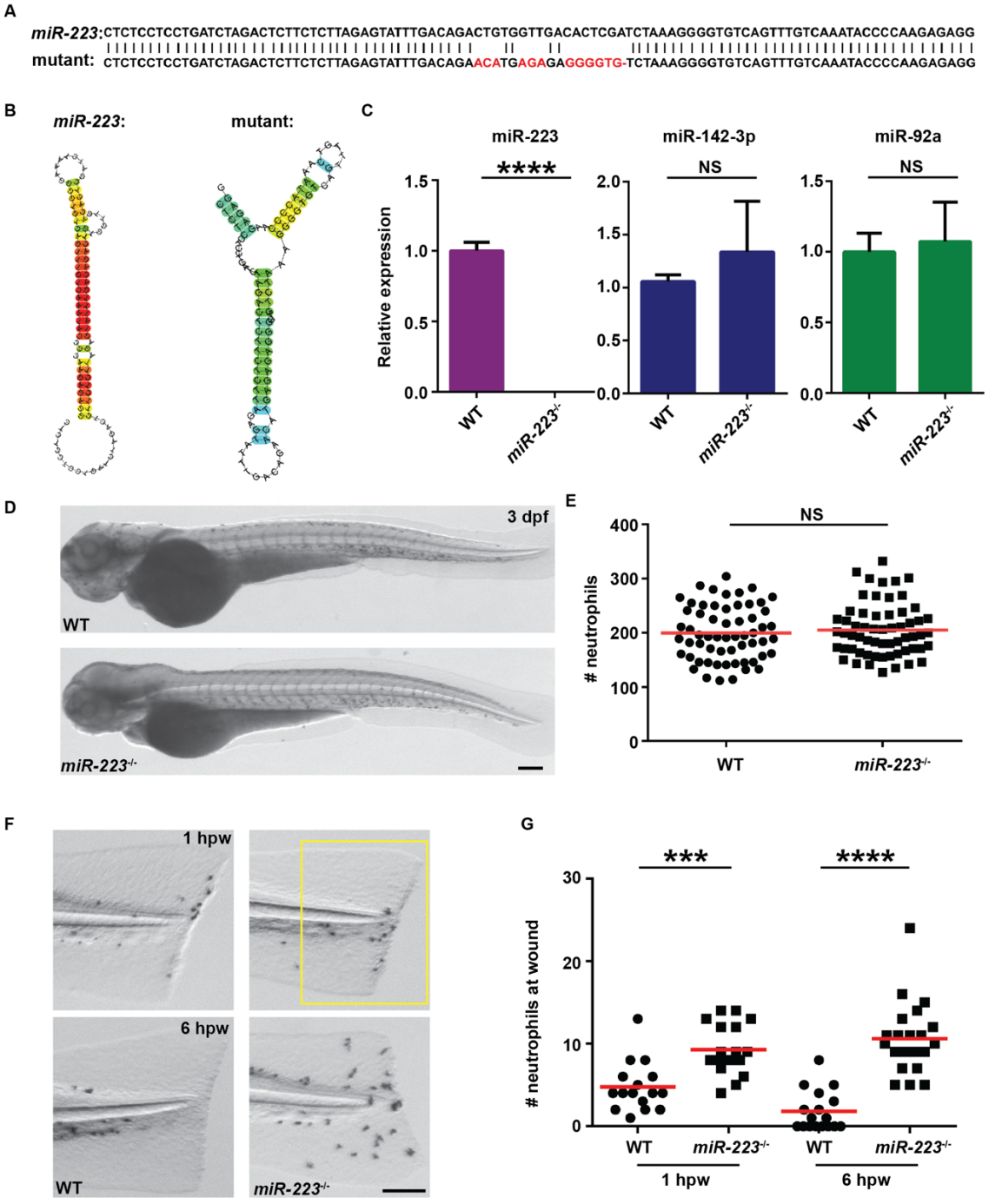
A
miR-223:CTCTCCTCCTGATCTAGACTCTTCTCTTAGAGTATTTGACAGACTGTGGTTGACACTCGATCTAAAGGGGTGTCAGTTTGTCAAATACCCCAAGAGAGG
mutant: CTCTCCTCCTGATCTAGACTCTTCTCTTAGAGTATTTGACAGAACATGAGAGAGGGGTG-TCTAAAGGGGTGTCAGTTTGTCAAATACCCCAAGAGAGG
B
miR-223:
mutant:
C
miR-223
miR-142-3p
miR-92a
****
NS
NS
Relative expression
1.5
1.0
0.5
0.0
2.0
1.5
1.0
0.5
0.0
1.5
1.0
0.5
0.0
WT
miR-223-/-
WT
miR-223-/-
WT
miR-223-/-
D
3 dpf
WT
miR-223-/-
E
NS
neutrophils
400
300
200
100
0
WT
miR-223-/-
F
1 hpw
6 hpw
WT
miR-223-/-
G
***
****
neutrophils at wound
30
20
10
0
WT
miR-223-/-
WT
miR-223-/-
1 hpw
6 hpw

We next investigated the function of miR-223 in a self-resolving inflammation model. Specifically, a tailfin transection injury in 3 dpf embryos results in a rapid recruitment of neutrophils that peaks at 1 hour post wounding (1 hpw), which is spontaneously resolved by 6 hpw. Significant increases in neutrophils at the wound region in *miR-223*$^{-/-}$ embryos were detected at both time points (Fig. 2-2F and G). The *miR-223*$^{+/-}$ embryos has a phenotype comparable to *miR-223*$^{-/-}$, possibly due to the self-reinforced expression of miR-223 (Fazi et al., 2005). As a result, adult fish (*miR-223*$^{+/+}$ and *miR-223*$^{-/-}$) from the same parents (*miR-223*$^{+/-}$) were used to produce embryos for experiments. To better identify the source of neutrophils at the wound vicinity at 6 hpw, photoconversion-enabled neutrophil fate-mapping was performed (Deng et al., 2011) (Fig. 2-3 A). Green neutrophils present at the wound at 1 hpw were photo-converted into red neutrophils. Five hours later, the percentage of red neutrophils remaining at the wound in *miR-223*$^{-/-}$ was modestly higher than that in WT, indicating a defect in neutrophil reverse migration (migration away from the wound) (Fig. 2-3B, C). Furthermore, the number of green neutrophils at the wound in 6 hpw *miR-223*$^{-/-}$ was significantly higher than that in WT, suggesting a continuous recruitment of neutrophils in the *miR-223*$^{-/-}$ (Fig. 2-3D). Altogether, the excessive neutrophilic inflammation in *miR-223*$^{-/-}$ embryos was primarily a result of continuous neutrophil recruitment, with a minor defect in reverse migration.

Figure 2-3. Enhanced neutrophil recruitment in *miR-223*$^{-/-}$ embryos results from both continuous neutrophil recruitment and a defect in neutrophil reverse migration.

(A) Schematics of photoconversion-enabled neutrophil fate-mapping assay. Embryos from *Tg(miR-223*$^{-/-}$*, mpx: Dendra2)* or *Tg(mpx: Dendra2)* were used. Photolabled neutrophils remaining at the wound indicate a defect in reverse migration. (B) Representative confocal images of embryos at three time points: before, immediately after, and 5 hours after photoconversion. Red neutrophils are photoconverted neutrophils. Red star indicates the injury site. (C) Percentage of red neutrophils remaining at the wound at 6 hpw. (D) Quantification of the number of green neutrophils at the wound at 6 hpw. Scale bars, 20 μm. * $P < 0.05$ and **** $P < 0.0001$, unpaired student *t*-test.

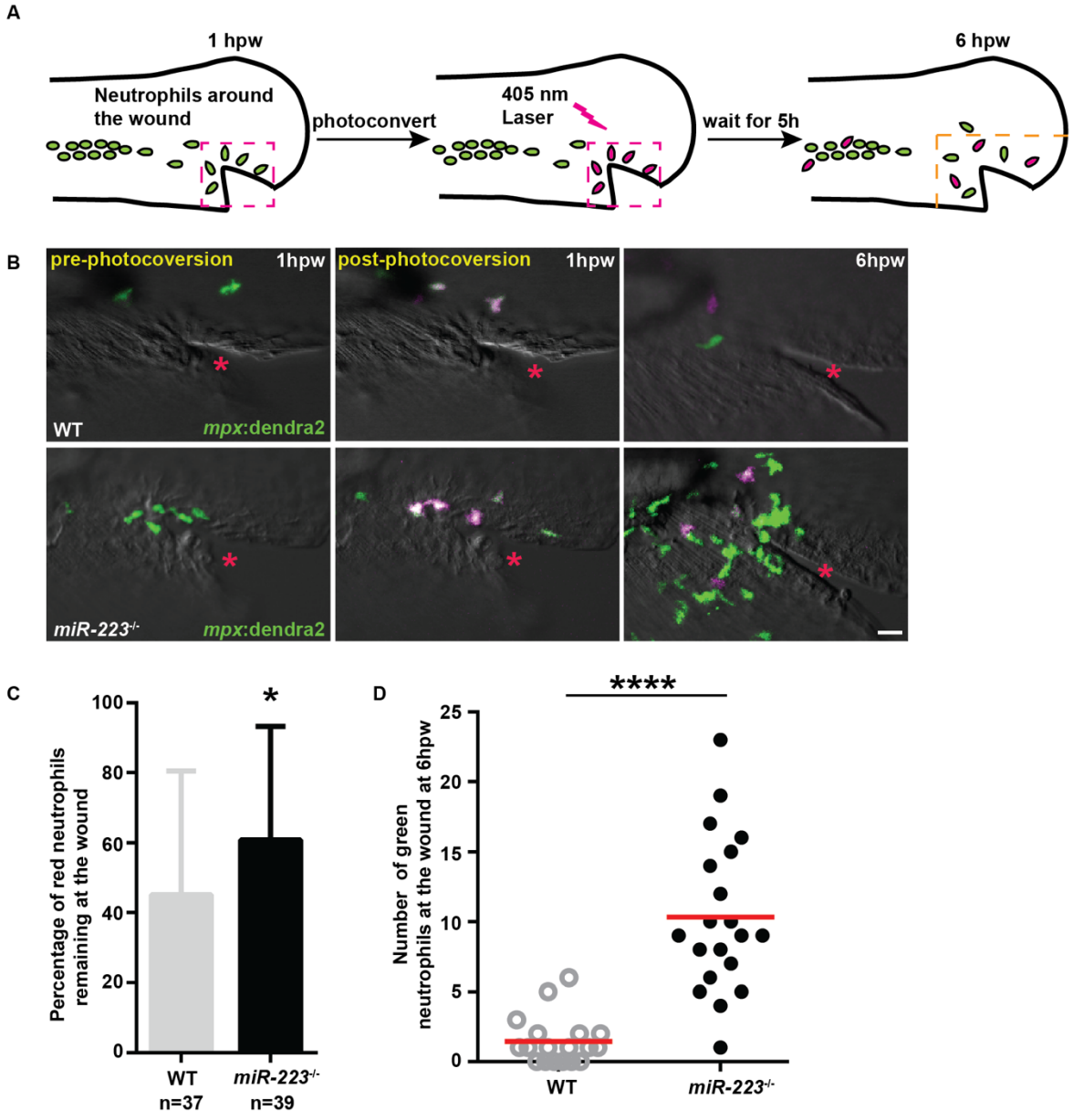
A
1 hpw
Neutrophils around the wound
photoconvert
405 nm Laser
wait for 5h
6 hpw
B
pre-photocoversion
1hpw
post-photocoversion
1hpw
6hpw
WT
mpx:dendra2
miR-223-/-
mpx:dendra2
C
Percentage of red neutrophils remaining at the wound
100
80
60
40
20
0
*
WT
n=37
miR-223-/-
n=39
D
Number of green neutrophils at the wound at 6hpw
25
20
15
10
5
0
****
WT
miR-223-/-

Neutrophil-intrinsic miR-223 is required to control neutrophilic inflammation

Since miR-223 has been known as a myeloid specific miRNA, we next determined whether miR-223 regulates neutrophil wound response cell-autonomously. To specifically knock down miR-223 in neutrophils, a miR-223 sponge, containing six bulged binding sites of miR-223, was expressed under the lysozyme C (*lyzC*) promoter (Hall et al., 2007) (Fig. 2-4A). Indeed, embryos expressing the miR-223 sponge accumulated more neutrophils at the wound at 6 hpw (Fig. 2-4B, C and Video 1). To further confirm the neutrophil intrinsic role of miR-223, a neutrophil-specific *miR-223*-overexpression line, *Tg(lyzC: miR-223-RFP)*^{pu9} was generated and crossed into the *miR-223*$^{-/-}$ background (Fig. 2-4D). The neutrophil specific rescue partially restored the miR-223 expression level, and partially rescued the over-inflammation phenotype (Fig. 2-4E, F), suggesting that miR-223 regulates inflammation, at least partially, inside neutrophils. A control rescue with RFP alone did not yield any phenotype (Fig. 2-4D, E, G)

Figure 2-4. Neutrophil intrinsic miR-223 regulates neutrophilic inflammation.

(A) Schematics of *Tol2-lyzC-Gal4-crys-CFP* construct, injected into wild-type embryos to generate the transgenic line *Tg(lyzC:Gal4-Vp16, crys:CFP)*^{pu8}; *Tol2-UAS-miR-223* sponge that contains 6 bulged miR-223 binding sites after the UAS element and the Dendra2 control plasmid. (B, C) miR-223 sponge or Dendra2 control plasmids in A were injected into embryos from *Tg(lyzC: Gal4-Vp16, crys: CFP)* ^{pu8} and *Tg(lyzC: mCherry-H2B)* cross. Tailfins were transected at 3 dpf. Representative images at indicating time points are shown in B, and neutrophil recruitment at 6 hpw is shown in C. (D) Schematics of *Tol2-lyzC-miR-223/RFP* constructs, injected into wild-type embryos to generate the transgenic line *Tg(lyzC: RFP-miR-223)* ^{pu9} and the control line *Tg(lyzC: RFP)* ^{pu10}. (E) The transgenic lines illustrated in D were crossed into the *miR-223*$^{-/-}$ background. The siblings without RFP were used as negative control. miR-223 expression in indicated groups was quantified by RT-qPCR. (F, G) Quantification of neutrophil recruitment to tail transection sites in embryos with miR-223 (F) or RFP control (G) expressed in neutrophils in the *miR-223*$^{-/-}$ background at 1 hpw and 6 hpw. Scale bars, 100 μm. One representative experiment of three independent repeats is shown. * $P < 0.05$, ** $P < 0.01$, *** $P < 0.001$, and **** $P < 0.0001$, unpaired student *t*-test (C, F, G) or one-way ANOVA (E).

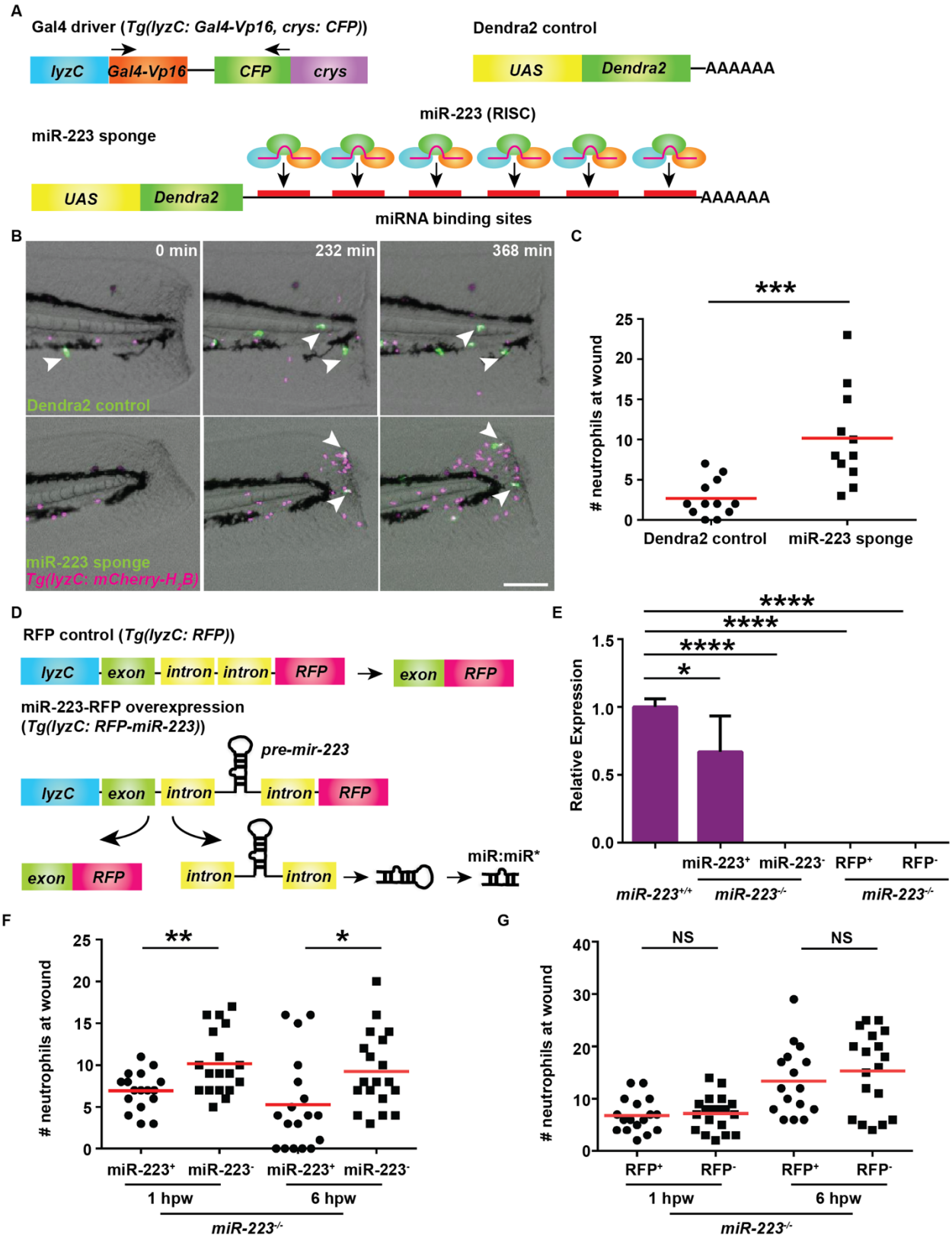
A
Gal4 driver (Tg(lyzC: Gal4-Vp16, crys: CFP))
lyzC
Gal4-Vp16
CFP
crys
Dendra2 control
UAS
Dendra2
AAAAAA
miR-223 (RISC)
miR-223 sponge
UAS
Dendra2
AAAAAA
miRNA binding sites
B
0 min
232 min
368 min
Dendra2 control
miR-223 sponge
Tg(lyzC: mCherry-H2B)
C
***
neutrophils at wound
25
20
15
10
5
0
Dendra2 control
miR-223 sponge
D
RFP control (Tg(lyzC: RFP))
lyzC
exon
intron
intron
RFP
exon
RFP
miR-223-RFP overexpression
(Tg(lyzC: RFP-miR-223))
pre-mir-223
lyzC
exon
intron
intron
RFP
exon
RFP
intron
intron
miR:miR*
E
****
****
****
*
Relative Expression
1.5
1.0
0.5
0.0
miR-223+
miR-223-
RFP+
RFP-
miR-223+/+
miR-223-/-
miR-223-/-
F
**
*
neutrophils at wound
25
20
15
10
5
0
miR-223+
miR-223-
miR-223+
miR-223-
1 hpw
6 hpw
miR-223-/-
G
NS
NS
neutrophils at wound
40
30
20
10
0
RFP+
RFP-
RFP+
RFP-
1 hpw
6 hpw
miR-223-/-

NF-κB pathway is activated in *miR-223*$^{-/-}$ embryos

To fully understand how miR-223 regulates neutrophilic inflammation, microarray analysis of both WT and *miR-223*$^{-/-}$ embryos, unwounded or at 1 and 6 hpw was performed. Transcriptome analysis revealed that 166, 115, and 114 genes (that have known human orthologues) were upregulated over 1.5 fold in *miR-223*$^{-/-}$ at indicated time points (Fig. 2-5A). This cut-off was selected according to a pervious report that miR-223 modulates gene expression at modest levels (Baek et al., 2008). The top four pathways altered are inflammatory response, cancer, organismal injury and abnormalities, and reproductive system disease. Among the genes involved in inflammatory response, those in the interferon pathways and NF-κB pathways were enriched.

To identify the biological relevant pathway, a CRISPR screen was performed, aiming to identify genes whose suppression would rescue the over-inflammation phenotype in *miR-223*$^{-/-}$ embryos. The genes initially screened were: *Irf3* and *Irf7* (interferon regulatory transcription factors), *Ifng1* and *Ifng2* (type 2 interferons), *Crfb5* and *Crfb17* (type 1 or type 2 interferon receptor subunits (Aggad et al., 2010), *Stat1a/b* and *Jak2a* (signaling molecules), *Myd88* (the adaptor of TLR and IL1R), *Caspa* (*Caspase1* orthologue), and *Il1b* (pro-inflammatory cytokine) (Fig. 2-5B). A sgRNA targeting GFP which knocked out GFP expression in zebrafish with high efficiency was used as a control (Fig. 2-6A, B). Among all the genes screened, only the *Myd88* sgRNAs injected embryos exhibited a rescue of the over-inflammation phenotype (Fig. 2-6C). The *Crfb17* sgRNAs injected embryos displayed an opposite phenotype, suggesting that interferon-γ may provide a feed-back inhibition of over-inflammation induced with miR-223 loss of function, but requires further characterization. This result of *Myd88* knock out was confirmed in three independent experiments (Fig. 2-7A). When the *Myd88* sgRNA target sites were sequenced, 98.6% of the alleles contain indels (Fig. 2-8A). Further validation was done with a specific inhibitor of the canonical NF-κB pathway, BAY (11-7085), which blocks the phosphorylation of the inhibitory I-κB (Fig. 2-7B). Collectively, miR-223 suppresses neutrophilic inflammation, at least partially, through downregulating the NF-κB pathway.

Figure 2-5. Genes in the NF-κB and interferon pathways are upregulated in *miR-223*$^{-/-}$ embryos.

(A) Microarray was performed for both WT and *miR-223*$^{-/-}$ embryos unwounded and at 1h and 6 h post wounding. Upregulated genes in *miR-223*$^{-/-}$ embryos were grouped into five classes at each time point. Inflammatory response related genes were selected for further pathway analysis. (B) Schematics of the genes in three signaling pathways that were selected for CRISPR/Cas screening: interferon pathway, NF-κB pathway, and related inflammasome pathway.

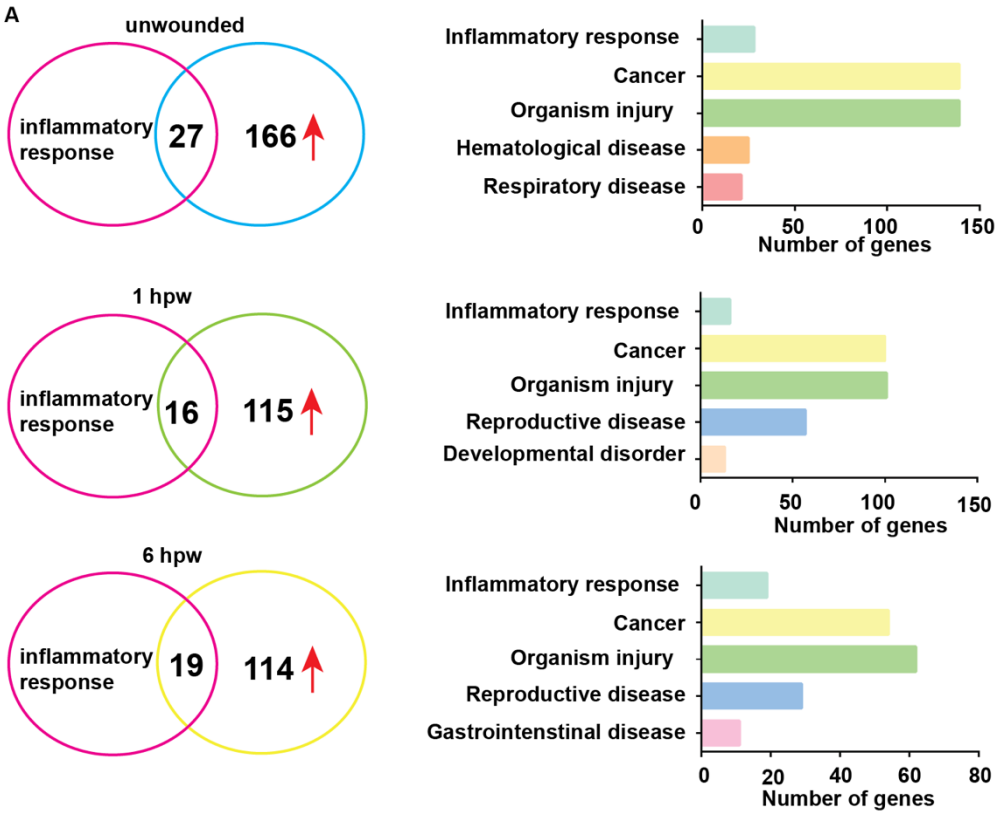
A
unwounded
inflammatory response
27
166
Inflammatory response
Cancer
Organism injury
Hematological disease
Respiratory disease
0
50
100
150
Number of genes
1 hpw
inflammatory response
16
115
Inflammatory response
Cancer
Organism injury
Reproductive disease
Developmental disorder
0
50
100
150
Number of genes
6 hpw
inflammatory response
19
114
Inflammatory response
Cancer
Organism injury
Reproductive disease
Gastrointenstinal disease
0
20
40
60
80
Number of genes

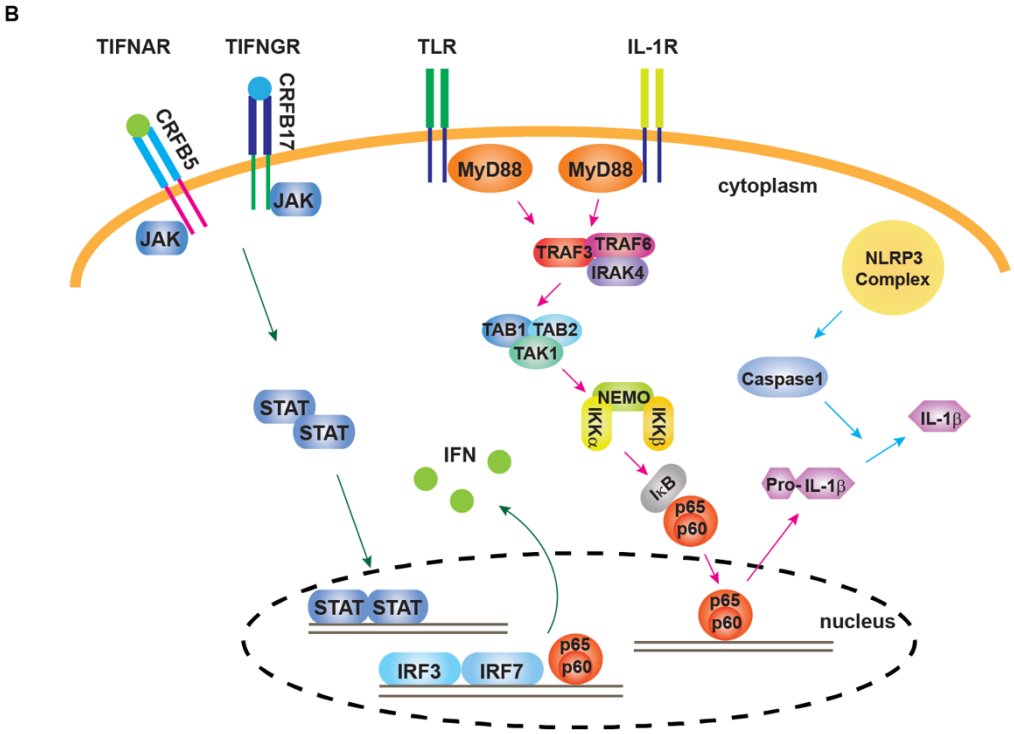
B
TIFNAR
TIFNGR
TLR
IL-1R
CRFB5
CRFB17
JAK
JAK
MyD88
MyD88
cytoplasm
TRAF3
TRAF6
IRAK4
NLRP3 Complex
TAB1
TAB2
TAK1
Caspase1
NEMO
IKKα
IKKβ
IL-1β
STAT
STAT
IFN
IκB
p65
p60
Pro-IL-1β
STAT
STAT
p65
p60
nucleus
IRF3
IRF7
p65
p60

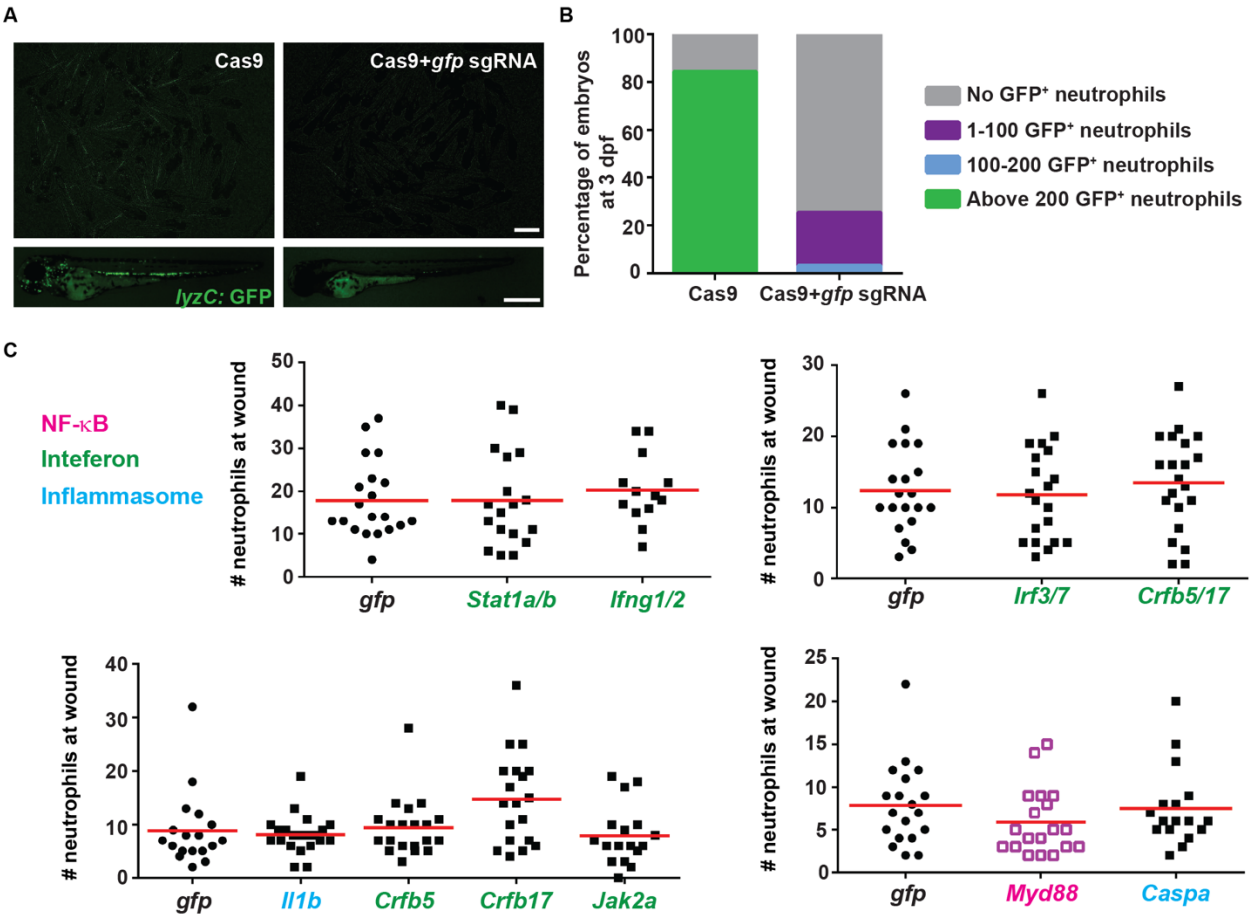

Figure 2-6. Myd88 knock out rescues over-inflammation in *miR-223*$^{-/-}$ embryos.

(A, B) Representative images and quantification of efficiency of transient knock out of GFP using the CRISPR/Cas system. Single guide RNAs targeting GFP were injected into embryos from *Tg(lyzC: GFP)* together with Cas9 proteins, or Cas9 protein alone. The number of green neutrophils at 3 dpf was counted. (C) CRISPR screening. Two separate sgRNAs were designed for each gene. Pooled sgRNAs targeting one gene or two genes were injected with Cas9 protein into *miR-223*$^{-/-}$ embryos. Neutrophil recruitment to the wound at 6 hpw was quantified using *gfp* sgRNA as a control. Genes in the three pathways were color coded separately.

Figure 2-7. miR-223 regulates NF-κB pathway by suppressing *Cul1a*, *Cul1b*, *Traf6*, and *Tab1*.

(A) Quantification of neutrophil recruitment at 6 hpw in *miR-223*$^{-/-}$ embryos injected with sgRNAs targeting *Myd88*, using *gfp* sgRNAs as the control. (B) Quantification of neutrophil recruitment at 6 hpw in *miR-223*$^{-/-}$ embryos treated with BAY (1 uM) or DMSO (1%). (C) Schematics of the canonical NF-κB signaling pathway. (D) The expression of *Cul1a*, *Cul1b*, *Traf6*, and *Tab1* in WT and *miR-223*$^{-/-}$ embryos in unwounded embryos or at 1 hpw as determined by RT-qPCR. (E) Dual luciferase reporter assay showing specific suppression of Renilla luciferase depending on the 3'UTRs of *Cul1a*, *Cul1b*, *Traf6*, and *Tab1* by miR-223. (F) Quantification of neutrophil recruitment at 6 hpw in *miR-223*$^{-/-}$ embryos injected with sgRNAs targeting both *Cul1a* and *Cul1b* or the *gfp* sgRNAs control. Data are representative of three independent experiments (A, B, F) or are pooled from three independent experiments (D, E; mean ± s.d.). * $P < 0.05$, ** $P < 0.01$, and *** $P < 0.001$, unpaired student *t*-test and paired student *t*-test in E.

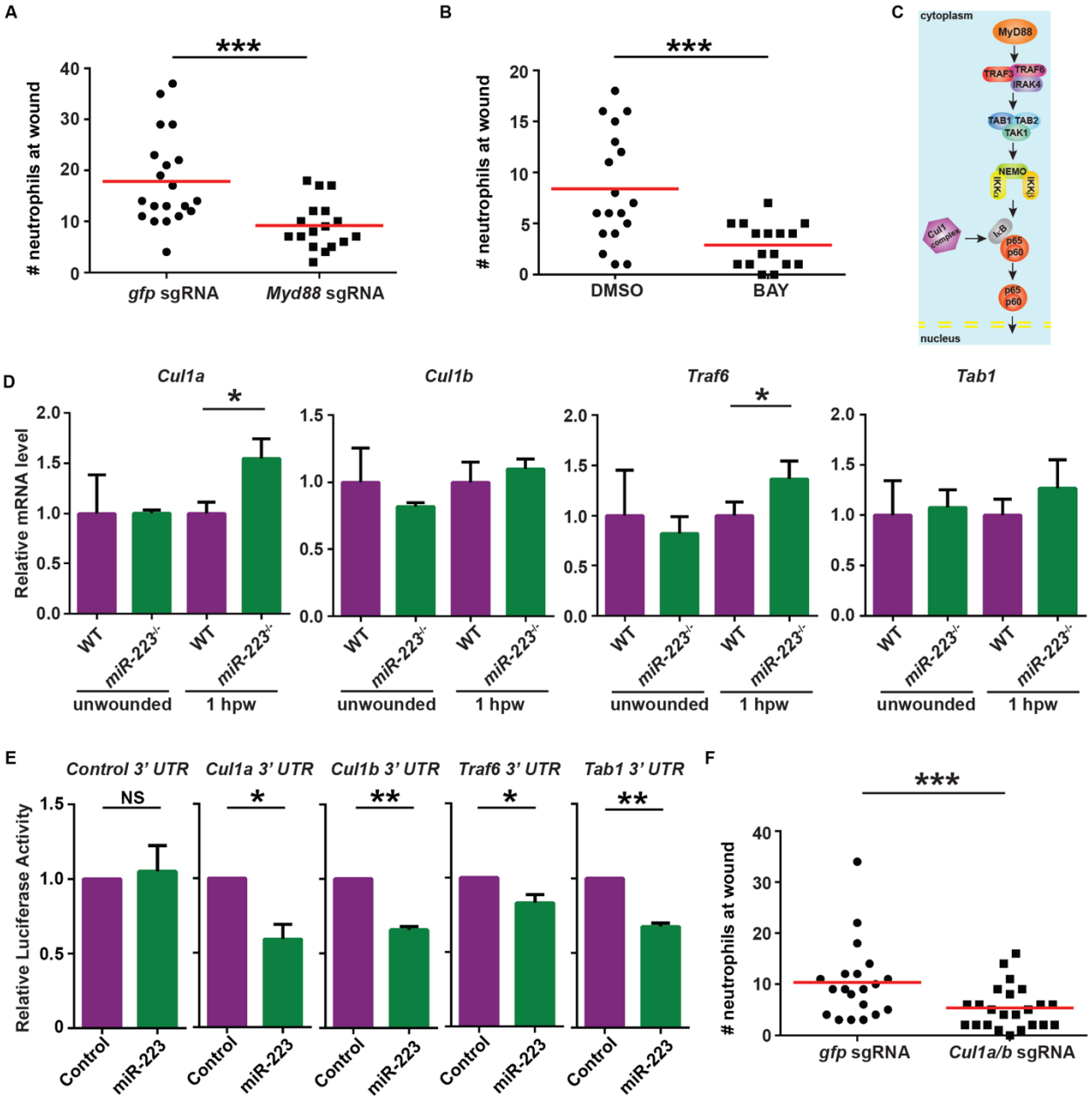
A
***
neutrophils at wound
40
30
20
10
0
gfp sgRNA
Myd88 sgRNA
B
***
neutrophils at wound
20
15
10
5
0
DMSO
BAY
C
cytoplasm
MyD88
TRAF3
TRAF6
IRAK4
TAB1
TAB2
TAK1
NEMO
IKK
IKK
Cul1 complex
I-κB
p65
p60
p65
p60
nucleus
D
Cul1a
Cul1b
Traf6
Tab1
*
*
Relative mRNA level
2.0
1.5
1.0
0.5
0.0
WT
miR-223-/-
WT
miR-223-/-
unwounded
1 hpw
E
Control 3' UTR
Cul1a 3' UTR
Cul1b 3' UTR
Traf6 3' UTR
Tab1 3' UTR
NS
*
**
*
**
Relative Luciferase Activity
1.5
1.0
0.5
0
Control
miR-223
F
***
neutrophils at wound
40
30
20
10
0
gfp sgRNA
Cul1a/b sgRNA

miR-223 directly suppresses *Cul1a/b, Traf6* and *Tab1*

Despite the established importance of the canonical NF-κB pathway in inflammation, a direct link of this pathway with miR-223 has not been reported. We used three algorithms (Target scan, PicTar, and miRanda(Grimson et al., 2007; John et al., 2004; Krek et al., 2005)) and identified four genes in the NF-κB pathway: *Cul1a*, *Cul1b*, *Traf6* and *Tab1* as potential miR-223 targets (Fig. 2-7C). CUL1 is an essential component of the SCF (complex of SKP1, CUL1, and F-box protein) E3 ubiquitin ligase. The SCF E3 ligase complex (SKP1-Cul1-β-TrCP1) ubiquitinates IκB and activates the canonical NF-κB pathway (Villeneuve et al., 2010). *Cul1a* and *Cul1b* are duplicated orthologous in zebrafish. *TRAF6* (TNF receptor associated factor protein 6) and *TAB1* (TGF-β activated kinase 1 binding protein 1) are signaling components in the canonical NF-κB pathway. The mRNA levels of *Cul1a* and *Traf6* were significantly elevated in *miR-223*$^{-/-}$ at 1 hpw, suggesting that they are regulated by miR-223 (Fig, 2-7D). However, there is a lack of reduction in *Cu1b* and *Tab1* transcripts, which may reflect the fact that miRNAs do not always degrade the target mRNAs (Cipolla, 2014). To verify the direct suppression of *Cul1a*, *Cul1b*, *Traf6*, and *Tab1* by miR-223, dual-luciferase reporter assays were performed. As expected, miR-223 significantly inhibited the expression of luciferase reporters fused with the 3'UTRs of *Cul1a*, *Cul1b*, *Traf6*, or *Tab1*, but not with a control 3'UTR (Fig, 2-7E). Additionally, transient knocking out of *Cul1a* and *Cul1b* reduced neutrophil recruitment in *miR-223*$^{-/-}$ embryos at 6 hpw, further validating *Cul1a* and *Cul1b* as physiological relevant miR-223 targets (Fig. 2-7F). The mutation efficiency of *Cul1a* and *Cul1b* was 79.6% and 60.8%, respectively (Fig. 2-8B, C). Taken together, miR-223 negatively regulates the canonical NF-κB signaling through suppressing the expression of *Cul1a*, *Cul1b*, *Traf6*, and *Tab1*.

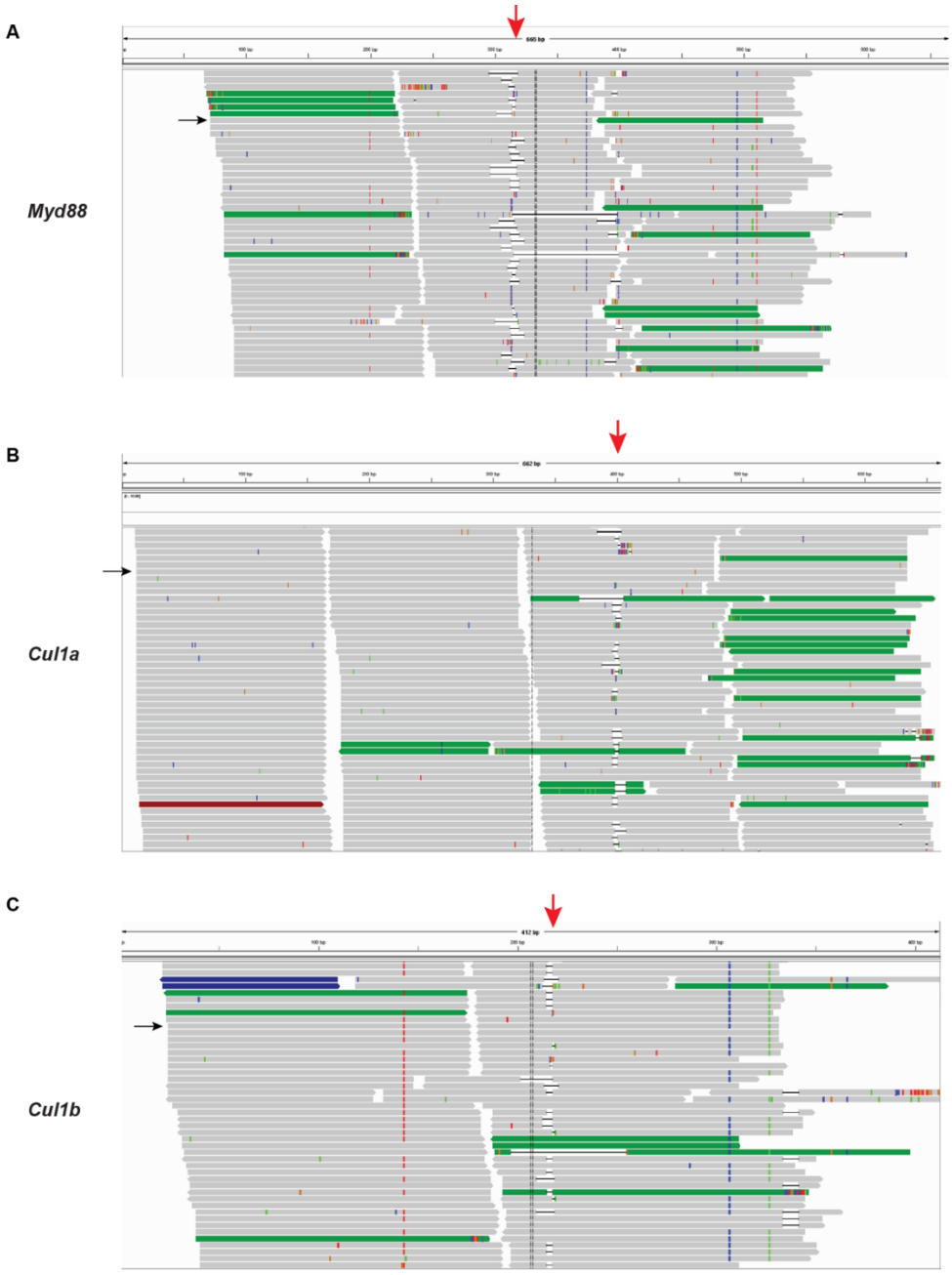

Figure 2-8. Mutation efficiency of transient knock out of *Myd88*, *Cul1a*, and *Cul1b* with the CRISPR/Cas system.

The gene locus targeted by sgRNAs was amplified by PCR and sequenced by next-generation sequencing from embryos injected with sgRNAs and Cas9 protein. (A-C) Representative images showing the alignment of individual reads to the reference sequence of indicating gene by Integrative Genomics Viewer. Red arrow represents one locus of the gene targeted by sgRNAs. Black arrow presents a read with wild-type sequence of the gene.

Loss of miR-223 elevates NF-κB activation in basal epithelial cells

To determine the dynamics of the NF-κB activation, we utilized a NF-κB reporter line *Tg(NFκB:GFP),* where GFP transcription is controlled by NF-κB recognition sequences (Kanther et al., 2011). *miR-223*$^{-/-}$ embryos displayed elevated GFP signal in the tail fin at steady state, as well as at the wound margin at 6 hpw (Fig. 2-9A, B and Video 2), which is consistent with our microarray results (Fig. 2-10). As expected, the NF-κB inhibitor BAY, significantly down regulated GFP expression at the wound (Fig. 2-9C). Interestingly, the GFP^{+} cells in the fin were immobile with an epithelium-like morphology (Fig. 2-9D). The tailfin epithelium in zebrafish larva is composed of one apical layer and one basal layer. With immunofluorescence, we discovered that the GFP signal was restricted to the Tp63 (Lee and Kimelman, 2002) positive basal layer (Fig. 2-9E). Collectively, the NF-κB pathway was elevated in basal epithelial cells in *miR-223*$^{-/-}$ embryos.

miR-223 suppresses NF-κB activation in basal epithelial cells in a phagocytes-dependent and -independent fashion

Since miR-223 is highly expressed in phagocytes, we then sought to determine whether the elevated wound signal is a result of hyperactive phagocytes. Morpholinos that disrupt macrophages development (*Pu.1*) (Rhodes et al., 2005) and inhibit neutrophil and macrophage motility (*Rac2)* (Deng et al., 2011; Rosowski et al., 2016b) were used to remove all phagocytes at the wound margin (Fig. 2-9F). The elevated NF-κB signal in wounded epithelial cells was partially inhibited in the phagocyte-deficient *miR-223*$^{-/-}$ embryos (Fig. 2-9G), suggesting both intra- and extra-phagocyte regulation.

Furthermore, the elevated NF-κB signal in unwounded fin was not affected by phagocytes (Fig. 2-11), suggesting a surprising possibility that miR-223 directly regulates the NF-κB pathway in epithelial cells, whereas no, or very low, expression of miR-223 in epithelial cells was reported. Thus, whether miR-223 is expressed in the epithelium was determined. Neutrophils, macrophages, and basal epithelial cells were sorted from the 3 dpf embryos. The quality of cell sorting was validated by RT-PCR using lineage specific markers (Fig. 2-12A). Mature miR-223 was enriched 2-fold in basal epithelial cells compared with the whole embryo (Fig. 2-12B).

Figure 2-9. NF-κB pathway is elevated in basal epithelial cells in *miR-223*$^{-/-}$ embryos.

The NF-κB reporter line *Tg(NF-κB:GFP)* was crossed into the *miR-223*$^{-/-}$ and matched WT background. (A, B) Representative images and quantification of GFP signal. Mean fluorescence intensity (MFI) in the yellow square (A) in unwounded embryos or at the wound edge at 6 hpw was quantified. White arrows: neuromast cells constitutively expressing NF-κB signal. (C) Quantification of GFP signal at the wound edge at 6 hpw in *miR-223*$^{-/-}$ embryos treated with DMSO or BAY. (D) Representative confocal image of GFP^{+} cells in *miR-223*$^{-/-}$ embryos. (E) Immunofluorescence of GFP and Tp63 (basal cell marker) in *Tg(miR-223*$^{-/-}$*, NF-κB:GFP)* embryos. Nucleus were stained with DAPI. Representative confocal images of vertical view are shown in E. (F, G) Embryos from WT and *miR-223*$^{-/-}$ were injected with *Pu.1* (200 μM) and *Rac2* (100 μM) mopholinos. (F). Representative images showing the efficiency of the two morpholinos. Yellow arrowhead: macrophage; white arrowhead: neutrophils. (G) Quantification of GFP signal at the wound edge at 6 hpw in WT and *miR-223*$^{-/-}$ embryos. Scale bars, 100 μm (in A, F), or 20 μm (in D, E). Data are representative of three independent experiments. ** $P < 0.01$ and **** $P < 0.0001$, unpaired student *t*-test (B, C), or two-way ANOVA (G).

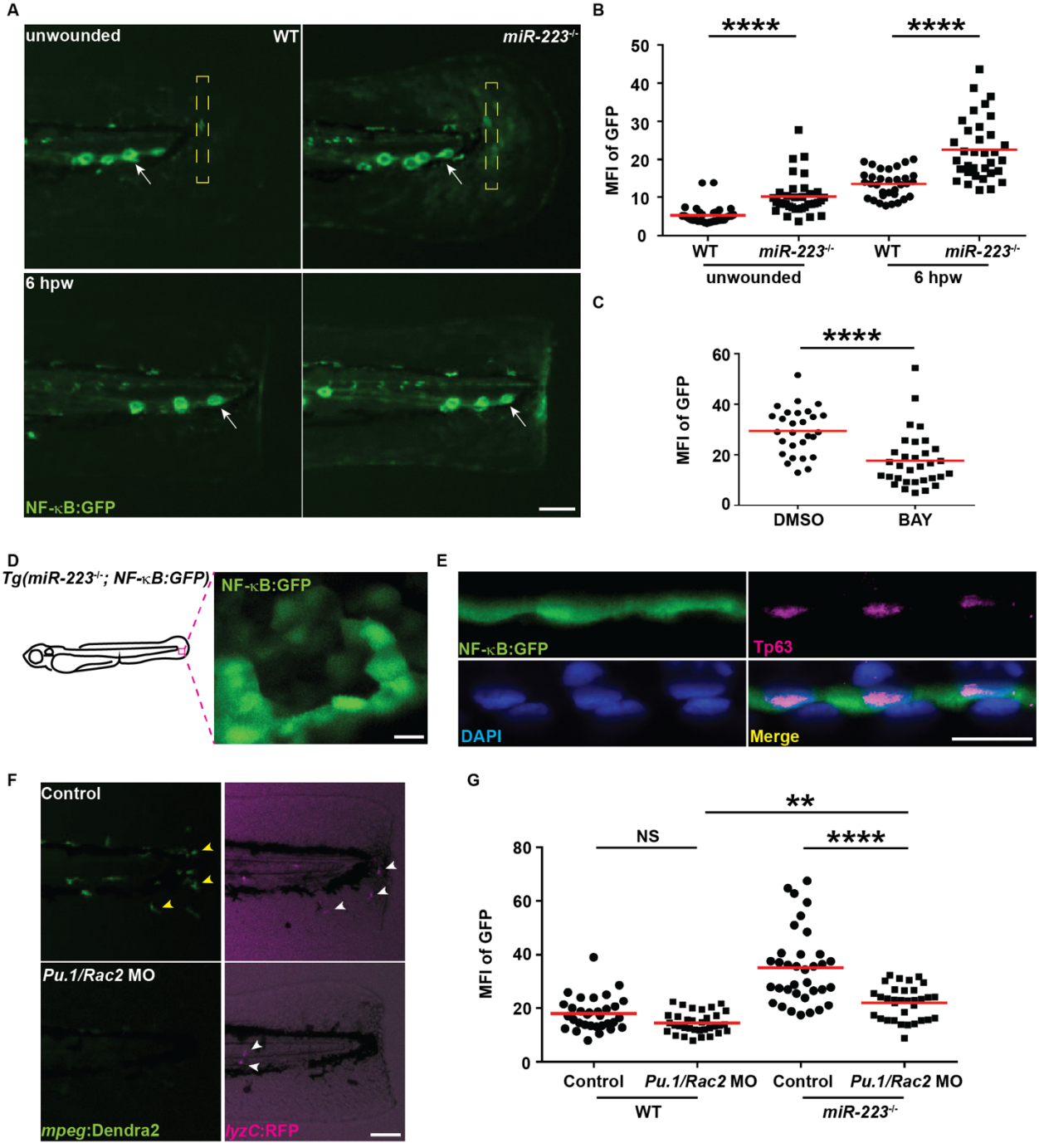
A
unwounded
WT
miR-223-/-
6 hpw
NF-κB:GFP
B
****
****
MFI of GFP
50
40
30
20
10
0
WT
miR-223-/-
WT
miR-223-/-
unwounded
6 hpw
C
****
MFI of GFP
60
40
20
0
DMSO
BAY
D
Tg(miR-223-/-; NF-κB:GFP)
NF-κB:GFP
E
NF-κB:GFP
Tp63
DAPI
Merge
F
Control
Pu.1/Rac2 MO
mpeg:Dendra2
lyzC:RFP
G
**
NS
****
MFI of GFP
80
60
40
20
0
Control
Pu.1/Rac2 MO
Control
Pu.1/Rac2 MO
WT
miR-223-/-

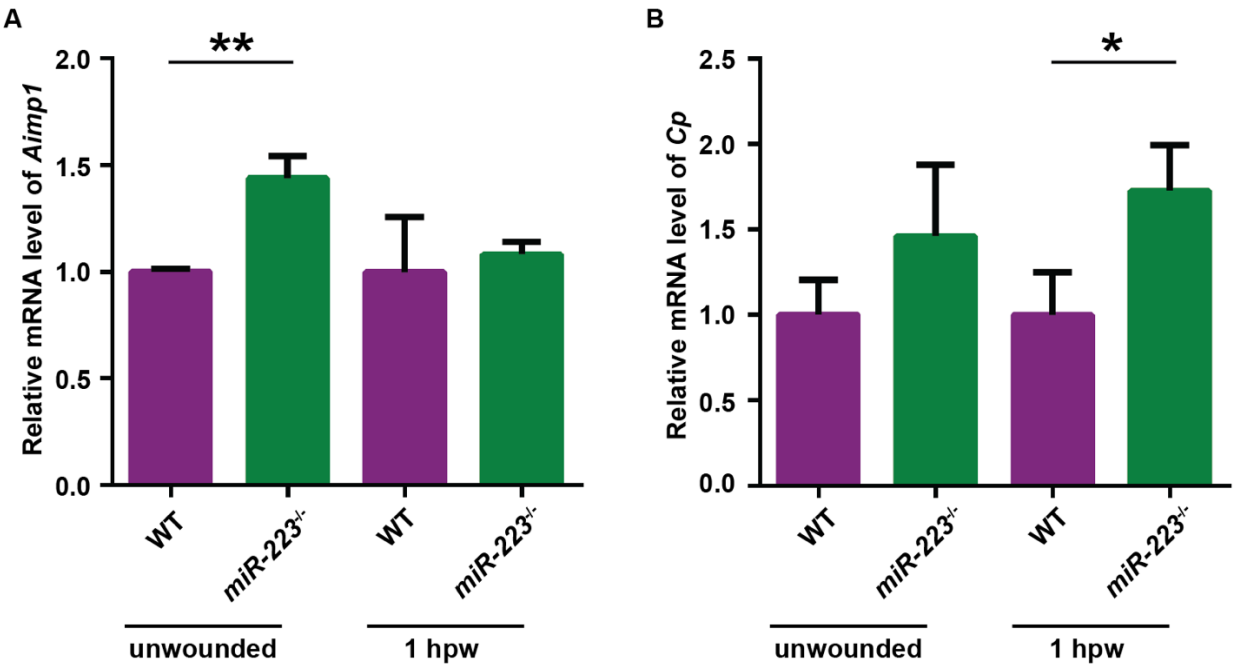

Figure 2-10. NF-κB related genes are upregulated in unwounded embryos and at 1 hpw.

(A, B) Relative expression of indicated genes was measured by RT-qPCR before wounding and at 1 hpw in WT and *miR-223*$^{-/-}$ embryos. Data are pooled from three independent experiments (mean and s.d.). * $P < 0.05$ and ** $P < 0.01$, unpaired student *t*-test.

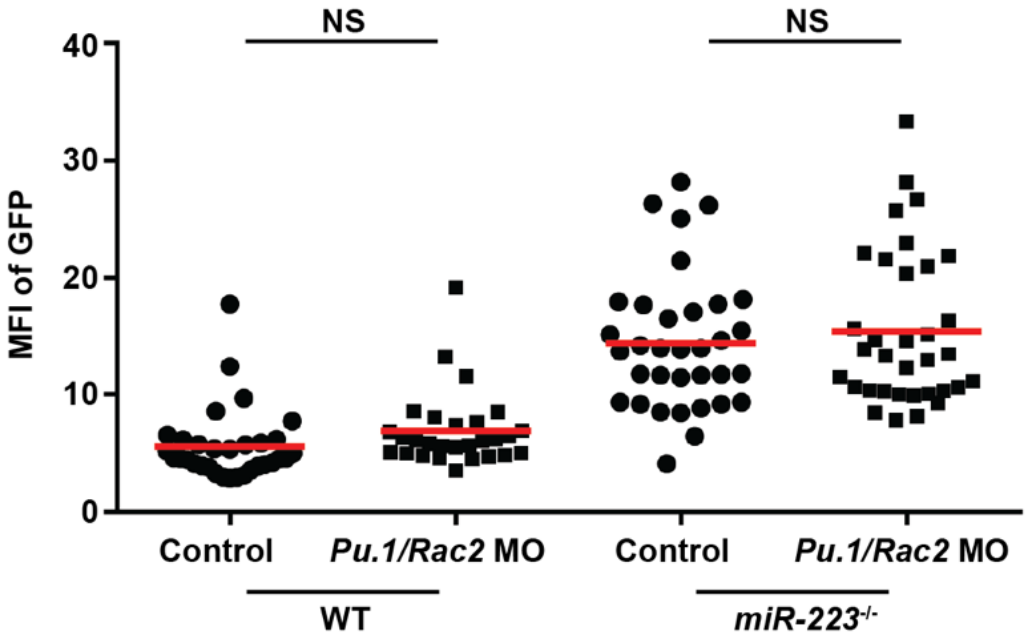

Figure 2-11. Phagocytes do not regulate NF-κB activation in uninjured zebrafish tail fin.

Quantification of NF-κB signal in the tail in unwounded WT and *miR-223*$^{-/-}$ embryos. Data are representative of three independent experiments. NS, $P > 0.05$, unpaired student *t*-test.

To demonstrate that basal epithelium-intrinsic miR-223 regulates the NF-κB pathway, an *RFP-miR-223 sponge* mRNA was injected into embryos at the 4-cell stage. It was previously reported that injecting mRNAs at the 4-8-cell stage led to mosaic expression predominantly in basal epithelial cells (Gault et al., 2014) and the same observation was confirmed using *Tdtomato-CAAX* mRNA (Fig. 2-12C). When the RFP-miR-223 sponge mRNA was delivered this way, its expression was also restricted to the close proximity to the apical layer (Fig. 2-12D). Embryos expressing the RFP-miR-223 sponge had elevated NF-κB signals at the wound edge and enhanced neutrophil wound response at 6 hpw, compared to embryos receiving the RFP control (Fig. 2-12E, F and G). To further validate that miR-223 down regulates the target gene expression in basal epithelial cells, transcripts associated with the ribosomes in the basal epithelium were isolated. We have optimized the published protocol (Heiman et al., 2014) such that no contamination from the phagocytes were detected (Fig. 2-12H). The translation of *Cul1a/b*, *Traf6*, and *Tab1,* but not *Cxcl8* was indeed enhanced in the miR-223 deficient larvae after wounding (Fig. 2-12I). Therefore, miR-223 in basal epithelial cells regulates neutrophilic inflammation and the NF-κB pathway in a cell autonomous manner.

To be noted, apical epithelial cells also contain modest, yet detectable levels of miR-223 (Fig. 2-13A and B). Therefore a transgenic line that expresses the miR-223 sponge specifically in apical epithelial cells, *Tg(krt4: RFP-miR-223 sponge)*^{pu12} was generated, in which a significantly enhanced recruitment of neutrophils was also observed (Fig. 2-13C). Interestingly, the NF-κB signal was not present in the apical epithelial cells, but again was restricted to the basal cells, although not significantly elevated (Fig. 2-13D,E and F), suggesting that miR-223 in the apical layer regulates neutrophil recruitment in a way separable from the NF-κB activation in the basal layer.

Furthermore, accelerated tailfin regeneration was observed in miR-223 deficient larvae, especially at 72 hpw and 96 hpw (Fig. 2-13G and H), possibly due to enhanced NF-κB activation which is known to promote cell proliferation (Brantley et al., 2001). This result further supports that miR-223 regulates physiological processes in epithelial cells.

Figure 2-12. miR-223 suppresses NF-κB activation in basal epithelial cells in a cell-intrinsic manner.

(A, B) Macrophages, neutrophils and basal epithelial cells were sorted from 3 dpf embryos. (A) RT-PCR of lineage specific markers. *mpeg*: macrophage marker; *mpx*: neutrophil marker*;* t*p63*: basal epithelial cell marker; *myoD*: muscle cell marker; *ef1a*: loading control. WE: whole embryo. NTC: non-template control. (B) Quantitative RT-PCR of miR-223. (C) *Tdtomato-CAAX* mRNA was injected into *Tg(krt4: GFP)*^{pu11} embryos at 4-cell stage. Representative confocal images from the lateral view of 3 dpf larvae are shown. (D) *RFP-miR-223 sponge* mRNA was injected into *Tg(krt4: GFP)*^{pu11} embryos at 4-cell stage. A representative confocal image from the vertical view of 2 dpf larvae is shown. (E, F) *Tg(NF-κB:GFP)* were injected with *miR-223* sponge or the RFP control mRNA at 4-cell stage. Representative images and quantification of GFP signal at the wound edge at 6 hpw are shown. (G) Quantification of neutrophil recruitment to the wound in embryos injected with *miR-223* sponge or *RFP* mRNA at 4-cell stage. (H, I) Tol2-*tp63*-GFP-L10a was injected into WT or *miR-223*$^{-/-}$ embryos. At 3 dpf, cell specific mRNA-ribosome complexes were isolated by anti-GFP antibodies at 1 hpw. (H) RT- PCR of lineage specific markers as described in A. (I) RT-qPCR of indicated genes. Data are pooled from three independent experiments (mean + s.d.). Scale bars, 20 um (in C, D) or 100 μm (in E). Data are representative of three independent experiments (F, G) or of two independent experiments (A, B). * $P < 0.05$, ** $P < 0.01$, and **** $P < 0.0001$, unpaired student *t*-test.

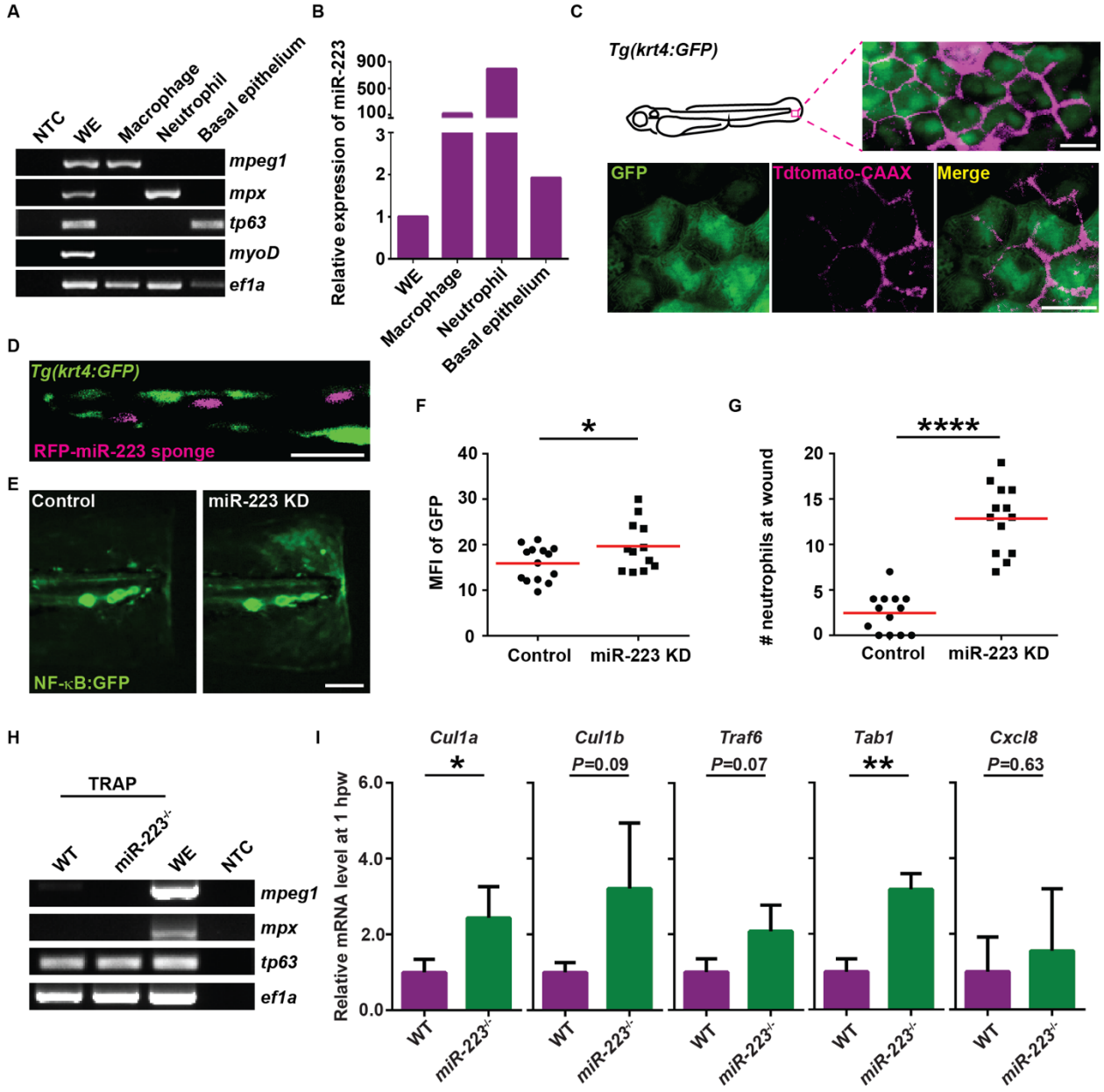
A
NTC
WE
Macrophage
Neutrophil
Basal epithelium
mpeg1
mpx
tp63
myoD
ef1a
B
Relative expression of miR-223
900
500
100
3
2
1
0
WE
Macrophage
Neutrophil
Basal epithelium
C
Tg(krt4:GFP)
GFP
Tdtomato-CAAX
Merge
D
Tg(krt4:GFP)
RFP-miR-223 sponge
E
Control
miR-223 KD
NF-κB:GFP
F
*
MFI of GFP
40
30
20
10
0
Control
miR-223 KD
G
****
neutrophils at wound
20
15
10
5
0
Control
miR-223 KD
H
TRAP
WT
miR-223-/-
WE
NTC
mpeg1
mpx
tp63
ef1a
I
Cul1a
*
Cul1b
P=0.09
Traf6
P=0.07
Tab1
**
Cxcl8
P=0.63
Relative mRNA level at 1 hpw
6.0
4.0
2.0
0.0
WT
miR-223-/-

Figure 2-13. Fin regeneration is accelerated in miR-223 deficient embryos.

(A) Apical epithelial cell were sorted from the *Tg(krt4:GFP)*^{pu11} and RT-PCR of lineage specific markers were performed as described in Fig 5A, *krt4*: apical epithelial cell marker. (B) RT-qPCR of miR-223. (C) Quantification of neutrophil recruitment at 6 hpw in embryos from *Tg(krt4: RFP-miR-223 sponge)*^{pu12} *and Tg(krt4: RFP)*^{pu13}. (D, E) *Tg(krt4: RFP-miR-223 sponge)*^{pu12} *and Tg(krt4: RFP)*^{pu13} were crossed with *Tg(NF-κB:GFP).* Representative images and quantification of GFP signal at the wound edge at 6 hpw. (F) Representative confocal images of embryos from *Tg(NF-κB:GFP/krt4: RFP-miR-223 sponge)*^{pu12} at 6 hpw. (G, H) Tailfin regeneration in WT and miR-223$^{-/-}$ embryos. Tailfin transection was performed at 3 dpf. The length of regenerated tailfin was measured as the distance between the blue and yellow dash lines. (G) Representative images of tailfins at indicated time points. (H) Quantification of the length of tailfin at different time points (n>20 in each group). Scale bars, 100 μm (in D, G) or 20 um (in F). Data are representative of three independent experiments (C, E, H) or of two independent experiments (A, B). * $P < 0.05$, ** $P < 0.01$, and **** $P < 0.0001$, unpaired student *t*-test.

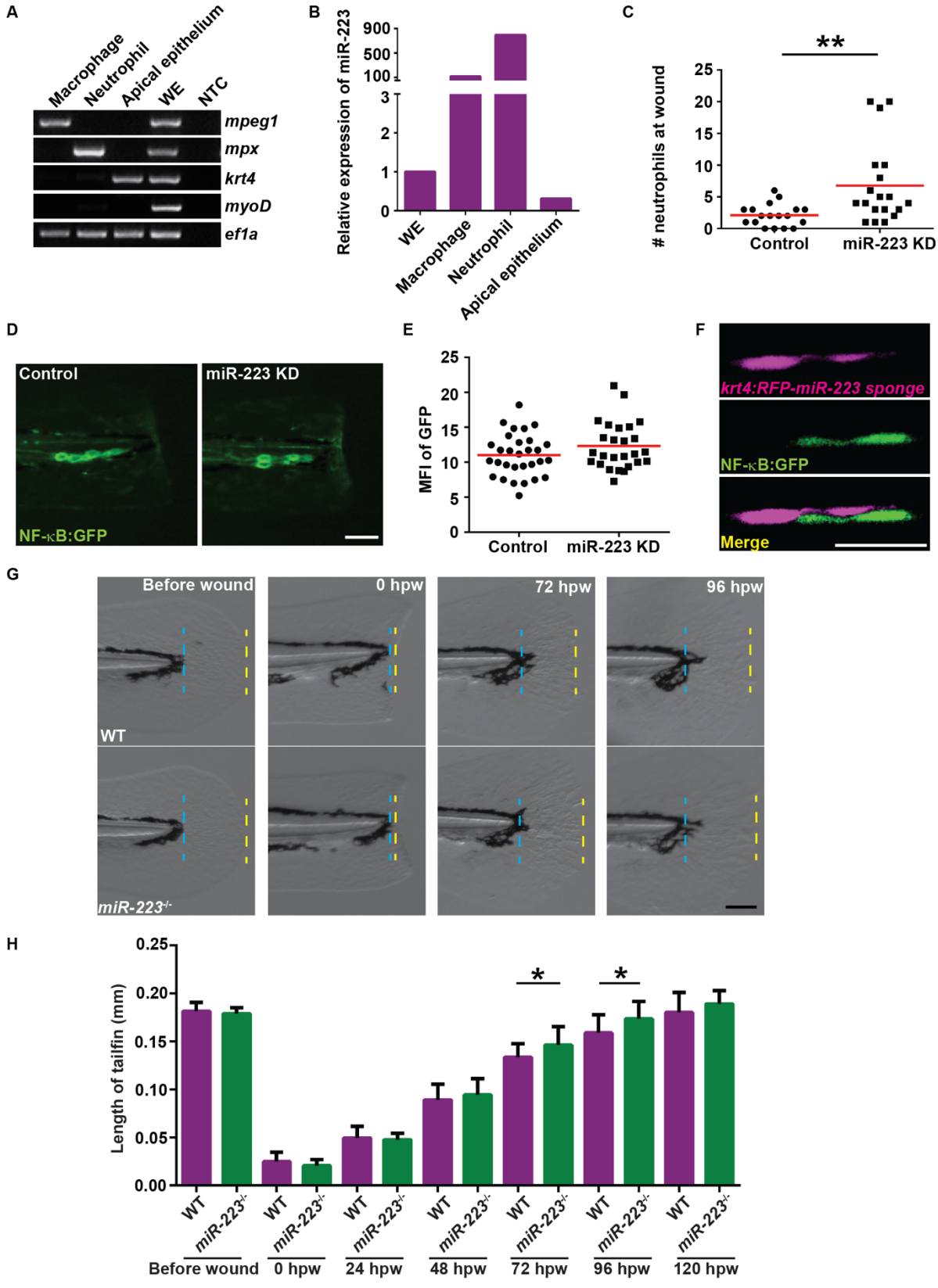
A
Macrophage
Neutrophil
Apical epithelium
WE
NTC
mpeg1
mpx
krt4
myoD
ef1a
B
Relative expression of miR-223
900
500
100
3
2
1
0
WE
Macrophage
Neutrophil
Apical epithelium
C
**
neutrophils at wound
25
20
15
10
5
0
Control
miR-223 KD
D
Control
miR-223 KD
NF-κB:GFP
E
MFI of GFP
25
20
15
10
5
0
Control
miR-223 KD
F
krt4:RFP-miR-223 sponge
NF-κB:GFP
Merge
G
Before wound
0 hpw
72 hpw
96 hpw
WT
miR-223-/-
H
Length of tailfin (mm)
0.25
0.20
0.15
0.10
0.05
0.00
*
*
WT
miR-223-/-
Before wound
0 hpw
24 hpw
48 hpw
72 hpw
96 hpw
120 hpw

miR-223 regulates NF-κB pathway in human bronchial epithelial cells

Zebrafish skin is a suitable model for human mucosal epithelium (Enyedi et al., 2016). To extend our findings to humans, the expression of miR-223 was evaluated in human cells. Indeed, we detected miR-223 in the immortalized human bronchial epithelial cells (HBECs), but not in the human embryonic kidney 293 cells (HEK293T). MiR-223 expression was further elevated in the H441 human lung cancer cell line (Fig. 2-14A). Moreover, human *CUL1* and *TAB2* were bioinformatically identified as potential targets of miR-223, which was further confirmed in luciferase reporter assays (Fig. 2-14B). Additionally, overexpression of miR-223 in HEK293T cells suppressed NF-κB activation with or without stimulation using heat-killed *P. aeruginosa*. In HBECs, miR-223 over expression suppressed, whereas its inhibition enhanced the activation of NF-κB after *P. aeruginosa* stimulation (Fig. 2-14C). Together, our results indicated that miR-223 regulates NF-κB pathway in human cells.

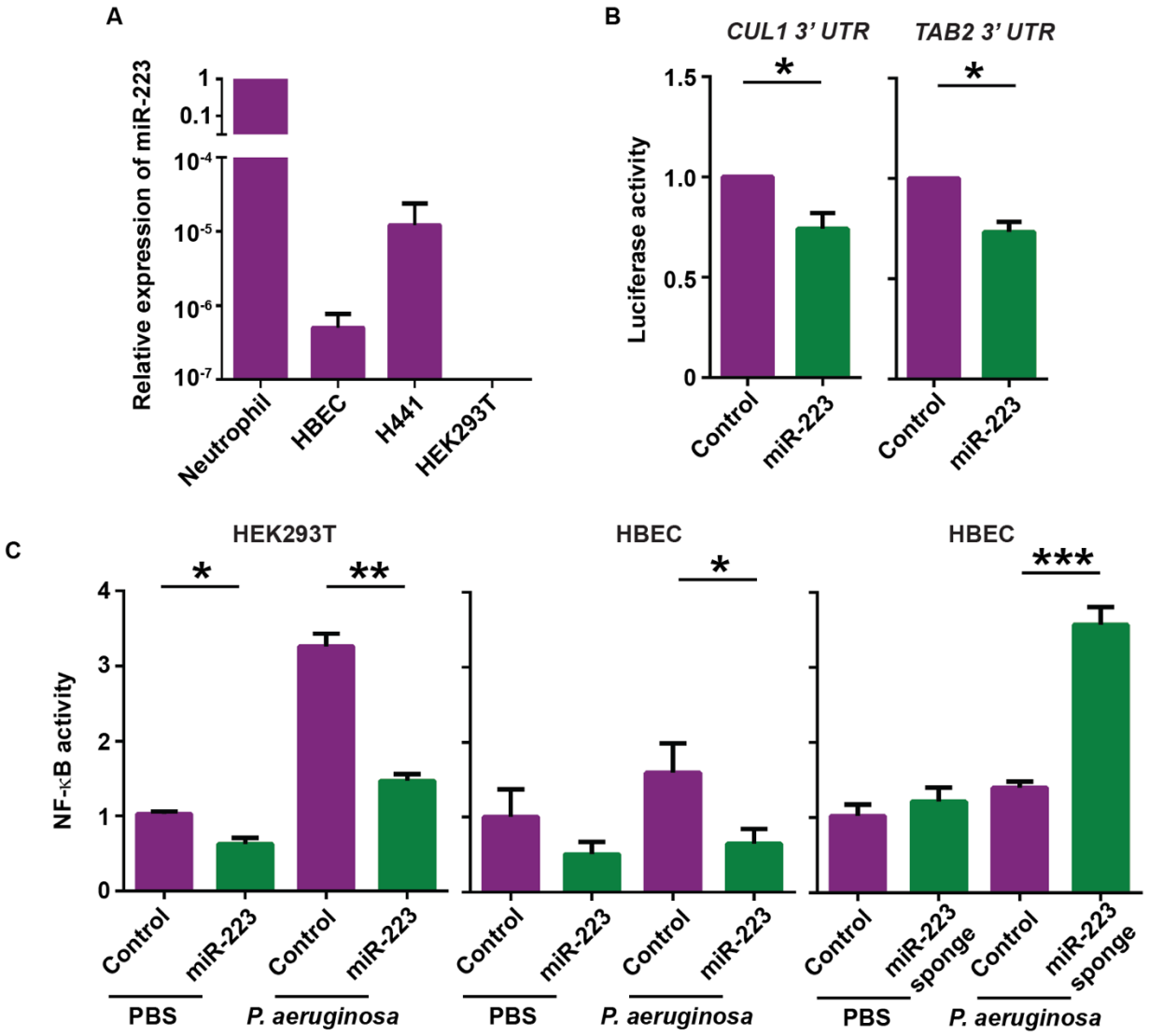

Figure 2-14. miR-223 regulates NF-κB activation in human bronchial epithelial cells.

(A) RT-qPCR of miR-223 expression in human neutrophils, human immortalized bronchial epithelial cells (HBEC), transformed lung cancer epithelial cells (H441) and HEK293T. (B) Dual luciferase reporter assay showing specific suppression of Renilla luciferase dependent on 3'UTRs of human *CUL1* and *TAB2* by miR-223. (C) NF-κB activity in HEK293T cells expressing miR-223 or control with or without *P. aeruginosa* stimulation. NF-κB activity in HBEC cells expressing miR-223/control or miR-223-sponge/control with or without *P. aeruginosa* stimulation. Data are pooled from three independent experiments (mean ± s.d.). * $P < 0.05$, unpaired student *t*-test in A, C, and D and paired student *t*-test in B.

Discussion

Here we have reported that miR-233 regulates distinct signaling pathways in multiple tissues that coordinate the resolution of neutrophilic inflammation (Fig. 2-15). In basal epithelial cells, miR-223 suppresses canonical NF-κB signaling by directly targeting multiple components in the signaling cascades. Phagocytes also contributes to suppress basal cell NF-κB activation during inflammation. In the apical epithelium, miR-223 promotes the resolution of neutrophilic inflammation in a separate mechanism. Our observation is in line with the seminal work performed by McDonald *et al* that complex overlapping chemokines and lipid mediators, produced by the phagocytes and injured tissue coordinate to recruit neutrophils to a sterile injury (McDonald et al., 2010).

The most surprising observation is that miR-223 modulates the inflammatory signaling, visualized by the NF-κB reporter, primarily in epithelial cells in a cell intrinsic manner. This phenomenon is in line with the report that the reactive oxygen species, which are essential for neutrophil wound response, are primarily restricted to the injured epithelium (Niethammer et al., 2009), whereas the phagocytes were not the primary source as previously speculated. Neutrophils are recruited to tissue injury sites by a hierarchical system of chemoattractive signals. Other signaling molecules possibly produced by the injured epithelium are the metalloproteases, such as mmp9 (LeBert et al., 2015) and mmp13 (Lisse et al., 2016), as well as ATP and proinflammatory lipid mediators, released as a consequence of osmotic swelling of the epithelial cells and their nucleus (Enyedi et al., 2016; Gault et al., 2014). In addition, the formyl-peptide signals produced by injured hepatocytes recruits neutrophils to the necrotic core in mice (McDonald et al., 2010). It remains to be determined how these signals are modulated by miR-223 and the related NF-κB pathway. It remains to be determined whether neutrophil maturation is also regulated by the function of miR-223 outside the phagocytes. Neutrophils in miR-223 knock out mice are hypermature and hyperactive (Johnnidis et al., 2008), however the mechanism is not clear.

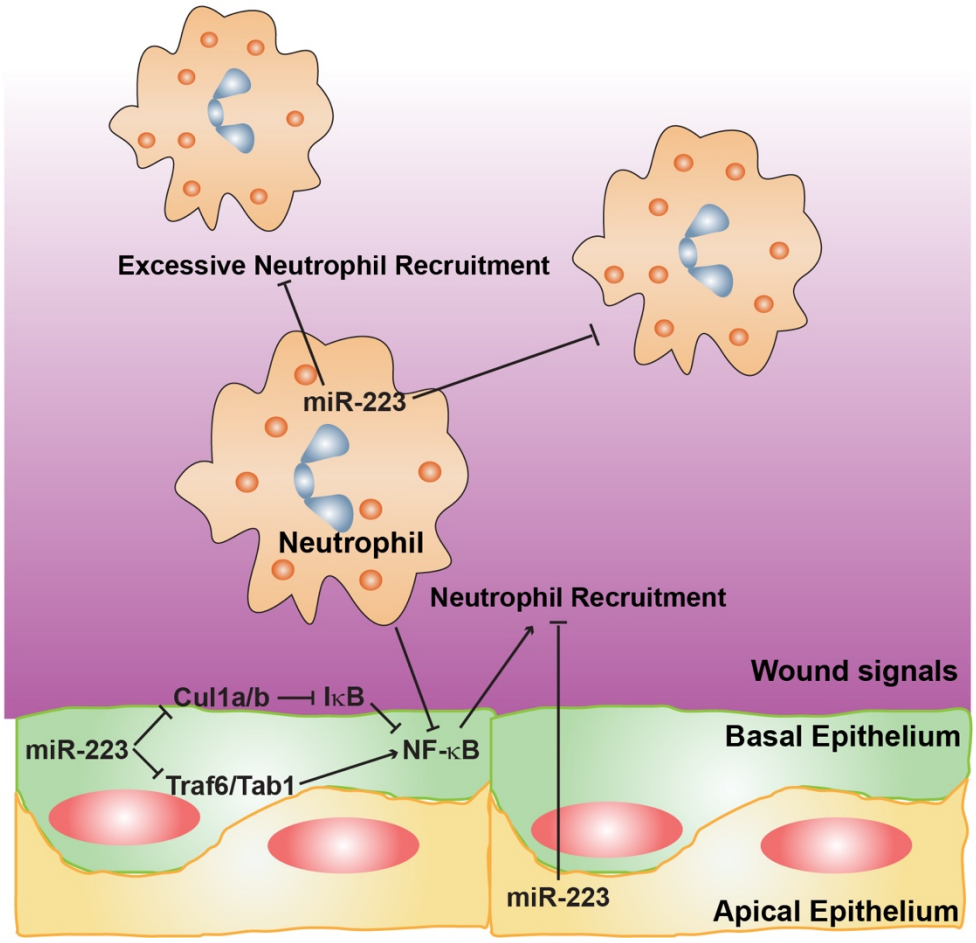

Figure 2-15. Proposed model of miR-223 in regulating neutrophilic inflammation.

Indeed, the importance of epithelial cells in inflammation is increasingly recognized. A good example is that epidermal cells utilize fatty acid β-oxidation, which again was previously investigated in immune cells, to fuel the production of matrix metalloproteinase and coordinated the immune response during cutaneous inflammation (Hall et al., 2014). Since the expression level of miR-223 changes under many disease conditions, further animal or human work is still needed to elucidate the physiological significance of miR-223-NF-κB in various disease conditions. It is speculated that zebrafish skin is a good model for human mucosal epithelium (Enyedi et al., 2016). Here we detected the presence of miR-223 in human bronchial epithelial cells, cells in the lower respiratory track that are critical for asthma pathogenesis (Erle and Sheppard, 2014). In line with our observation, miR-223 is upregulated in both bronchial and alveolar epithelial cells upon LPS challenge in mice (Sugatani and Hruska, 2007). In addition, a recent study (Maes et al., 2016) reported a significant up-regulation of miR-223 in sputum of patients with severe neutrophilic asthma, supporting a physiological role of miR-223 in mucosal epithelial cells.

Our result also indicates a neutrophil-intrinsic role of miR-223 in regulating neutrophil recruitment, which is consistent with the previous observation that miR-223 regulates neutrophil recruitment in a blood cell intrinsic manner (Dorhoi et al., 2013). Neutrophils isolated from miR-223 deficient mice produce more Cxcl2, and Ccl3 upon *Mycobacterial* infection. Cxcl2 is a neutrophil chemoattractant. Ccl3 stimulates neutrophils to produce proinflammatory mediates such as platelet-activation factor and lipid leukotriene B4 (LTB4) to recruit other neutrophils (Reichel et al., 2009). In an elegant study, Lämmermann *et al* have shown that neutrophils secret LTB4 in exosomes to amplify the range of neutrophil recruitment during neutrophil swarming (Lammermann et al., 2013; Majumdar et al., 2016).

Here we visualized that miR-223 deficient phagocytes also have a direct impact on the injured epithelium. Many molecules produced by the phagocytes, including reactive oxygen species, granule enzymes, inflammatory mediates, and neutrophil extracellular traps can lead to further tissue damage and amplifies inflammation. Many of these molecules are regulated by the NF-κB transcription factor, or are direct miR-223 targets in human neutrophils such as the cysteine proteases cathepsin L and Z (Baek et al., 2008). It is also possible that activated phagocytes deliver additional miR-223 into the epithelium via exosomes or microvesicles, as demonstrated recently in mice (Neudecker et al., 2017). Inhibiting the Cxcl8 receptor Cxcr2 or the high affinity LTB4

receptor Ltb4r1 did not reduce neutrophil recruitment in the miR-223 knockout (data not shown). It is likely that miR-223 regulates redundant or other inflammatory signals to coordinate neutrophil recruitment. Further work is required to fully dissect the mechanism.

The adaptor protein Myd88 was detected as a suppressor to the over-inflammation induced by miR-223 deficiency. Both the TLRs and the IL-1/18 receptor can activate the canonical NF-kB signaling through Myd88. Due to the poor characterization of the zebrafish IL-1/18 pathway and the high functional redundancy of the TLRs (Li et al., 2017; Sepulcre et al., 2009), it is difficult at present to pinpoint the receptor(s) that activates the NF-κB pathway during tissue injury. The nuclear factor NF-κB plays a complex role in inflammation and cancer (Hoesel and Schmid, 2013; Lawrence, 2009). On one hand, it promotes inflammation by producing pro-inflammatory cytokines and chemokines. On the other hand, it resolves inflammation by promoting leukocytes apoptosis, the production of anti-inflammatory cytokines and survival of somatic tissue under stress. Despite the vast number of predicted and validated miR-223 targets, here we report that miR-223 directly targets four different components in the canonical NF-κB pathway in zebrafish and human, providing a significant advance in miR-223 biology. In human cells, besides *CUL1* and *TAB2* (Fig. 6), *TRAF6* and *TAB1* also harbor miR-223 binding sites in their longest splice variants. Furthermore, miR-223 can suppress IKKα, downregulating the alternative NF-κB pathway (Li et al., 2010). Together, miR-223 possibly regulates the NF-κB activation differentially in various tissues, as disease progress, as a result of alternative splicing, or balancing the canonical and the alternative pathways. In light of the complexed biological function of the NF-κB pathway, our work provides a mechanistic understanding of the multifaceted and multilayered role of miR-223 in inflammatory diseases and cancer.

CHAPTER 3. NEUTROPHIL-SPECIFIC KNOCKOUT DEMONSTRATES A ROLE FOR MITOCHONDRIA IN REGULATING NEUTROPHIL MOTILITY IN ZEBRAFISH

Abstract

Neutrophils are fast moving cells essential for host immune functions. Although they primarily rely on glycolysis for ATP, isolated primary human neutrophils depend on mitochondrial membrane potential for chemotaxis. Whether mitochondria regulate neutrophil motility in vivo, however, and the underlying molecular mechanisms remain obscure. Here, we visualized mitochondria in an interconnected network that localizes to the front and rear of migrating neutrophils using a novel transgenic zebrafish line. To disrupt mitochondrial function genetically, we established a gateway system harboring the CRISPR/Cas9 elements for tissue-specific knockout. In a transgenic line, neutrophil-specific disruption of mitochondrial DNA polymerase, *polg*, significantly reduced the velocity of neutrophil interstitial migration. In addition, inhibiting the mitochondrial electron transport chain or the enzymes that reduce mitochondrial reactive oxygen species also inhibited neutrophil motility. In addition, the reduced cell motility resulted from neutrophil-specific knockout of *sod1* was rescued with *sod1* mRNA overexpression or treating with scavengers of reactive oxygen species. Together, our work has provided the first in vivo evidence that mitochondria regulate neutrophil motility, tools for the functional characterization of mitochondria related genes in neutrophils, and insights into immune deficiency seen in patients with primary mitochondrial disorders.

Introduction

Cell motility, crucial for development, immunity, wound healing and cancer metastasis, is central to homeostasis in both health and disease. Mitochondria are the powerhouse for energy production and integrated regulators for cell signaling, modulating intracellular calcium concentration and apoptosis, producing metabolic intermediates and reactive oxygen species (ROS). Polarized localization of mitochondria is observed in isolated cancer cells and lymphocytes in culture and is thought to drive cell migration, presumably by localized ATP production (Bao et al., 2015; Campello et al., 2006; Desai et al., 2013). In addition, mitochondria regulate redox and calcium signals that are also relevant to cell migration.

Neutrophils are fast moving cells and the first line of defense against invading pathogens. Polarized localization of the actin cytoskeleton and intracellular signaling molecules is essential for neutrophil motility, chemotaxis and immune functions. Regarding the energy source required for neutrophil function, the Warburg effect has long been appreciated that neutrophils utilize glycolysis in oxygenated environment for ATP production (Maianski et al., 2004; Warburg, 1956). Isolated primary human neutrophils have a partially dysfunctional mitochondrial network with low expression of electron transport chain components, low rates of respiration and ATP production, and yet are able to maintain mitochondrial membrane potential. Disrupting mitochondria membrane potential or prolonged inhibition of the F0-ATPase inhibited neutrophil chemotaxis in 2D, without inducing cell apoptosis or inhibiting the activation of the respiratory burst or phagocytosis (Bao et al., 2015; Fossati et al., 2003). Of note, disrupting mitochondria membrane potential resulted in a much more profound phenotype than inhibiting the F0-ATPase activity alone (Fossati et al., 2003), suggesting that mitochondria possibly also regulate neutrophil chemotaxis via mechanisms other than ATP production. In addition, previous studies were limited by the dependency on pharmacological inhibitors, due to the fact that neutrophils are terminally differentiated and not genetically tractable. Genetic evidences for the importance of mitochondria related pathways in neutrophil chemotaxis are scarce.

It is well accepted that leukocytes in vitro and in tissue display distinct behaviors and may utilize separate signaling mechanisms (Lammermann et al., 2008; Yamahashi et al., 2015). The biological relevance of mitochondria for neutrophil migration in vivo has not been characterized. It is noted that patients with primary mitochondrial disorders are indeed highly susceptible to opportunistic bacterial and fungal infections that are typically controlled by neutrophils (Walker et al., 2014). The lack of an in vivo model significantly hinders the mechanistic characterization of how mitochondria regulate neutrophil function.

Zebrafish are a well-established model to study neutrophil biology (Deng and Huttenlocher, 2012). However, a lack of standard tissue-specific knockdown or knockout technique in the zebrafish field has limited the power of this model organism when studying developmental essential genes, such as those related to mitochondrial function. Recently, a tissue-specific knockout approach has been developed by the Zon group (Ablain et al., 2015). Here, we have further adapted this system

for use in zebrafish neutrophils. We have successfully disrupted mitochondrial DNA polymerase in neutrophils thereby providing the first evidence that the mitochondrial network plays an indispensable role in regulating neutrophil motility in vivo.

Results

Mitochondrial dynamics in migrating neutrophils

Mitochondria are morphologically dynamic organelles that travel along microtubules (Heggeness et al., 1978), and continuously divide and fuse to form small structures or interconnected networks. The localization of mitochondria in a migrating cell provides significant insight into the potential role of mitochondrial network. To observe mitochondrial dynamics in migrating zebrafish neutrophils, we generated a transgenic zebrafish line: *Tg(lyzC:mitoDendra2)*^{pu14}*,* expressing a green fluorescent protein, Dendra2, fused to a mitochondria-localization sequence. Total neutrophil numbers, distribution and motility were comparable with the standard *Tg(lyzC:GFP)* control line (Hall et al., 2007). A spinning disk confocal was used to capture the morphology and localization of the mitochondrial network in the randomly migrating cells in the head mesenchyme of the 3 days post fertilization (dpf) larvae (Lam et al., 2014). Mitochondria primarily formed a tubular structure that localize to the front and rear relative to the nucleus, but not necessarily enter cell protrusions or the uropods (Fig. 3-1). Similar observations were made when a neutrophil reversed the direction during random migration or during neutrophil wound response.

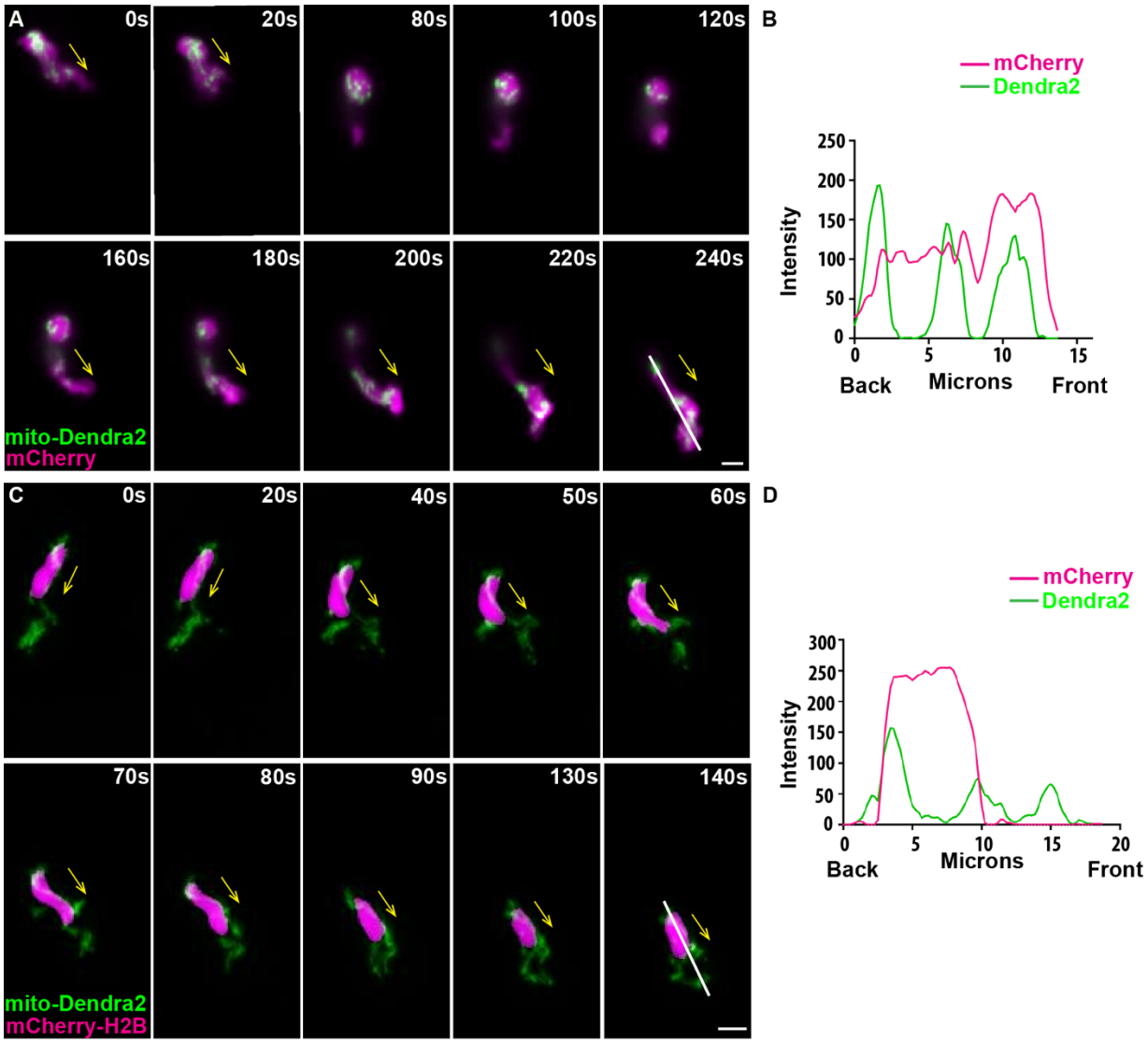

Figure 3-1. Mitochondria localize to both the front and the rear of neutrophils.

A). Random motility of neutrophils in the head mesenchyme of a 3 dpf larvae of *Tg(lyzC:mitoDendra2)*^{p14} crossed with *Tg(lyzC:mCherry)*. C) *Tg(lyzC:mitoDendra2)* ^{pu14} was crossed with *Tg(lyzC:mCherry-H2B)* to visualize mitochondria network relative to the nucleus. Montages of one representative movie out of 8 are shown. B, D) Quantifications of the fluorescence intensity along the indicated line in A or C. Scale bars: 5 µm.

A gateway cloning system for tissue specific knockout

To disrupt mitochondrial function genetically, elements in the CRISPR/Cas9 Vector developed by the Zon group (Ablain et al., 2015) were separately cloned into gateway entry vectors, to facilitate promoter switching and single guide RNA (sgRNA) cloning. Briefly, the p5E vector contains a tissue-specific promoter to restrict the expression of the Cas9 protein. The pME vector contains DNA encoding a Cas9 protein with nuclear localization signals, linked with mCherry via a self-cleaved 2A peptide to label the target cells. The p3E vector contains U6 promoters and a common scaffold to allow transcription of gene specific sgRNAs. An SV40 polyA sequence to stabilize the cas9-2A-mCherry transcript is also in the p3E. Since zebrafish have had a genome duplication event, we designed the p3E to harbor one or two U6-scaffold cassettes to allow simultaneous expression of two sgRNAs for knocking out both paralogues when needed. Two different U6 promoters, U6a and U6c (Yin et al., 2015) were used to reduce the frequency of homologous recombination of repeat sequences. After gateway recombination, a single plasmid is obtained that allows expression of mCherry and Cas9 in the selected tissue and ubiquitous expression of two sgRNAs for tissue specific knockouts (Fig. 3-2A). For control, a longer sequence without predicted binding sites in the zebrafish genome were used, based on the observation that longer sgRNAs have greatly reduced efficiency (Doench et al., 2014) (Fig. 3-2C).

Mitochondrial DNA polymerase regulates neutrophil motility in vivo

The first mitochondria related gene selected for in vivo characterization was *polg*, a nuclear encoded gene that encodes the catalytic subunit of the DNA polymerase gamma, the only DNA polymerase for mitochondrial DNA synthesis. Pathogenic variants of *POLG* cause *POLG*-related disorders, presenting a broad clinical spectrum in human patients (Stumpf et al., 2013). To determine whether *polg* regulates neutrophil motility, a sgRNA against *polg* was selected using CRIPSRScan for neutrophil-specific inhibition (Moreno-Mateos et al., 2015). It targets exon 15 that encodes the Thumb, the catalytic domain, with no predicted off-target sites (Fig. 3-2B, C). A control line, *Tg(lyzC:nls-cas9-2A-mCherry/U6a/c:control sgRNA)*^{pu15} (TS-ctrl) and the transgenic line targeting *polg* in neutrophils, *Tg(lyzC:nls-cas9-2A-mCherry/U6a:polg sgRNA)*^{pu16} (TS-polg), were generated. We obtained 2 founders for each line and the fish were raised to F2 generation. Both lines have similar numbers of neutrophils at 3 dpf. To confirm that *polg* was edited in neutrophils, we isolated the neutrophils from the stable lines and confirmed in vivo editing in the neutrophil DNA from the TS-polg line using the T7E1 mutagenesis detection assay (Fig. 3-2D).

We further deep sequenced this locus and detected an average mutation efficiency of 39.52% in two individually sorted samples with in-frame (46.57%) and out-of-frame (53.43%) mutations resulted from deletions or insertions (Fig. 3-3), likely resulted from non-homologues end joining when DNA double strand breaks caused by CRISPR/Cas9 were repaired (Lindsay et al., 2016). In addition, the relative abundance of the mitochondrial DNA was significantly reduced in neutrophils sorted from the TS-polg line compared with those sorted from the TS-ctrl line (Fig. 3-2E). We then quantified the velocity of neutrophil motility in the head mesenchyme. A significant reduction in the speed was detected in the TS-polg line at both 3 dpf and 5 dpf (Fig. 3-2F,G, Fig. 3-4), indicating that *polg* is required for optimal cell migration.

Figure 3-2. Neutrophil-specific knockout of *polg* reduced neutrophil motility.

A). Schematic of the design of gateway vectors to clone constructs for neutrophil-specific knockout. B) Schematics of the gene structure and protein domains of zebrafish *polg* gene. The sgRNA targets exon 15 in the forward strand. C) Sequences of sgRNAs (control or *polg*) produced using our vectors. Note the first G (blue) is included in the backbone. D,E) Neutrophils were sorted from 3 dpf embryos of *Tg(lyzC:nls-cas9-2A-mCherry/U6a/c:control sgRNA)* ^{pu15} (TS-ctrl) and *Tg(lyzC:nls-cas9-2A-mCherry/U6a:polg sgRNA)* ^{pu16} (TS-polg) lines. D) T7E1 assay was performed to show the in vivo editing of the *polg* locus. E) The ratio of mitochondrial DNA/nuclear DNA content was measured by qPCR in two separate sorts. ****, $P<0.0001$, one-way ANOVA. F) Representative images and G) Quantification of neutrophil motility in the head mesenchyme of 3 dpf larvae. One representative result of three biological repeats was shown. n = 64 for ctrl and n = 76 for polg from 4 different larvae. ****, $P<0.0001$ by Mann-Whitney test. Scale bar: 50 μm.

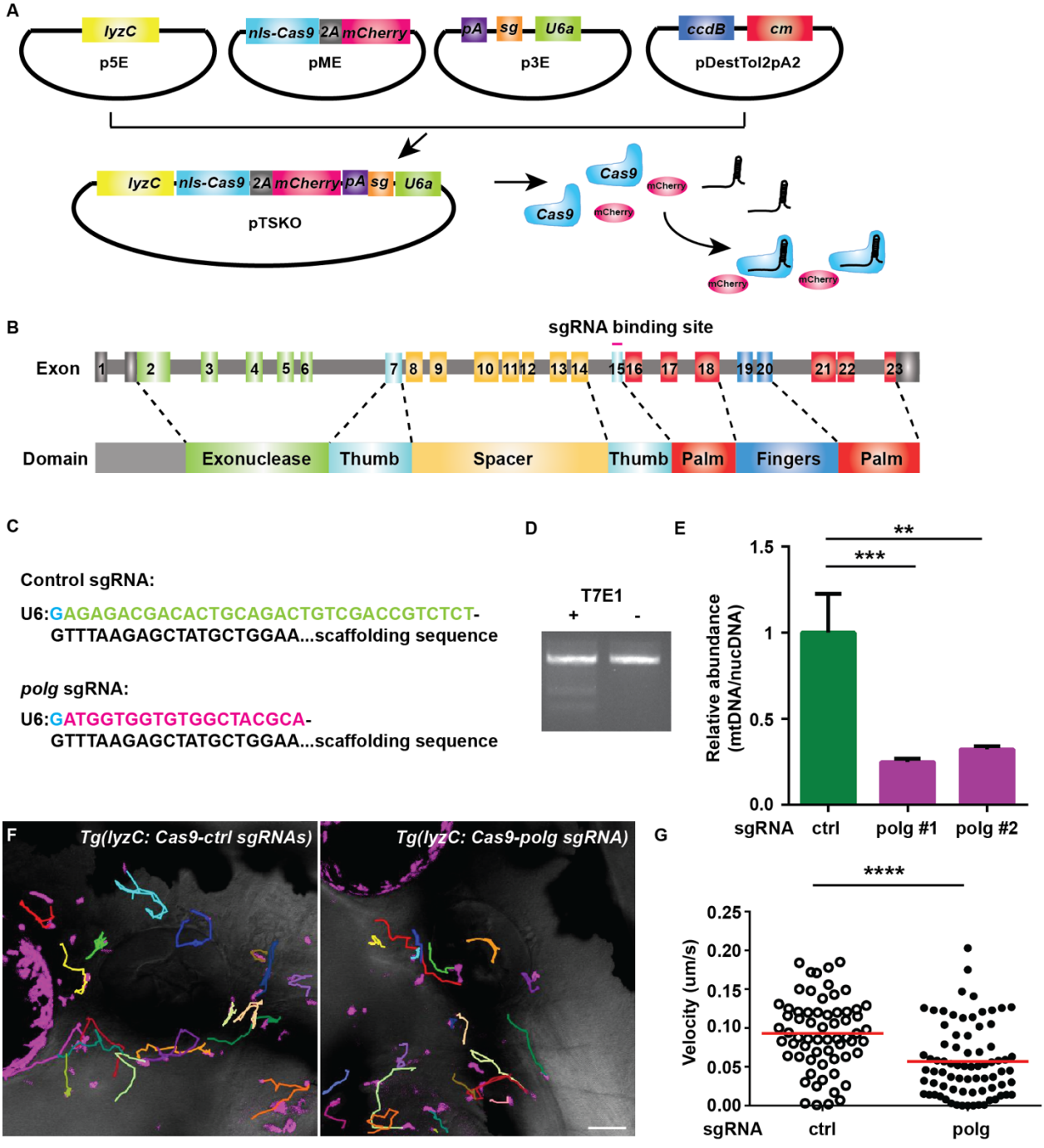
A
lyzC
p5E
nls-Cas9 2A mCherry
pME
pA sg U6a
p3E
ccdB cm
pDestTol2pA2
lyzC nls-Cas9 2A mCherry pA sg U6a
pTSKO
Cas9
mCherry
B
sgRNA binding site
Exon
1 2 3 4 5 6 7 8 9 10 11 12 13 14 15 16 17 18 19 20 21 22 23
Domain
Exonuclease
Thumb
Spacer
Thumb
Palm
Fingers
Palm
C
Control sgRNA:
U6:GAGAGACGACACTGCAGACTGTCGACCGTCTCT-
GTTTAAGAGCTATGCTGGAA...scaffolding sequence
polg sgRNA:
U6:GATGGTGGTGTGGCTACGCA-
GTTTAAGAGCTATGCTGGAA...scaffolding sequence
D
T7E1
+
-
E
**
***
Relative abundance (mtDNA/nucDNA)
1.5
1
0.5
0.0
sgRNA
ctrl
polg #1
polg #2
F
Tg(lyzC: Cas9-ctrl sgRNAs)
Tg(lyzC: Cas9-polg sgRNA)
G
****
Velocity (um/s)
0.25
0.20
0.15
0.10
0.05
0.00
sgRNA
ctrl
polg

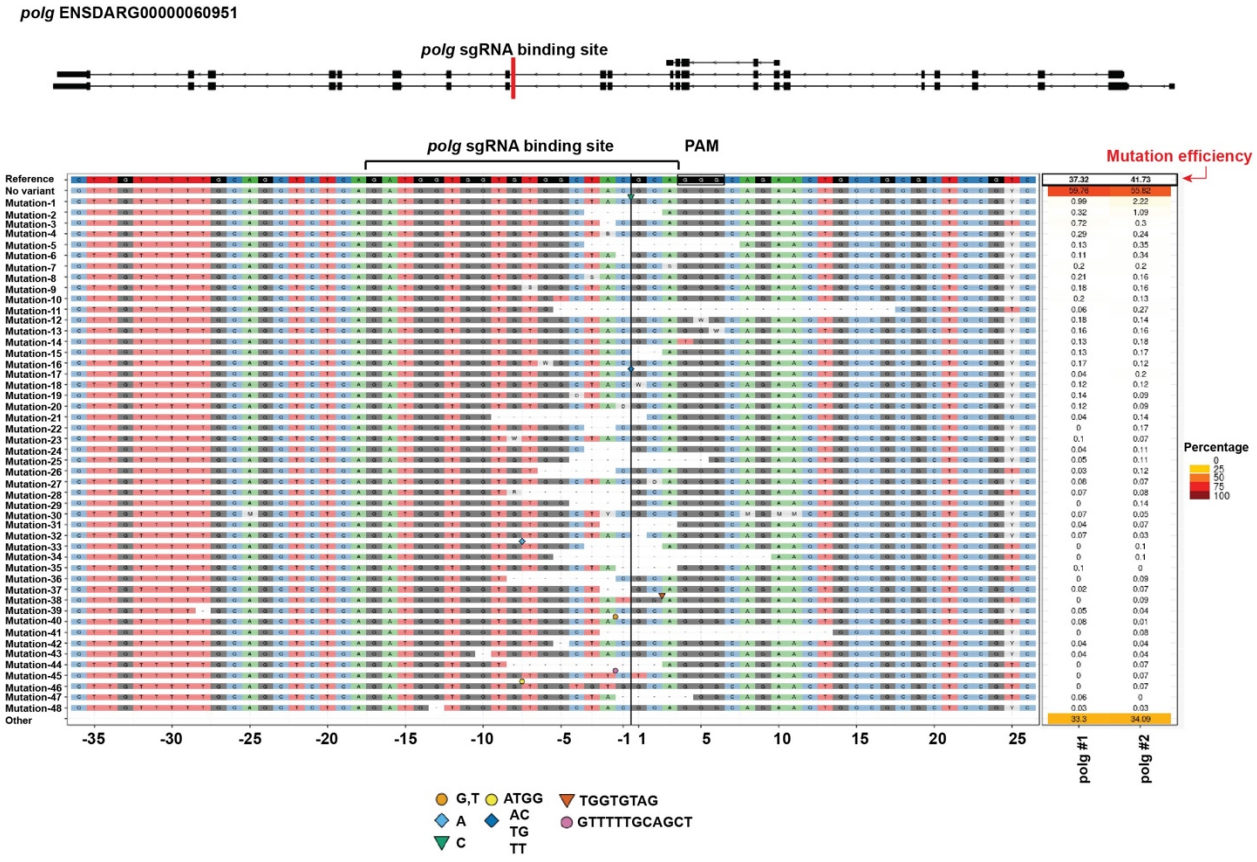

Figure 3-3. In vivo editing in the *polg* locus in *Tg(lyzC:nls-cas9-2A-mCherry/U6a:polg sgRNA)* ^{pu16}.

Neutrophils were sorted via FACS from 3 dpf embryos. Genomic DNA was extracted and the polg locus around the sgRNA cleavage site was PCR amplified and sequenced. The 48 most frequent types of mutations from two separate sorts are shown. Point mutations, deletions and insertions are all observed. Symbols indicate various forms of insertion.

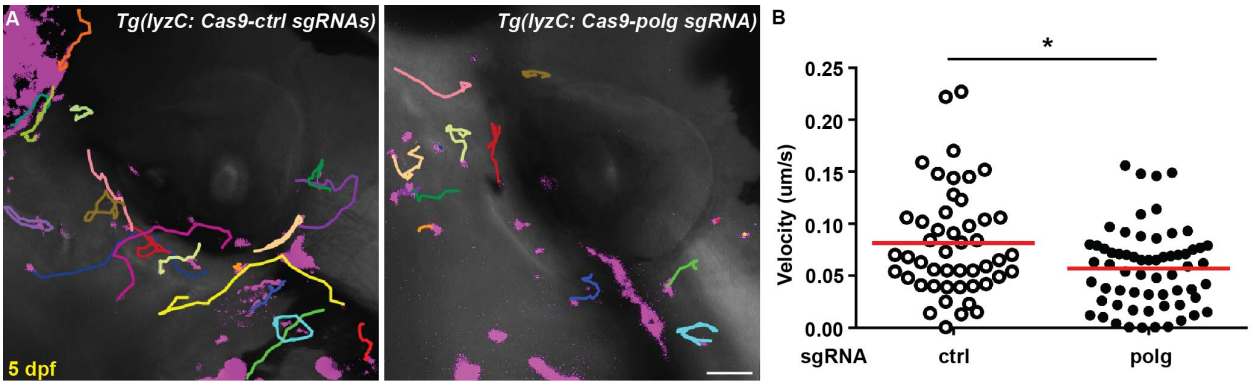

Figure 3-4. Neutrophil-specific knockout of *polg* reduced neutrophil motility at 5 dpf.

A) Representative images and B) Quantification of neutrophil motility in the head mesenchyme of 5 dpf embryos. One representative result of three biological repeats was shown. n = 48 for ctrl and n = 63 for polg from 4 different larvae. *, $P<0.05$ by Mann-Whitney test. Scale bar: 50 μm.

Mitochondrial electron transport chain regulates neutrophil motility in vivo

One of the consequences of *polg* loss-of-function and depletion of mitochondrial DNA is the reduced enzymatic activity of the electron transport chain (ETC) components, 13 of which are encoded by the genes on the mitochondrial DNA (Anderson et al., 1981). The mitochondria uncouplers FCCP and CCCP rapidly disrupted mitochondria inner membrane potential and abrogated neutrophil chemotaxis in primary human neutrophils ex vivo (Bao et al., 2015; Fossati et al., 2003). The complex I inhibitors Rotenone and Metformin significantly reduced neutrophil recruitment in an acute LPS-induced lung inflammation mouse model (Zmijewski et al., 2008), although this treatment was not neutrophil targeted. We then determined whether proper function of mitochondrial ETC is required for neutrophil motility in vivo. FCCP or CCCP treatment resulted in rapid fish death, precluding the suitability of the mitochondria uncouplers for in vivo use. Mitochondria complex I inhibitor Rotenone, and complex III inhibitor Antimycin significantly reduced neutrophil motility in zebrafish (Fig. 3-5A, B). Similar to the observations of human primary neutrophils ex vivo (Zmijewski et al., 2008), inhibitor treatment did not trigger cell apoptosis.

To further confirm that mitochondrial ETC is essential for neutrophil migration, we disrupted it genetically. Neutrophils migrate individually, allowing functional characterization of a subset of genetically perturbed cells without generating stable lines. To test the feasibility of transient gene disruption in vivo, we injected the 1-cell stage embryos with the plasmid carrying two different sgRNAs targeting *rac2*, a gene required for neutrophil motility (Deng et al., 2011; Rosowski et al., 2016a) (Fig. 3-5C). At 3 dpf, larvae contains 5~10 mCherry expressing neutrophils in the head mesenchyme were selected for live imaging and quantification. A majority of these neutrophils lost motility (Fig. 3-5D and E), demonstrating the effectiveness of the tissue-specific knockout strategy in vivo. We then designed sgRNAs against *ndufs2* and *uqcrc1*, core components in complex I and III, respectively (Mimaki et al., 2012; Smith et al., 2012). Transient knockout of these two genes also resulted in a reduction in neutrophil motility (Fig. 3-5D, E), consistent with the results obtained using the pharmacological inhibitors.

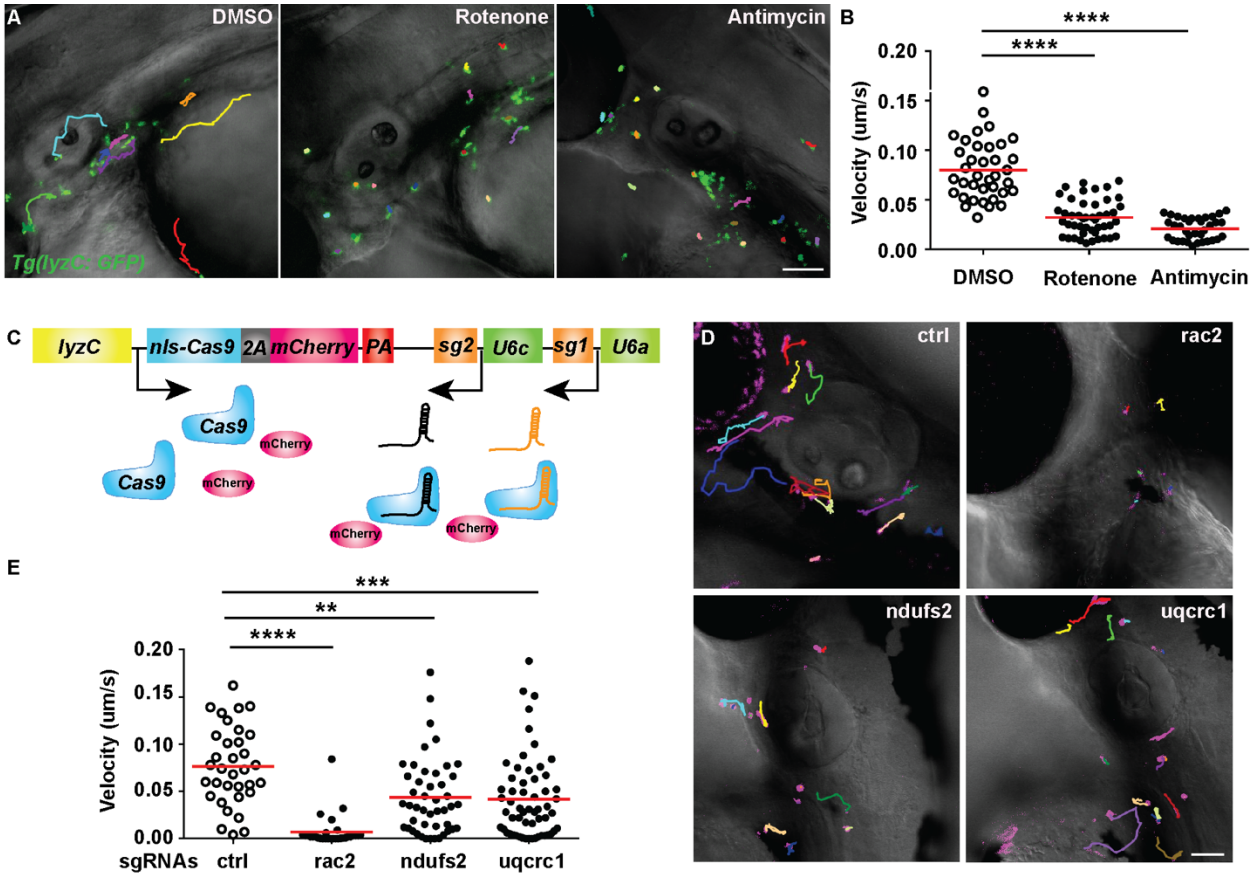

Figure 3-5. Mitochondria complex I and III regulate neutrophil motility.

A,B) *Tg(lyzC:GFP)* at 3 dpf was treated with DMSO, Retonone or Antimycin. A) Representative images and B) Quantification of neutrophil motility in the head mesenchyme. One representative result of three biological repeats was shown. n =37 for DMSO, n= 46 for Rotenone, and n= 35 for Antimycin from 4 different larvae. ****, $P<0.0001$ by Kruskal-Wallis test. C) Schematic of the vector used to produce 2 different sgRNAs. D) Representative images and E) Quantification of neutrophil motility in the head mesenchyme with neutrophil-specific transient knockout of *rac2* (positive control), *ndufs2* or *uqcrc1*. One representative result of three biological repeats was shown. n = 34 for ctrl, n= 30 for rac2, n = 46 for ndufs2, and n = 58 for uqcrc1 from 4 different larvae. ****, $P<0.0001$, ***, $P<0.001$, **, $P<0.01$ by Kruskal-Wallis test. Scale bars: 50 µm.

Mitochondrial redox status regulates neutrophil motility in vivo

Mitochondria complex I and III directly leak electrons to oxygen molecules and are the major source of intracellular ROS in many cell types. Treating neutrophils ex vivo with Rotenone increases the intracellular levels of superoxide and hydrogen peroxide (Zmijewski et al., 2008). We then determined whether mitochondrial redox status affects neutrophil motility. Using the same experimental design as in Fig. 3-5C, we transiently expressed constructs that specifically knockout *sod1* (superoxide dismutase 1 localized in the cytosol and intermembrane space of mitochondria) (Milani et al., 2011) and *sod2* (superoxide dismutase 2 localized in mitochondria matrix) (Peterman et al., 2015) in neutrophils. Both Sod1 and Sod2 mediate the reduction of superoxide (O_2^-). Neutrophils with loss-of-function in *sod1* and *sod2* displayed significantly reduced motility (Fig. 3-6A, B). The defect of neutrophil motility resulted from *sod1* knockout can be rescued with *sod1* mRNA over-expression (Fig. 3-6C, D), demonstrating the specificity of the knockout approach. In addition, the reduction of neutrophil motility induced by *sod1/2* deficiency was also rescued by the ROS scavenger NAC and/or a mitochondria targeted antioxidant mitoTEMPO (Fig. 3-6E-H), indicating that neutrophil motility is inhibited by excessive ROS when *sod1* or *sod2* is knocked out. We however, could not use *sod2* mRNA to rescue the neutrophil specific disruption of *sod2*, probably due to that 1). Fish embryos cannot tolerate high level of *sod2* over expression or 2). The mutated proteins form aggregates and act as dominant-negative (Perry et al., 2010). In contrast, treating zebrafish with pharmacological inhibitors to reduce ROS levels, or overexpression of Sod2 did not affect neutrophil motility (Fig. 3-7).

Figure 3-6. Mitochondria redox status regulate neutrophil motility.

A) Representative images and B) Quantification of neutrophil motility in the head mesenchyme with neutrophil-specific transient knockout of s*od1* and s*od2* using the plasmids described in Figure 3C. One representative result of three biological repeats was shown. n = 36 for ctrl, n= 40 for sod1, and n= 42 for sod2 from 4 different larvae. ****, $P<0.0001$ by Kruskal-Wallis test. C) Representative images and D) Quantification of neutrophil motility in embryos co-injected with the plasmid for *sod1* knockout in neutrophils and *sod1* mRNA or the *GFP* control mRNA. One representative result of three biological repeats was shown. n = 11 for *gfp mRNA* and n = 14 for *sod1 mRNA* from 4 different larvae. **, $P<0.01$ by Mann-Whitney test. E) Representative images and F) Quantification of neutrophil motility in embryos injected with the plasmid for *sod1* knockout in neutrophils and then treated with 1% DMSO, 200 μM NAC, or 50 μM mitoTEMPO from 1 dpf. One representative result of three biological repeats was shown. n =53 for DMSO, n = 34 for NAC, and n = 62 for mitoTEMPO from 4 different larvae. ****, $P<0.0001$ by Kruskal-Wallis test. G) Representative images and H) Quantification of neutrophil motility in embryos injected with the plasmid for *sod2* knockout in neutrophils and then treated with 1% DMSO, 200 μM NAC, or 50 μM mitoTEMPO from 1 dpf. One representative result of three biological repeats was shown. n = 49 for DMSO, n = 40 for NAC, and n = 31 for mitoTEMPO from 4 different larvae. **, $P<0.01$, and n.s., not significant, by Kruskal-Wallis test. Scale bars: 50 μm.

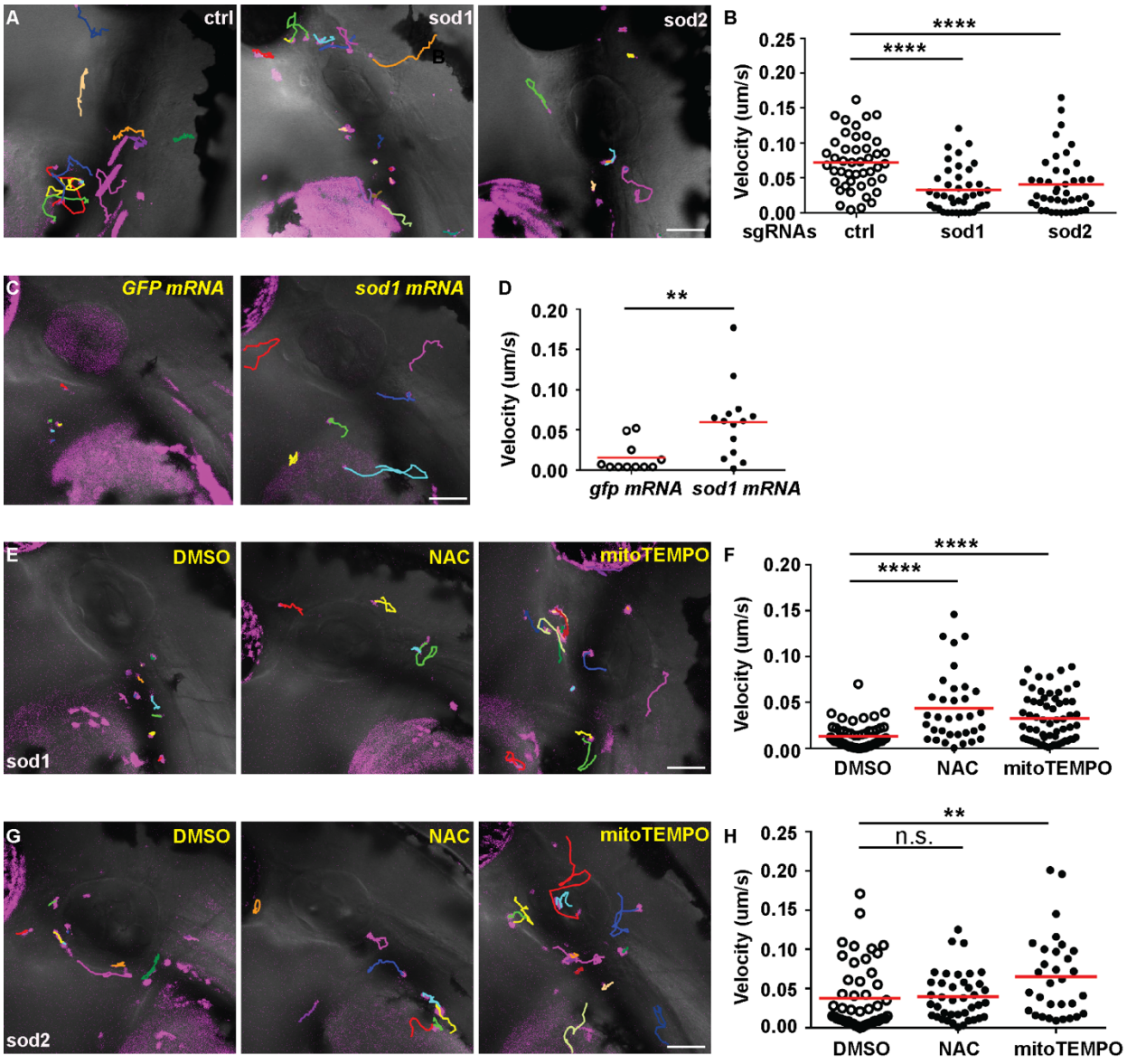
A
ctrl
sod1
sod2
B
****
****
Velocity (um/s)
0.25
0.20
0.15
0.10
0.05
0.00
sgRNAs
ctrl
sod1
sod2
C
GFP mRNA
sod1 mRNA
D
**
Velocity (um/s)
0.20
0.15
0.10
0.05
0.00
gfp mRNA
sod1 mRNA
E
DMSO
NAC
mitoTEMPO
sod1
F
****
****
Velocity (um/s)
0.20
0.15
0.10
0.05
0.00
DMSO
NAC
mitoTEMPO
G
DMSO
NAC
mitoTEMPO
sod2
H
**
n.s.
Velocity (um/s)
0.25
0.20
0.15
0.10
0.05
0.00
DMSO
NAC
mitoTEMPO

Figure 3-7. Decreasing the ROS level in neutrophils does not affect neutrophil migration.

A, B) *Tg (lyzC:GFP)* at 3 dpf was treated with DMSO, DPI, Celastrol or NAC. A) Representative images and B) Quantification of neutrophil motility in the head mesenchyme. One representative result of three biological repeats was shown. n = 32 for DMSO, n = 32 for DPI, n = 33 for Celastrol, n = 24 for NAC from 4 different larvae. n.s., not significant by one-way ANOVA. C) Representative images and D) Quantification of neutrophil number at the wound at 1 hpw in embryos treated with DMSO, DPI, or Celastrol. One representative result of three biological repeats was shown. n = 19 for DMSO, n = 21 for DPI, n = 17 for Celastrol. ****, $P<0.0001$ by Kruskal-Wallis test. E) Representative images and F) Quantification of neutrophil motility in the head mesenchyme with neutrophil specific transient overexpression of Sod2. n = 28 for ctrl and n = 27 for Sod2-2A-Catalase from 4 different larvae. n.s., not significant by Mann-Whitney test. Scale bars: 50 μm.

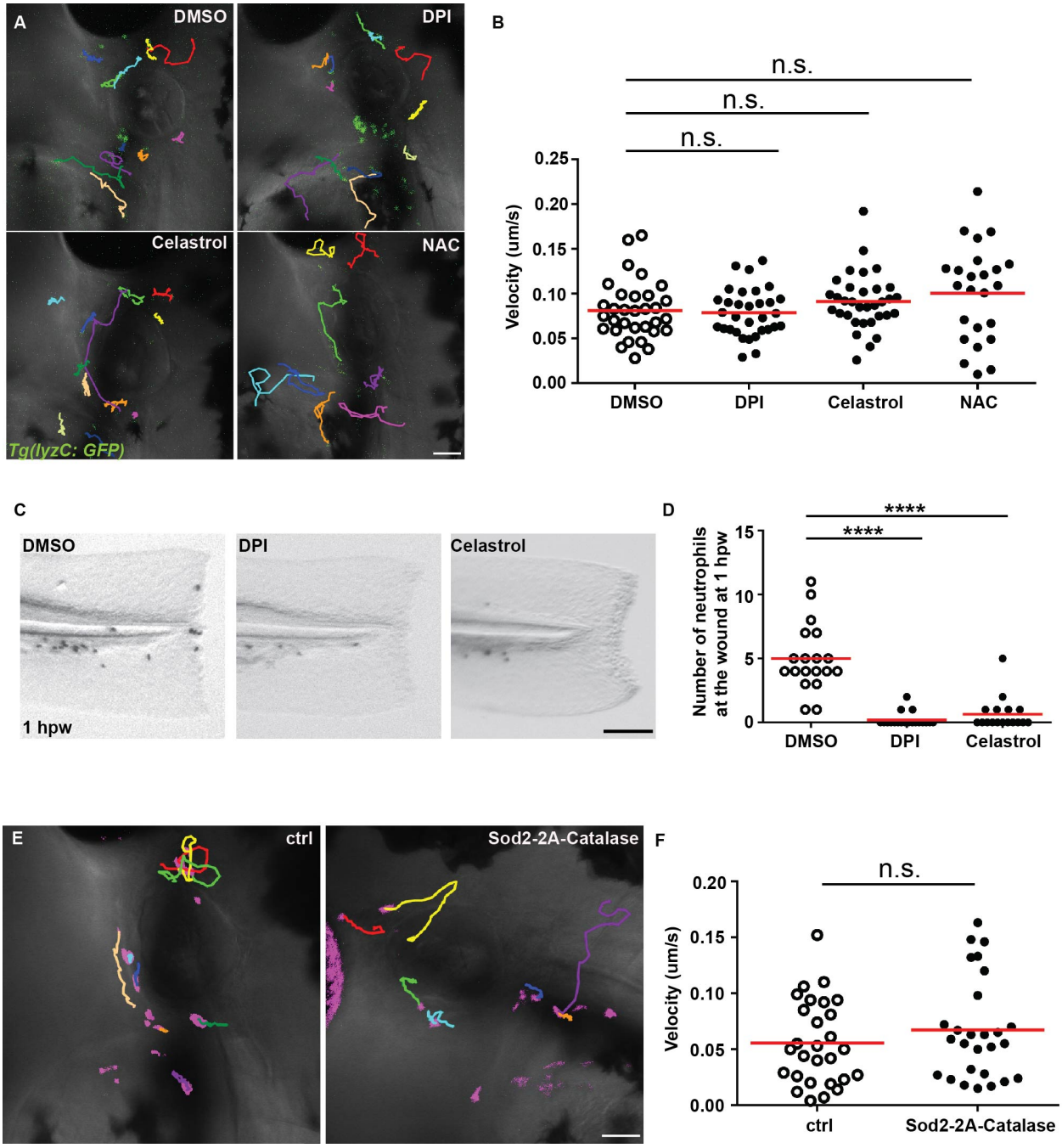
A
DMSO
DPI
Celastrol
NAC
Tg(lyzC: GFP)
B
n.s.
n.s.
n.s.
Velocity (um/s)
0.25
0.20
0.15
0.10
0.05
0.00
DMSO
DPI
Celastrol
NAC
C
DMSO
DPI
Celastrol
1 hpw
D
****
****
Number of neutrophils at the wound at 1 hpw
15
10
5
0
DMSO
DPI
Celastrol
E
ctrl
Sod2-2A-Catalase
F
n.s.
Velocity (um/s)
0.20
0.15
0.10
0.05
0.00
ctrl
Sod2-2A-Catalase

Discussion

Technically, we have explored the CRISPR/Cas9 system for leukocyte-specific knockout in zebrafish for the first time. We have optimized the original vector developed by the Zon group to allow easier switching of tissue specific promoters, visualization of Cas9 expressing cells and incorporation of two sgRNAs. The stable TS-polg line generated here displayed an inheritable phenotype, from founders to the F2 generation. The *lyzC* promoter drives Cas9 expression primarily in neutrophils starting at 2 dpf (Hall et al., 2007). At 3 dpf, the editing of the *polg* locus was detected, suggesting the fast acting nature of this system. However, mutation efficiency estimated using the T7E1 assay or deep sequencing is skewed by the necessary PCR amplification step. Another caveat with this stable line is that the phenotype disappears when crossed with other transgenic lines harboring the *lyzC* or the *mpx* promoter, but not with other lines. We speculate that the presence of another transgene after a neutrophil specific promoter competes with the transcription of Cas9 and thus reduces the efficiency of target editing. Further optimizations, such as using the GAL4-UAS system should be attempted in the future. Linking Cas9 with mCherry allows the visualization of the edited cells after transient expression without generating stable lines, significantly increasing the efficiency of scientific discovery. We chose mCherry so the generated TS-KO line can be used in conjunction with many GFP reporter lines in the zebrafish community. We have demonstrated the efficacy with sgRNAs against *rac2* and two mitochondrial ETC components. We have also demonstrated the specificity by mRNA and chemical rescue of the *sod1* disruption; although not all genes can necessarily be rescued with mRNA expression. We expect that a similar strategy can be used to assess gene functions in other tissues. Caution should be applied when interpreting negative results. Since it is extremely difficult to evaluate the efficiency of transient knockout in vivo, a conclusion that a gene is not related to the phenotype under investigation should not be reached.

Here we have provided the first evidence that *polg* is required for cell migration. Previously, the characterization of the immune function in *POLG*-related disorders are limited to the adaptive immune system. A heterozygous missense mutation of the *POLG* gene was identified in an infant with decreased T cell number and immunoglobulin numbers, although the significance is not clear (Reichenbach et al., 2006). Increased peripheral lymphocyte death is observed in patients with *POLG*-related disorders (Formichi et al., 2016), suggesting a role for *POLG* in maintaining the pool of adaptive immune cells. Unlike the adaptive immune cells, neutrophils are terminally

differentiated and short lived. It is likely that POLG performs functions in neutrophils other than long-term survival. It has been recently noted that POLG localizes to ER-mitochondria contact sites, which coincides with mitochondria fission (Lewis et al., 2016), providing another possible mechanism for POLG in regulating cell migration.

The mitochondrial network we observed here in neutrophils in vivo is significantly different from those observed in 2D. In isolated primary human neutrophils, mitochondria are devoid from the uropod, and a small fraction with higher membrane potential localize to cell protrusions (Bao et al., 2015). In contrast, mitochondria localize to the uropod of T cells and neutrophil-like cells (Campello et al., 2006). Mitochondria are recruited to the cell front in highly metastatic breast cancer cells to promote lamellipodia formation, migration, and invasion (Zhao et al., 2013). It is possible that both the formation of cell protrusion and tail contraction in vivo require proper mitochondria function whereas mitochondria not necessarily enter the structures. This tubular structure is consistent with the previous report in primary human neutrophils (Maianski et al., 2002) and in HL-60 cells (Maianski et al., 2004). In T cells and cancer cells, mitochondria fragmentation promotes cell motility, presumably by increasing proper mitochondria localization and local ATP concentration (Campello et al., 2006; Zhao et al., 2013). It is not clear whether this highly fused network benefits neutrophil migration. A fused network reduces mitophagy (Gomes et al., 2011) and promotes efficient ATP production (Rambold et al., 2015), which may be required to maintain cell homeostasis in addition to regulating cell migration.

Here we have shown that excessive ROS is detrimental to neutrophil migration, possibly resulted from oxidation of the cytoskeleton or signaling molecules. Despite multiple attempts using several ROS dyes such as CM-H2DCFDA and CellROX Green and the genetically encoded ROS sensor Hyper, we failed to label intra-neutrophil ROS to show that indeed the ROS levels are increased in sod1/2 knockouts. Since the biochemical functions of sod1 and sod2 are well characterized and the phenotypes are rescued with ROS scavenger treatment (Fig. 6), we are confident that the motility defect is resulted from increased ROS levels. In contrast, increases in ROS production, resulting from mutations that lead to mitochondrial dysfunction (Frezza et al., 2011), pharmacological mitochondria electron transport inhibition with Rotenone, or metabolic switch (Porporato et al., 2014), promotes cancer cell migration and invasion. Taken together, the physiological relevance of mitochondrial ROS levels and the dynamics of mitochondria networks

are highly context-dependent, displaying different features in various cell types in 2D and 3D, warranting further characterization in neutrophils.

In summary, we have characterized the localization of the mitochondria network in zebrafish neutrophils and provided the first evidence of the biological relevance of mitochondria in neutrophil migration in 3D. In addition, we have provided an animal model that allows rapid assessment of the contribution of developmental essential genes in neutrophil migration in vivo. We expect that a full understanding the different contributions of mitochondria related genes in neutrophil migration will provide mechanistic insights into immune deficiencies seen, and often overlooked, in patients with mitochondrial diseases.

CHAPTER 4. MITOFUSIN 2 REGULATES NEUTROPHIL ADHESIVE MIGRATION VIA SUPPRESSING RAC ACTIVATION

Abstract

Mitochondrial membrane potential is required for neutrophil migration, although the mechanism remains unclear. Here, we report that mitochondrial outer membrane protein mitofusin 2 (Mfn2) regulates neutrophil homeostasis in vivo. *Mfn2*-deficient neutrophils are released from the hematopoietic tissue and trapped in the vasculature in zebrafish embryos. Human neutrophil-like cells deficient with MFN2 fail to be arrested by activated endothelium under sheer stress or perform chemotaxis on substrates. Deletion of Mfn2 results in a significant reduction of neutrophil infiltration to the inflamed peritoneal cavity in mice. *Mfn2*-deficient neutrophil-like cells and mouse embryonic fibroblasts display heightened Rac activation. Mechanistically, MFN2 maintains mitochondria-ER interaction and prevents excessive elevation of cytosolic calcium and subsequent phosphorylation of CaMKII upon stimulation. Inhibiting CaMKII or the Rac GEF Tiam rescues the chemotaxis defect that results from Mfn2 depletion. Altogether, we identified an Mfn2-CaMKII-Tiam-Rac axis in regulating neutrophil migration and discovered a role of *MFN2* in regulating the actin cytoskeleton.

Introduction

Neutrophils, the most abundant circulating leukocytes in humans, constitute the first line of host defense. Upon stimulation by either pathogen or host-derived proinflammatory mediators, neutrophils are recruited to inflamed tissue using spatially and temporally dynamic intracellular signaling pathways. Activation of the surface receptors, primarily the G-protein-coupled receptors(de Oliveira et al., 2016; Gambardella and Vermeren, 2013; Mocsai et al., 2015; Pantarelli and Welch, 2018), leads to the activation of phosphatidylinositol 3-kinases (PI3K) which produces phosphatidylinositol (3,4,5)P3 and activates small GTPases such as Rac. Rac promotes actin polymerization at the leading edge and drives cell migration(Futosi et al., 2013). In parallel, G-protein-coupled receptors activate phospholipase C, which generates IP3 and activates the Ca^{2+} release from intracellular stores(Tsai et al., 2015). Although intracellular Ca^{2+} is a well characterized second messenger that activates Rac and regulates cell migration in slowly migrating cells(Price et al., 2003b; Tsai et al., 2015), its role in neutrophil migration is less clear.

Cell migration requires the coordination of multiple cellular organelles, including mitochondria. Mitochondria carry out oxidative phosphorylation to produce ATP, regulate intracellular redox status and intracellular distribution of Ca^{2+}, which are involved in cell migration. In addition, mitochondria morphology changes via fusion and fission(Campello and Scorrano, 2010) to adapt to variable metabolic needs under different conditions. Mitochondria fission is believed to promote cell migration by providing localized mitochondria and ATP production(Campello et al., 2006; Zhao et al., 2013).

In neutrophils, mitochondrial biology is distinct and contradictory. The Warburg effect is well-documented in neutrophils that they primarily use glycolysis for ATP(Borregaard and Herlin, 1982). Neutrophils have a few mitochondria with low respiration rates and low enzymatic activity of the electron transport chain(Peachman et al., 2001). However, maintaining mitochondria membrane potential is required for chemotaxis. Disrupting mitochondria membrane potential by pharmacological inhibitors abolished chemotaxis of isolated primary neutrophils(Bao et al., 2015; Bao et al., 2014; Fossati et al., 2003). Although mitochondria-derived ATP possibly regulates neutrophil chemotaxis in vitro(Bao et al., 2015), removal of extracellular ATP improves neutrophil chemotaxis in vivo(Li et al., 2016). These conflicting reports prompted us to search for mechanisms delineating the role of mitochondria in neutrophil migration outside the realm of ATP or cellular energy(Bi et al., 2014; Schuler et al., 2017; Zanotelli et al., 2018).

Neutrophils are terminally differentiated and undergo apoptosis within 24 hours in culture and thus not genetically tractable. We have overcome this hurdle by developing a neutrophil- specific knockout platform in zebrafish(Zhou et al., 2018). The zebrafish is a suitable model for neutrophil research because of a highly conserved innate immune system. In our previous work, we have confirmed the requirement of mitochondrial membrane potential, biosynthesis and electron transport chain in the migration of zebrafish neutrophils(Zhou et al., 2018). In addition, we have visualized a highly fused tubular network of mitochondria in zebrafish neutrophils, which is consistent with a previous report investigating primary human neutrophils(Maianski et al., 2002). Here we present evidence that Mitofusin 2 (Mfn2) regulates Rac activation to coordinate neutrophil adhesive migration. In addition, we have revealed a previously unknown function of Mfn2 in regulating the actin cytoskeleton, contributing to the understanding and management of patients with mitochondrial diseases.

Results

Neutrophils depleted with *mfn2* accumulate in zebrafish vasculature

To address whether this highly fused network benefits neutrophil migration, in the present study, we disrupted proteins regulating mitochondrial shape in zebrafish neutrophils. Mitofusins Mfn1 and Mfn2 are required for mitochondrial outer membrane fusion(Chen et al., 2003) and Opa1 regulates inner membrane fusion(Song et al., 2007). In embryos produced from the transgenic line, *Tg(lyzC:Cas9-mfn2 sgRNAs)*^{pu22} which expresses two independent sgRNAs targeting *mfn2*, the majority of neutrophils circulated in the bloodstream (Fig. 4-1a, b). This is in sharp contrast to the control or the wild-type embryos in which over 99% of neutrophils are retained in the caudal hematopoietic tissue or in the head mesenchyme(Harvie and Huttenlocher, 2015). This abnormal distribution of neutrophils was further confirmed in a second transgenic line expressing a different set of sgRNAs targeting *mfn2*, *Tg(lyzC:Cas9-mfn2 sgRNAs#2)*^{pu23} (Fig. 4-1a, b). Neutrophils were sorted from both lines and respective loci targeted by the 4 sgRNAs were deep sequenced. The overall mutation frequency ranged from 24% to 60%. In contrast, circulating neutrophils were not observed in embryos expressing sgRNAs targeting *opa1,* although the velocity of neutrophil migration in the head mesenchyme was significantly reduced (Fig. 4-2), indicating that decreased neutrophil retention in tissue is not simply due to defects in mitochondrial fusion.

Next, we determined whether neutrophils in the vasculature were able to respond to acute inflammation induced by a tail transection or performing chemotaxis to LTB_4. Significant defects in both assays were observed in the line with neutrophil specific *mfn2* deletion (Fig. 4-1c-f, d). Taken together, *mfn2* regulates neutrophil tissue retention and extravasation in zebrafish.

Figure 4-1. Mfn2 regulates neutrophil homeostasis in zebrafish.

a) Schematics of the gene structure and protein domains of the zebrafish *mfn2* gene. The first set of sgRNAs (purple lines) targets exon 3 and exon 8 in the forward strand, and the second set (blue lines) targets exon 3 and exon 13 in the forward strand. b) Representative images of neutrophils in the zebrafish trunk of the transgenic lines with neutrophil specific *mfn*2 disruption at 3 dpf. Magenta arrows: neutrophils in the caudal hematopoietic tissue; yellow arrows: neutrophils in the vasculature. c) Representative images and d) quantification of neutrophil recruitment to the wound edge at 1 hpw. Blue arrows: neutrophils migrated to the wound. e) Representative tracks and f) quantification of neutrophil recruitment to the fin at 30 min post LTB_4 treatment. Blue arrows: neutrophils in the fin. One representative result of three biological repeats is shown in d and f. *, $P<0.05$, ****, $P<0.0001$, unpaired *t*-test. Scale bar: 50 μm..

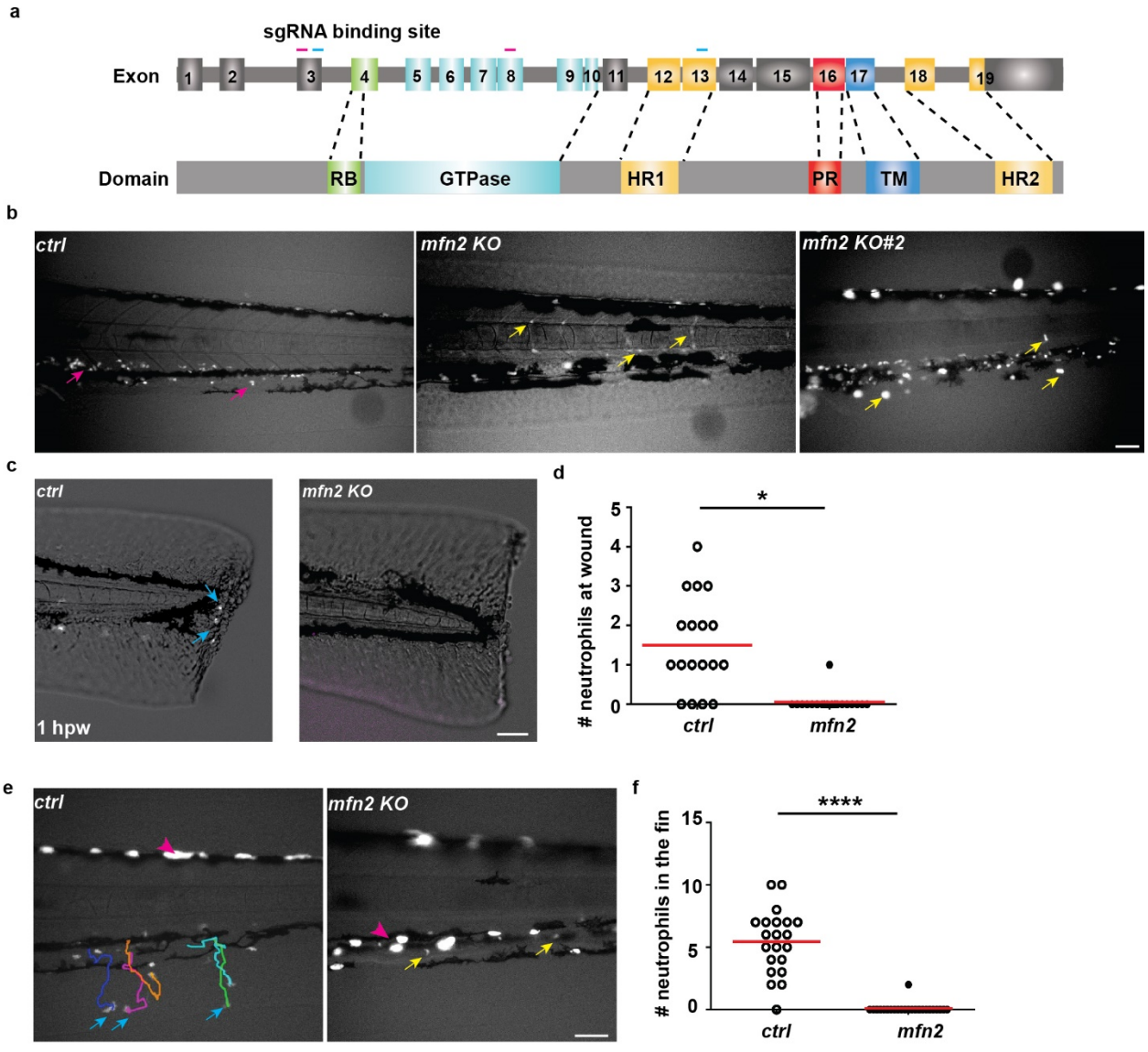
a
sgRNA binding site
Exon
1 2 3 4 5 6 7 8 9 10 11 12 13 14 15 16 17 18 19
Domain
RB GTPase HR1 PR TM HR2
b
ctrl
mfn2 KO
mfn2 KO#2
c
ctrl
mfn2 KO
1 hpw
d
neutrophils at wound
*
ctrl
mfn2
e
ctrl
mfn2 KO
f
neutrophils in the fin
****
ctrl
mfn2

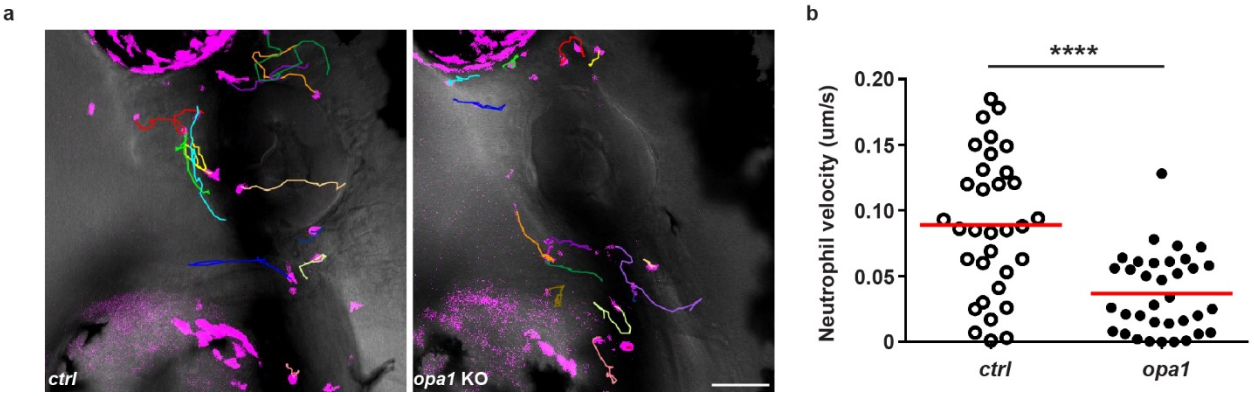

Figure 4-2. Disrupting *opa1* reduces neutrophil motility in zebrafish.

a) Representative tracks and b) Quantification of neutrophil motility in the head mesenchyme of the control line and the line with neutrophil specific *opa1* knockout at 3 dpf. One representative result of three biological repeats is shown. ****, $P<0.0001$, unpaired *t* test. Scale bar: 50 μ

MFN2 regulates adhesion and adhesive migration in human neutrophil-like cells

To get to the mechanism how Mfn2 regulates neutrophil migration, we knocked down *MFN2* in human neutrophil-like cells, HL-60, using shRNAs and obtained two individual lines with 80% and 50% reduction of MFN2(Fig. 4-3a). No difference in apoptosis or cell maturation was noticed in the cell lines (Fig. 4-4). First, we measured neutrophil static adhesion to fibrinogen-coated substrates. Differentiated HL-60 cells (dHL-60) expressing one shRNA targeting *MFN2* (*MFN2-sh1)* displayed significantly decreased adhesion in the absence or presence of N-Formylmethionyl-leucyl-phenylalanine (fMLP) (Fig. 4-3b). The second shRNA *MFN2-sh2* also caused a reduction in neutrophil adhesion, but it was not significant. To recapitulate the phenotype in zebrafish where neutrophils depleted with *mfn2* failed to adhere to the vasculature, we measured cell adhesion to activated endothelial cells under shear stress. A majority of *MFN2*-deficient cells failed to adhere to endothelial cells. A small fraction of cells rolled on top of endothelial cell but were eventually flushed away, suggesting a defect in forming tight adhesions (Fig. 4-3c, d). We then determined whether *MFN2* is required for neutrophil chemotaxis on collagen coated 2-dimensional surfaces, which also requires cell adhesion. As expected, both shRNAs interfered with neutrophil chemotaxis towards fMLP (Fig. 4-5a, b). To further validate the specificity of the shRNA, a sh1 resistant *MFN2* was introduced to the knock down cells and indeed the defect in chemotaxis was rescued (Fig. 4-5c-e). Intriguingly, when we knocked down MFN1, which shares a similar structure and function to MFN2, in dHL-60 cells, no defects in chemotaxis were detected (Fig. 4-6). To investigate whether Mfn2 is required for neutrophil infiltration in mice, we bred *Mfn2* flox/flox mice(Chen et al., 2007) with the *S100A8-Cre* strain(Abram et al., 2013) for neutrophil specific depletion. With 50% of Mfn2 protein reduction in neutrophils obtained in this strain, significant reduction of neutrophil infiltration into the inflamed peritoneal cavity was observed (Fig. 4-5f, g). Blood cell composition was not altered by Mfn2 depletion (28% and 32% granulocytes in the Cre^{+} and Cre^{-} lines, respectively), consistent with a previous report that *Mfn2* does not regulate blood cell development under hemostatic condition(Luchsinger et al., 2016). Therefore, MFN2 is required for neutrophil chemotaxis and infiltration into tissue in mammals.

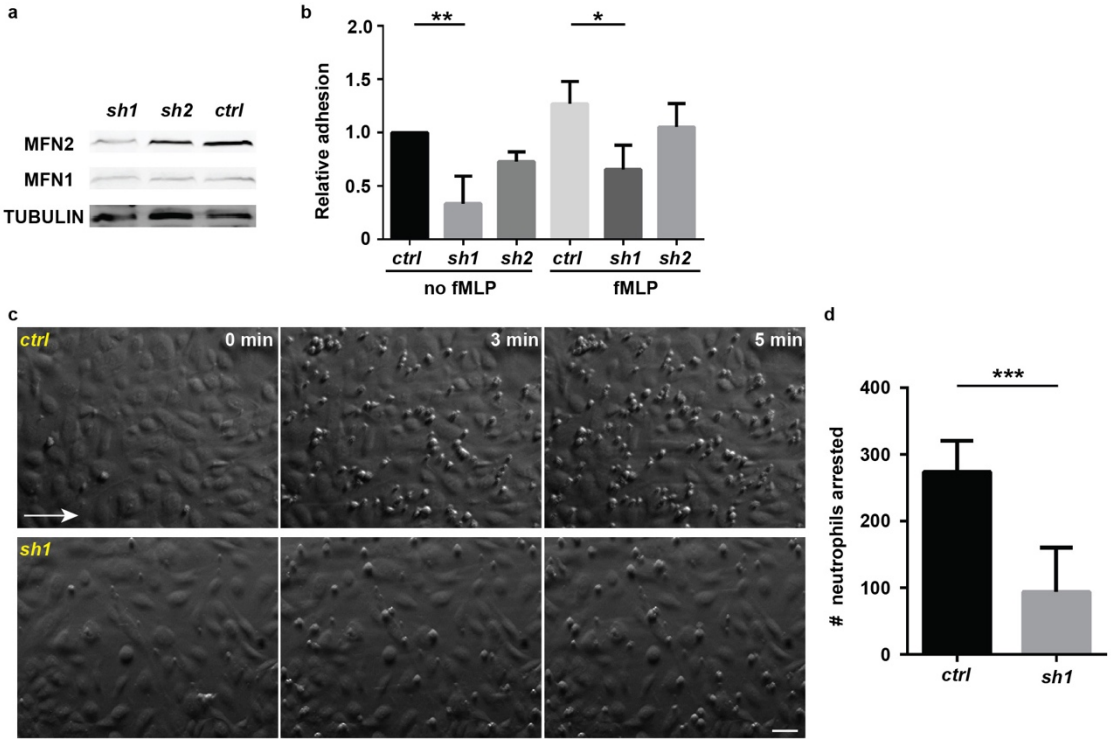

Figure 4-3. MFN2 regulates adhesion of dHL-60 cells.

a) Western blot determining the expression level of MFN2 in indicated cell lines. *ctrl*: standard control shRNA; *sh1*: shRNA targeting MFN2; *sh2*, another shRNA targeting MFN2. b) Relative adhesion of neutrophils to fibrinogen coated substrate in the absence and presence of fMLP. c) and d) Adhesion of neutrophils under sheer stress. HUVEC monolayer was activated with TNFα and neutrophils were flowed on top of the monolayer for 5 min. c) Representative images showing neutrophils arrested by HUVEC at different time points. White arrow: flow direction. d) Quantitation of numbers of neutrophils arrested at 5 min. Data were pooled from three independent experiments. *, $P<0.05$; **, $P<0.01$, one-way ANOVA (b). ***, $P<0.001$, unpaired *t*-test (d). Scale bar: 50 μm.

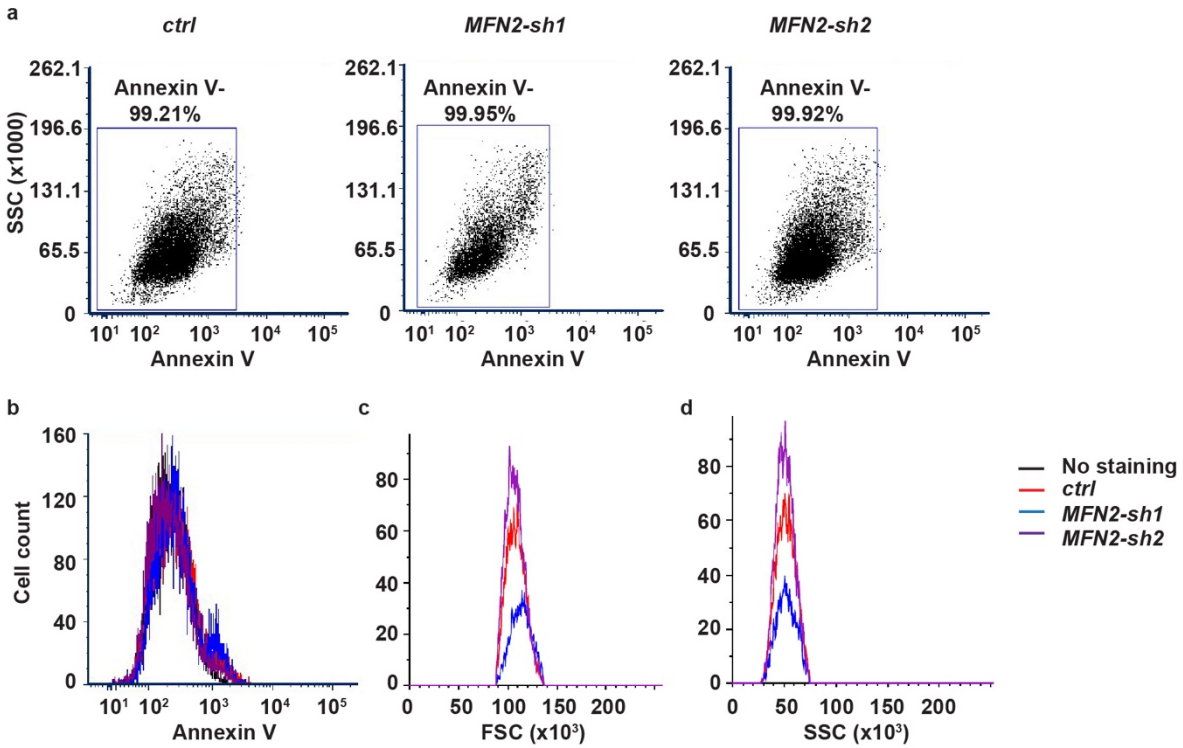

Figure 4-4. MFN2 deficiency does not induce apoptosis in dHL-60 cells.

Apoptosis was determined by Annexin V staining on the surface and followed by flow cytometry in indicated cell lines. a) Dot plot and b) Histogram of Annexin V staining. Status of cell differentiation was reflected by the similar size (FSC, in c) and granularity (SSC in d) of the control and the *MFN2* knockdown cells.

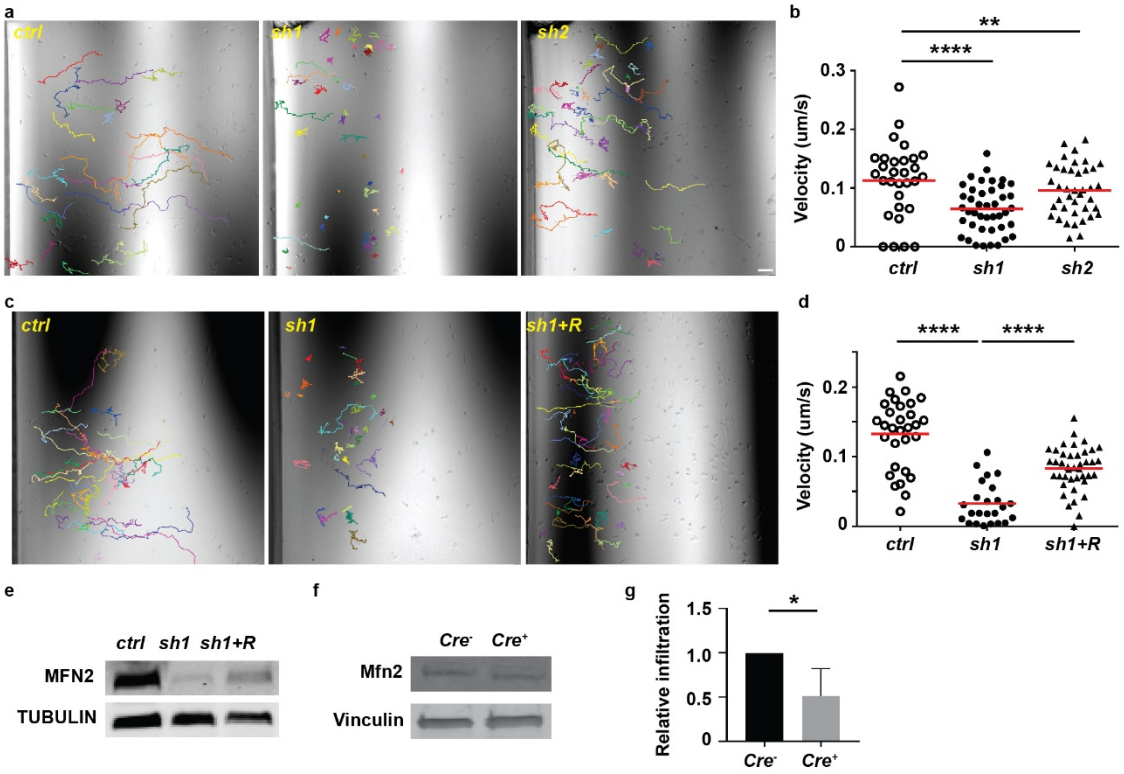

Figure 4-5. MFN2 regulates neutrophil migration in vitro and in vivo.

a) Representative images with individual tracks of neutrophil chemotaxis to fMLP. b) Quantification of velocity of neutrophil chemotaxis to fMLP. c) and d) A *sh1* resistant *MFN2* gene was reintroduced to the MFN2 knock down cells expressing *sh1*. c) Quantification and d) Representative images with individual tracks of neutrophils migrating toward fMLP. One representative result of three biological repeats is shown in b and d. **, $P<0.01$, ****, $P<0.0001$, one-way ANOVA. Scale bar: 50 μm. e) Western blot showing the expression level of MFN2 in indicated cell lines. f) Western blot showing the expression level of Mfn2 in mice neutrophils isolated from *Mfn2$^{flox/flox}$; S100A8:Cre+* or the control *Mfn2$^{flox/flox}$; S100A8:Cre-* littermates. g) Neutrophil infiltration to peritoneal cavity in indicated mice. Percentage of neutrophils in the lavage was normalized to that in sex-matched littermates in each experiment. *, $P<0.05$, paired *t*-test.

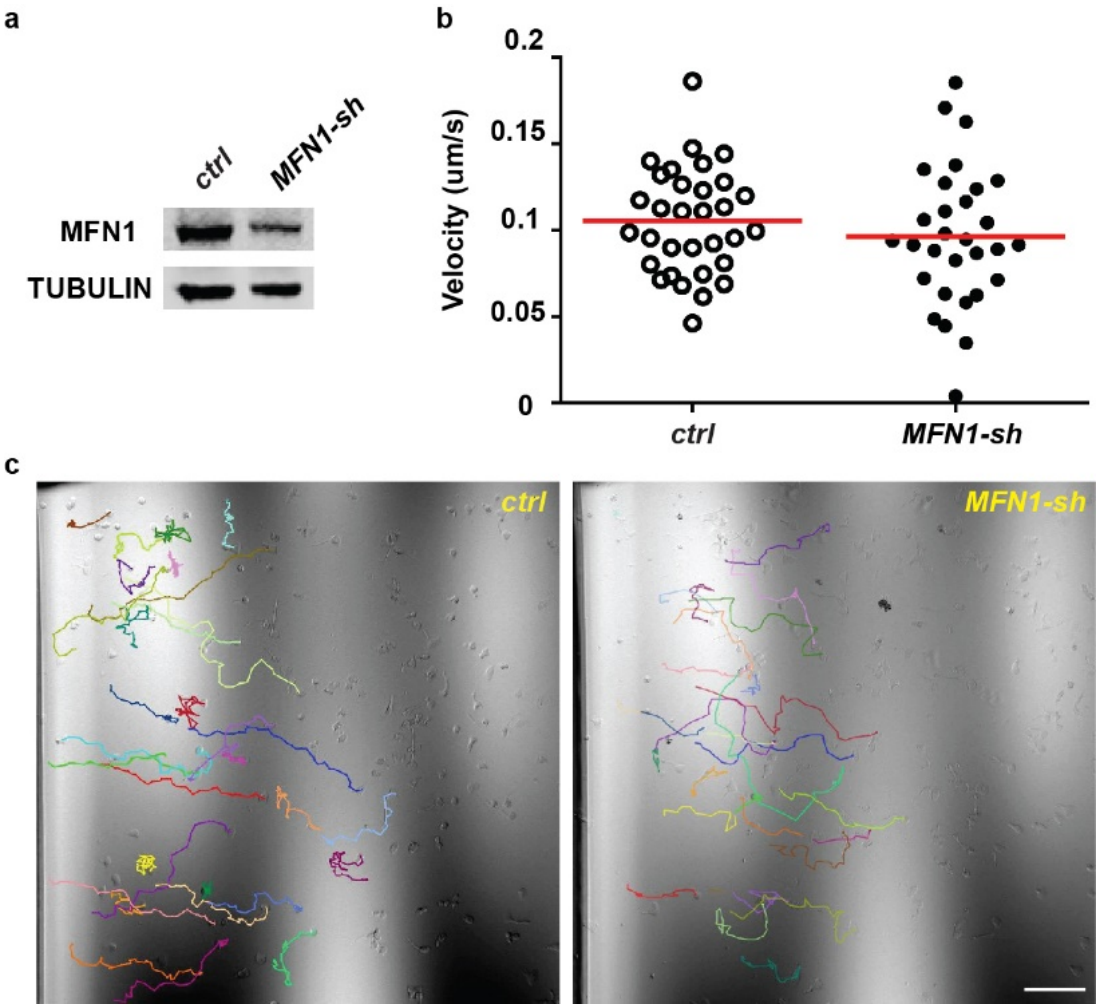

Figure 4-6. MFN1 does not regulate adhesive migration of dHL-60 cells.

a) Western blot showing the expression level of MFN1 in the control cell line or the one stably expressing a shRNA targeting *MFN1*. b) Quantification and c) Representative tracks of dHL-60 cells migrating toward fMLP. One representative result of three repeats is shown. Scale bar: 100 μm.

Mfn2 regulates the actin cytoskeleton and migration of mouse embryonic fibroblasts

In addition to neutrophils, we investigated the function of Mfn2 in mouse embryonic fibroblasts (MEF). *Mfn2-null* MEFs were round with enriched actin filaments and Paxillin in the cell cortex, whereas *wt* MEFs were elongated with stress fibers when plated on both ligand-coated and uncoated substrates (Fig. 4-7a and Fig. 4-8a, b). *Mfn1*-deficient MEFs were rounded but retained stress fibers (Fig. 4-8c, d). The significant changes in actin organization suggest that *Mfn2-null* MEFs may migrate differently. Indeed, MEFs deficient with Mfn2 migrated slower when compared to *wt* cells during wound closure (Fig. 4-7c, d). In addition, right after plating, *wt* MEFs extended transient filopodia and lamellipodia and eventually elongated, whereas *Mfn2-null* MEFs generated extensive membrane ruffles and retained the circular shape (Fig. 4-7d and). *Mfn1-null* cells spread similarly to the *wt* cells (Fig. 4-8e). In summary, Mfn2 modulates the actin cytoskeleton and cell migration in MEFs.

Figure 4-7. Mfn2 regulates cytoskeleton organization and cell migration in MEFs.

a) Immunofluorescence of F-actin (phalloidin), microtubule and Mfn2 in *wt* and *Mfn2-null* MEFs. b) Immunofluorescence of F-actin and Paxillin in wt and *Mfn2-null* MEFs. c) Representative images of wt and *Mfn2-null* MEFs during wound closure at indicated time points. Yellow dash lines: wound edge. d) Quantification of the wound area in wt and *Mfn2-null* MEFs during wound closure. **, $P<0.01$, ***, $P<0.001$, ****, $P<0.0001$unpaired *t*-test. e) Representative images of wt and *Mfn2-null* MEFs during cell spreading at indicated time points. Scale bar: 10 μm (a and b), 20 μm in e and 200 μm in c.

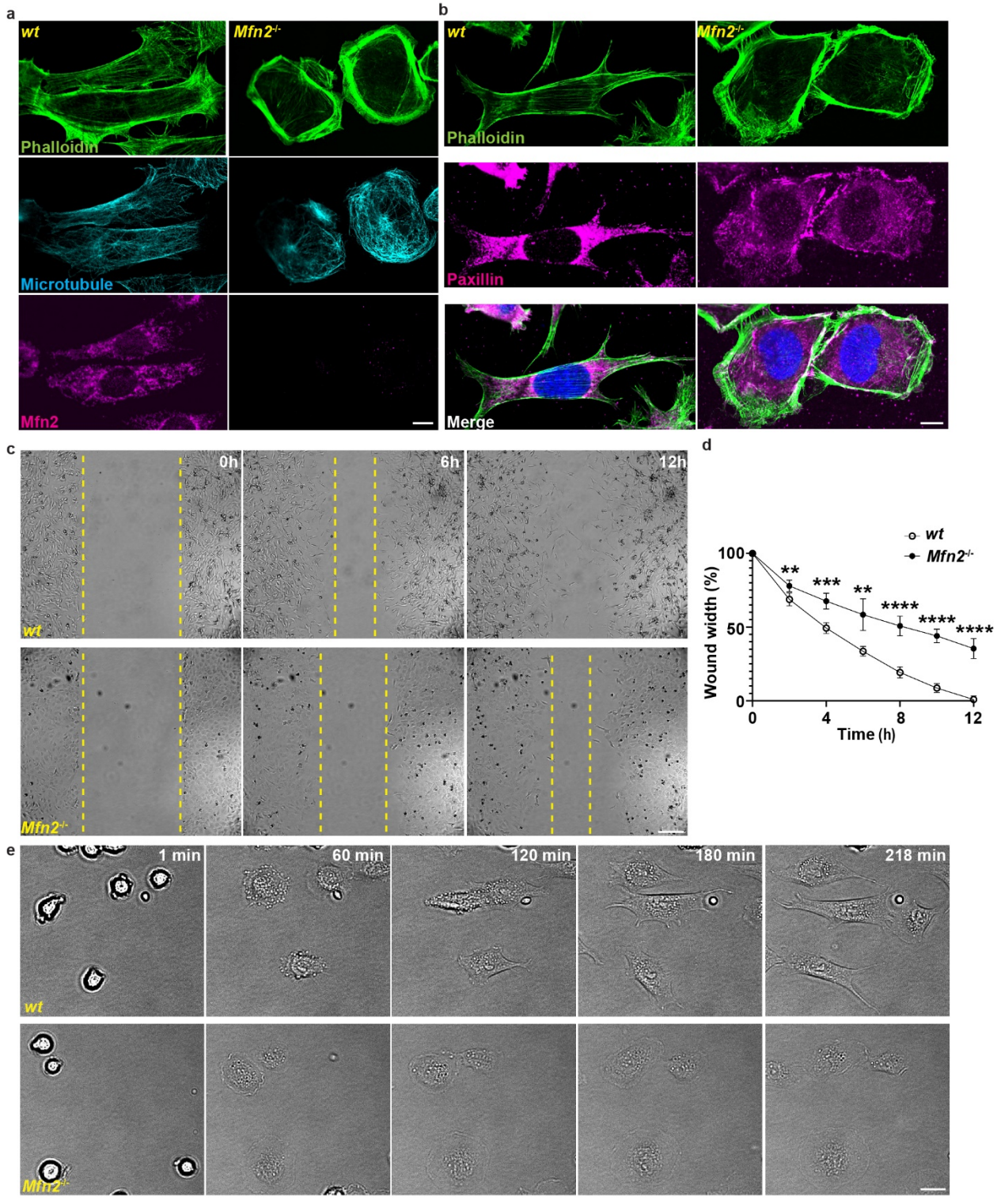
a
wt
Mfn2-/-
Phalloidin
Microtubule
Mfn2
b
wt
Mfn2-/-
Phalloidin
Paxillin
Merge
c
0h
6h
12h
wt
Mfn2-/-
d
wt
Mfn2-/-
Wound width (%)
100
50
0
0
4
8
12
Time (h)
**
***
**
****
****
****
e
1 min
60 min
120 min
180 min
218 min
wt
Mfn2-/-

Figure 4-8. Mfn1 does not regulate the actin cytoskeleton in MEFs.

a, b) Immunofluorescence of F-actin (Phalloidin) and nucleus (DAPI) in indicated cells plated on un-coated (a) or fibrinogen-coated (b) cover glasses. c) Immunofluorescence of F-actin (Phalloidin), microtubule and Mfn2 in *Mfn1-null* MEFs. d) Immunofluorescence of F-actin (Phalloidin) and Paxillin in *Mfn1-null* MEFs. e) Images of *Mfn1-null* MEFs spreading at indicated time points after plating. Scale bar: 10 μm in a-e

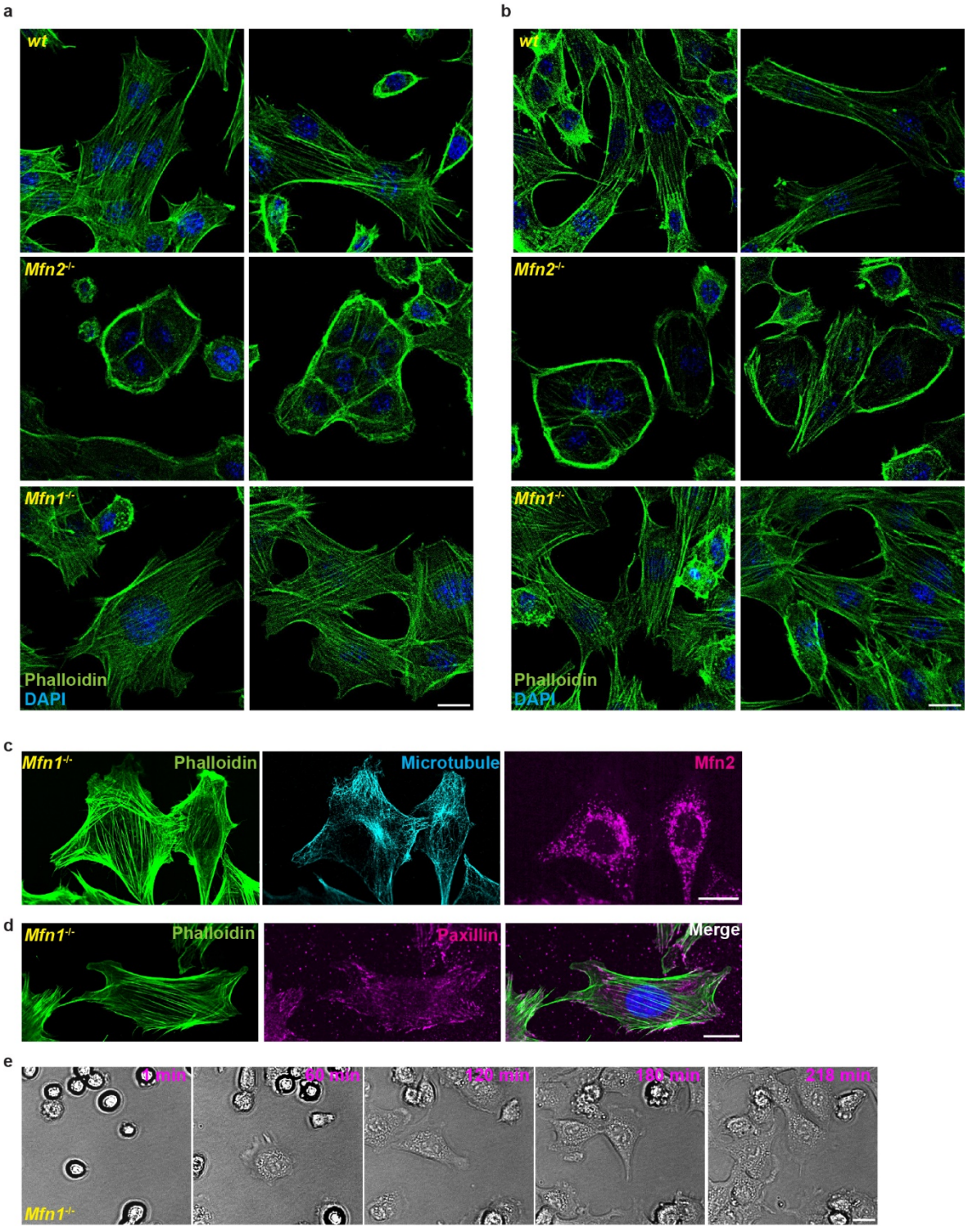
a
b
wt
Mfn2-/-
Mfn1-/-
Phalloidin
DAPI
c
Mfn1-/-
Phalloidin
Microtubule
Mfn2
d
Paxillin
Merge
e
0 min
60 min
120 min
180 min
219 min

MFN2 suppresses RAC activation

The predominant cortical actin, nascent focal contacts and extensive membrane ruffles in *Mfn2-null* MEF cells (Fig. 4-7) resembled the classic phenotype of fibroblasts expressing the constitutively active Rac(Hall, 1998), indicating that Mfn2 may negatively regulate Rac activation. We therefore performed a RAC-GTP pull-down to measure RAC activation in *MFN2*-deficient dHL-60 cells. Significantly increased amount of active RAC were detected in *MFN2-sh1* cells 5 min after fMLP stimulation (Fig. 4-9a, b). RAC-GTP colocalized with F-actins at cell protrusions as well as the retracting rear of the cells (Fig. 4-9c) and the lamellipodia in the *MFN2-sh1* cells accumulated more active RAC than that in the control cells. To determine whether RAC over activation contributes to the chemotaxis defect in *MFN2*-deficient dHL-60 cells, a RAC inhibitor NSC23766 was utilized. NSC23766 restored neutrophil adhesive migration in *MFN2-sh1* cells, at least partially, at a concentration that did not affect chemotaxis of control cells (Fig. 4-9d, e), suggesting that MFN2 regulates neutrophil migration through suppressing RAC activation.

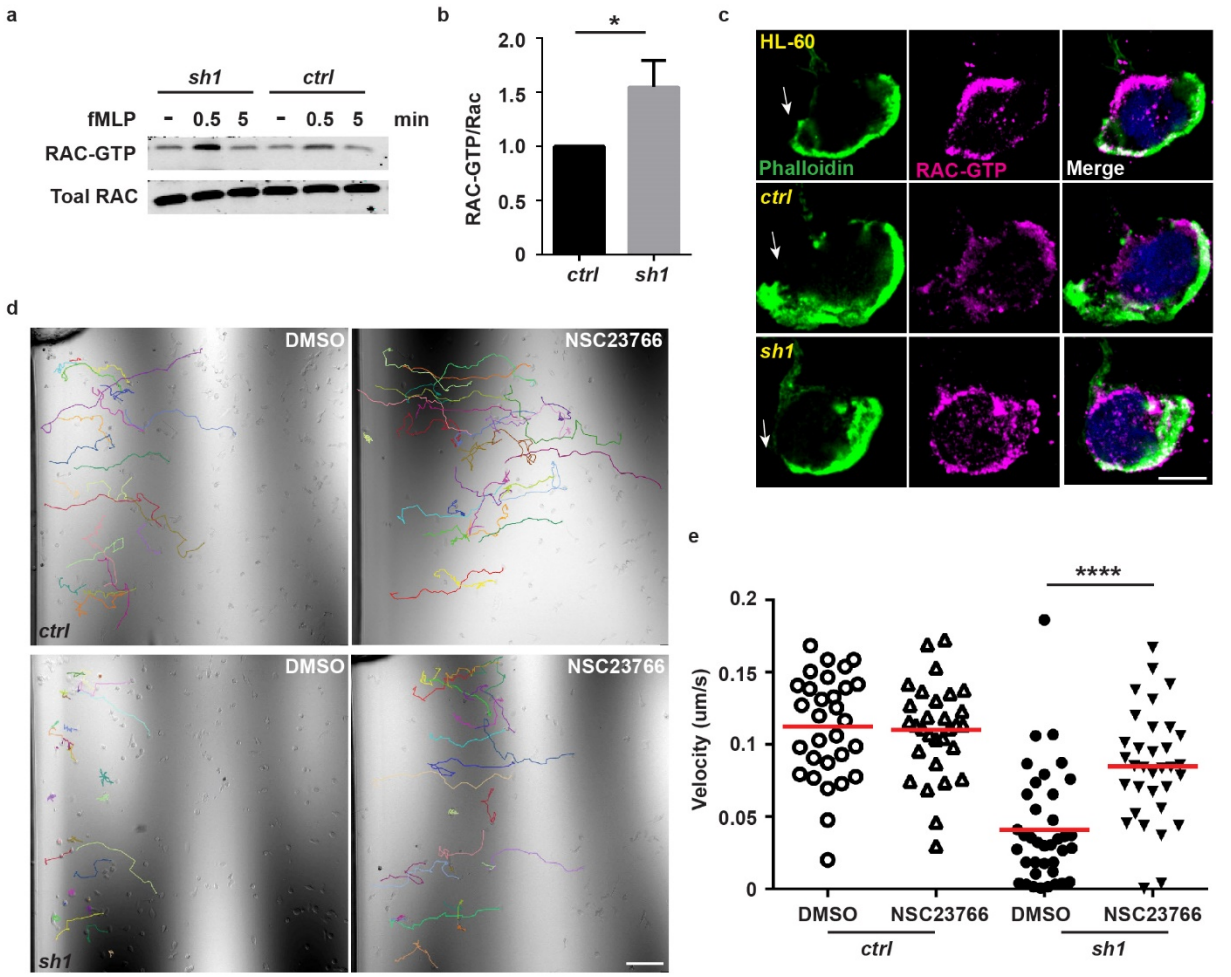

Figure 4-9. MFN2 suppresses RAC overactivation in dHL-60 cells.

a) Western blot determining the amount of RAC-GTP and total RAC protein in dHL-60 treated with fMLP at indicated time points. b) Quantification of RAC activation 5 min after stimulation with fMLP. c) Immunofluorescence of F-actin and GTP-RAC in indicated cell lines 3 min after stimulation with fMLP. Arrows: direction of cell polarization. d) Representative images with individual tracks. e) Quantification of velocity of neutrophil chemotaxis to fMLP in the presence of vehicle or the Rac inhibitor NSC23766. Data were pooled from three independent experiments in b. One representative result of three biological repeats was shown in e. *, $P<0.05$; ****, $P<0.0001$, unpaired *t*-test. Scale bar: 10 µm in c; 100 µm in d.

Mfn2 regulates mitochondria-ER tethering and calcium signaling in dHL-60 cells

We next investigated how MFN2 regulates RAC activation in neutrophils. Mfn2 localizes to both mitochondria and the ER membrane and regulates the tethering between the two organelles in MEF(Naon et al., 2016). To determine whether MFN2 mediates mitochondria-ER tethering in neutrophils, we determined the distribution of MFN2 in dHL-60 cells. MFN2 colocalized with both the mitochondria (stained with a TOMM20 antibody) and the ER (stained with a CALNEXIN antibody), and the Manders' colocalization coefficiency was 0.60±0.085 and 0.69±0.13, respectively (Fig. 4-10a, b). Mitochondria colocalized with the ER (Manders' colocalization coefficiency 0.52±0.097) and distributed throughout the cell body (Fig. 4-10a, b). The contact site between the mitochondria and the ER was also visualized using electron microscopy in dHL-60 cells (Fig. 4-11). When MFN2 was inhibited, mitochondria lost their structure and accumulated in the middle of the cell body and formed a clumpy structure similar to that in Mfn2 KO MEFs(Chen et al., 2003). Together, these results suggest that MFN2 mediates mitochondria-ER tethering in neutrophils.

The close proximity of the ER and the mitochondria regulates multiple cellular signaling pathways including calcium homeostasis(de Brito and Scorrano, 2008). Indeed, *MFN2*-deficient dHL-60 cells exhibited higher levels of cytosolic Ca^{2+} and reduced mitochondrial Ca^{2+} levels after fMLP stimulation (Fig. 4-10c, d). Furthermore, mitochondrial membrane potential and the ROS level in mitochondria were also reduced when MFN2 was depleted, especially post fMLP stimulation (Fig. 4-12a-d). This is consistent with the notion that mitochondrial Ca^{2+} activates the electron transportation chain(Glancy et al., 2013). On the contrary, the ATP levels were not affected in the MFN2 knock down dHL-60 cells (Fig. 4-12e), in line with the observation that mitochondria are not a major source of ATP in neutrophils(Amini et al., 2018; Borregaard and Herlin, 1982). We attempted to buffer cytosolic Ca^{2+} using BAPTA to determine whether elevated cytosolic Ca^{2+} is responsible for the chemotaxis defects in MFN2 knock down cells. However, a global cytosolic Ca^{2+} inhibition abrogated the ability of dHL-60 to migrate (Fig. 4-13), consistent with the previous observation that cytosolic Ca^{2+} possibly is tightly regulated spatially and/or temporally for neutrophil migration(Mandeville and Maxfield, 1997; Marks and Maxfield, 1990). In summary, depletion of *MFN2* alters cellular Ca^{2+} homeostasis but not ATP in neutrophils.

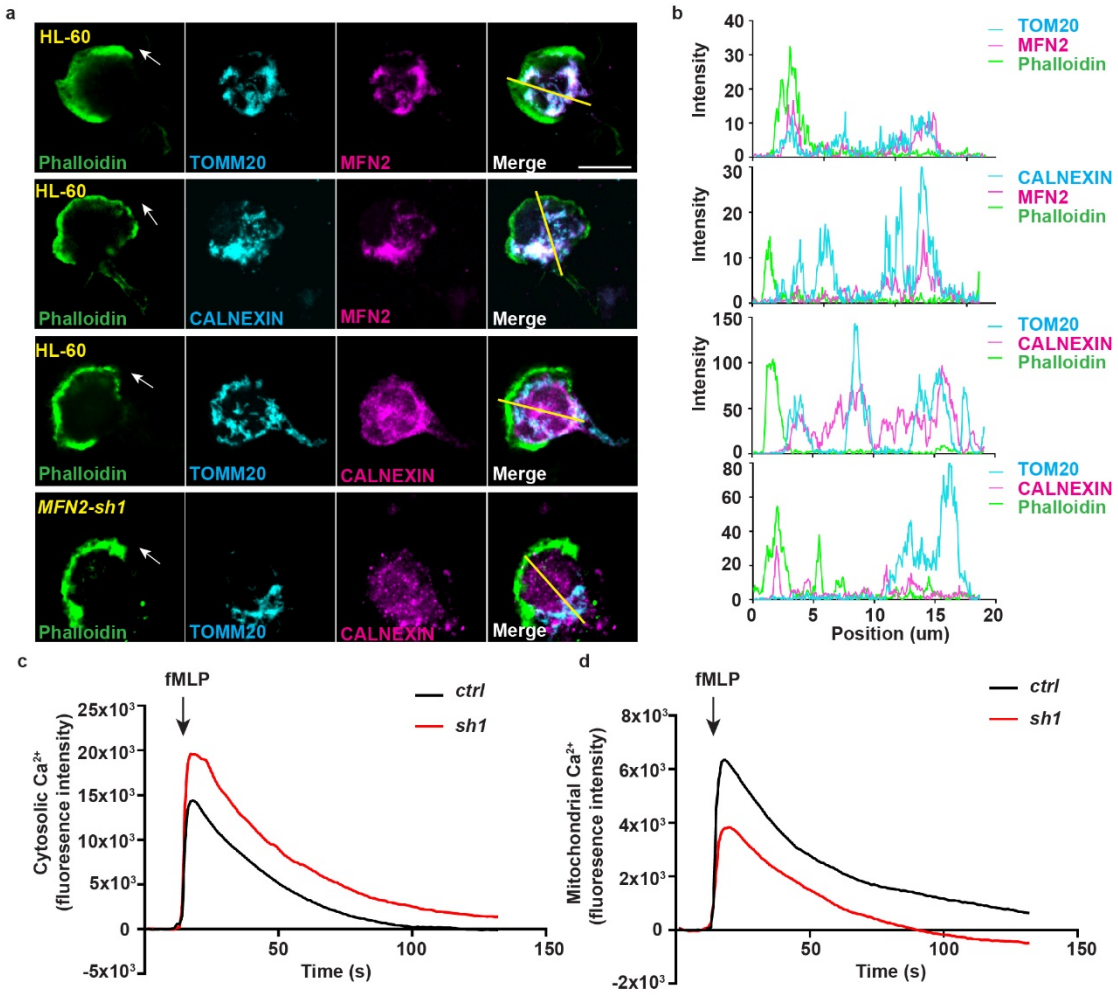

Figure 4-10. MFN2 regulates ER-mitochondria interaction and intracellular Ca^{2+}.

a) Immunofluorescence of F-actin (phalloidin), mitochondria (TOMM20), MFN2 and ER membrane (CALNEXIN) in indicated cells 3 min post fMLP stimulation. Arrows: direction of cell polarization. b) Plot profiles of the fluorescence intensity (MFI) along the corresponding yellow lines in a. c) Cytosolic Ca^{2+} in the control or MFN2 knockdown cell lines after fMLP stimulation. d) Mitochondrial Ca^{2+} in the control or MFN2 knockdown cell lines after fMLP stimulation. One representative result of three biological repeats is shown in c and d

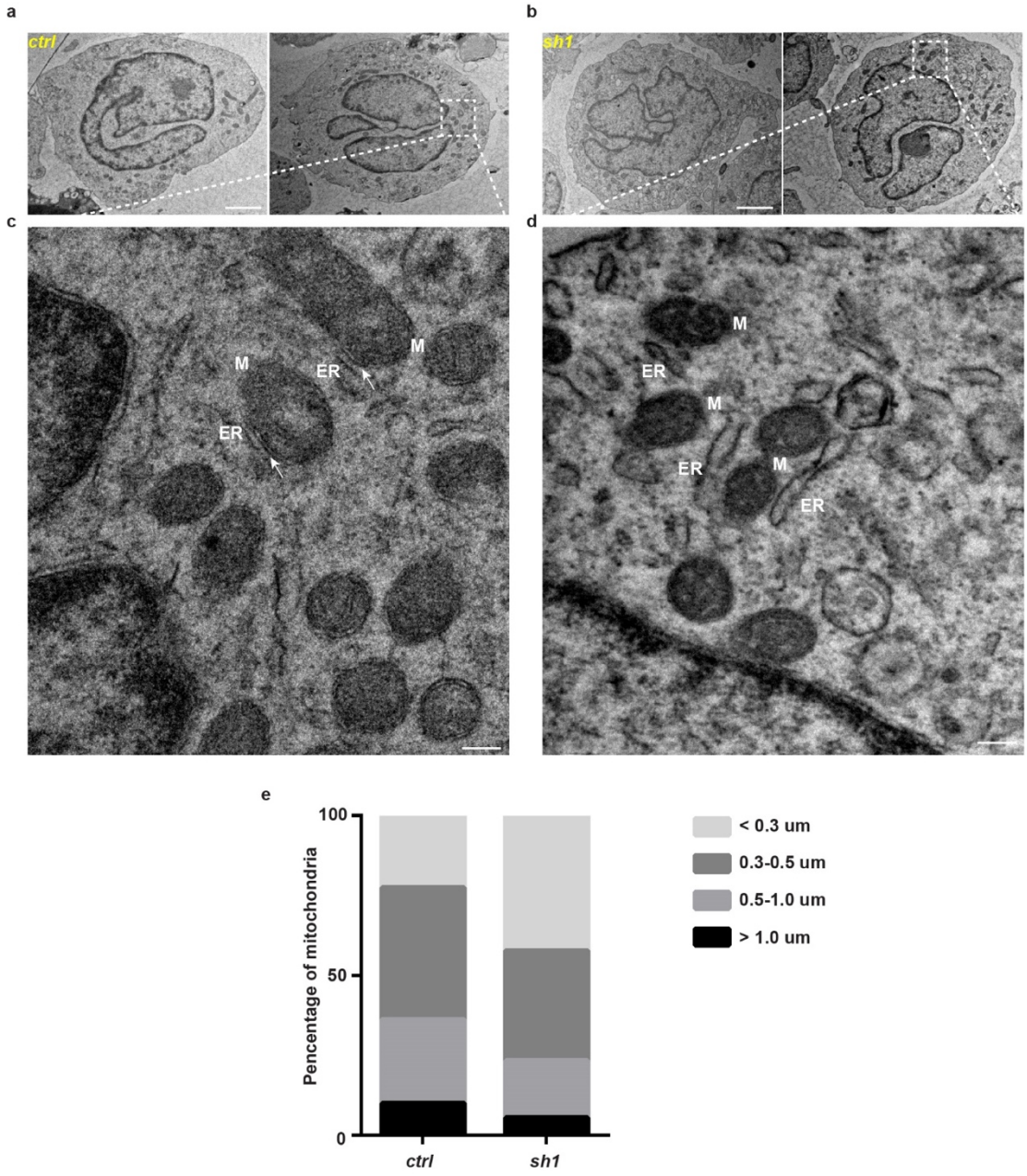

Figure 4-11. Electron microscopy of mitochondria and ER in MFN2 knock down dHL-60 cells.

a, b) Representative electron microscopy images of control and MFN2 knockdown dHL-60 cells. c, d) Enlarged images of the white box in a) and b). M: mitochondria, ER: endoplasmic reticulum. White arrows: contact sites between mitochondria and ER. e) Quantification of the length of mitochondria in control and *MFN2-sh1* dHL-60 cells. Scale bar: 2 μm in a and b; 0.2 μm in c and d.

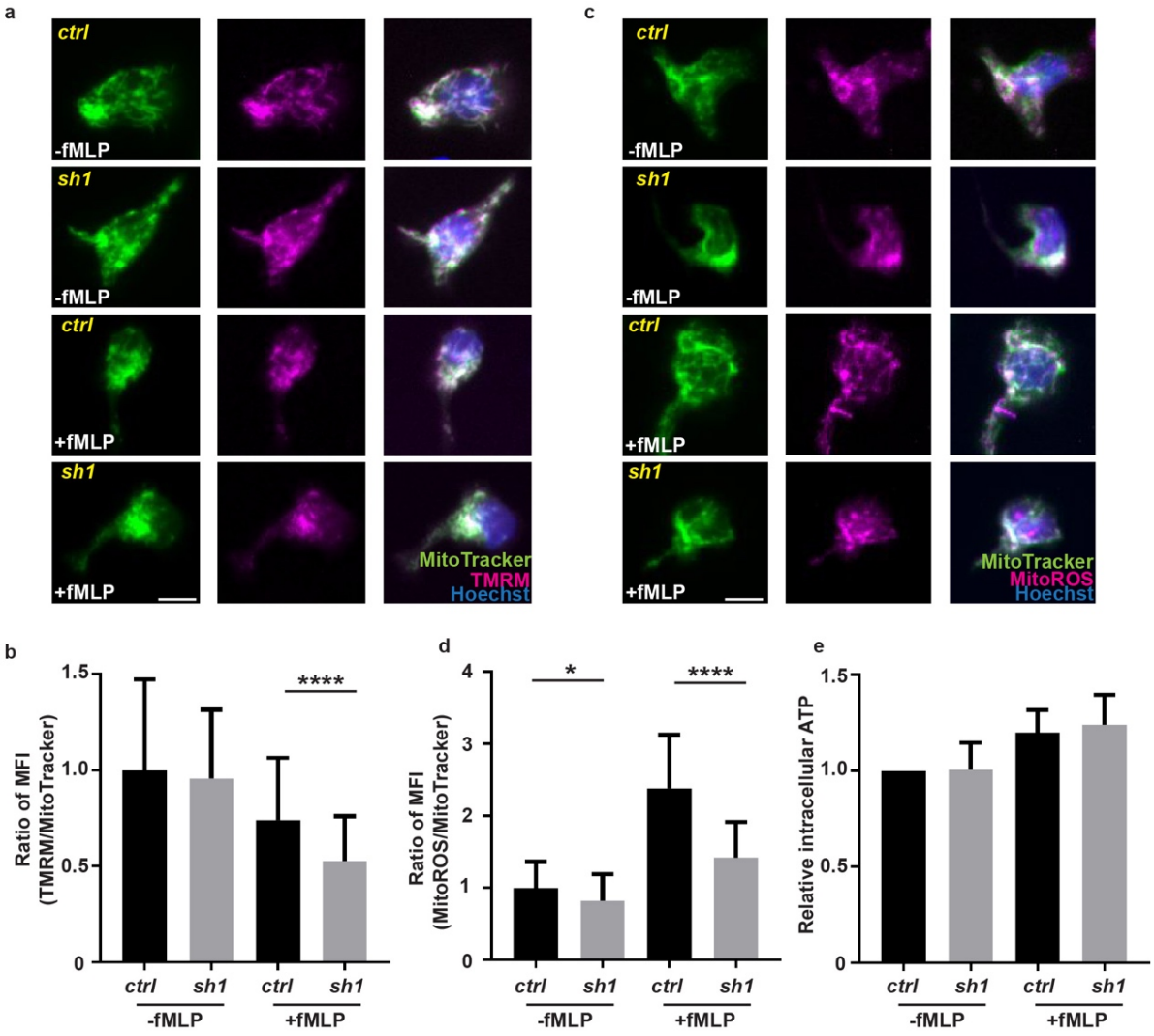

Figure 4-12. MFN2 regulates mitochondrial membrane potential and ROS, but not ATP in dHL-60 cells.

a) Fluorescence of mitochondria (MitoTracker), membrane potential (TMRM), and nucleus (Hoechst) in the control or *MFN2* knockdown cell lines with or without treatment of fMLP for 3 min. b) Quantification of the mean fluorescence intensity of TMRM normalized with MitoTracker. c) Fluorescence of mitochondria (MitoTracker), mitochondrial ROS (MitoROS), and nucleus (Hoechst) in indicated cells with or without treatment of fMLP for 3 min. d) Quantification of mean fluorescence intensity of MitoROS normalized with MitoTracker. e) Quantification of total cellular ATP levels with or without treatment of fMLP for 3 min.*, $P<0.05$; ****, $P<0.0001$, by unpaired *t*-test. Scale bar: 10 μm in a and c.

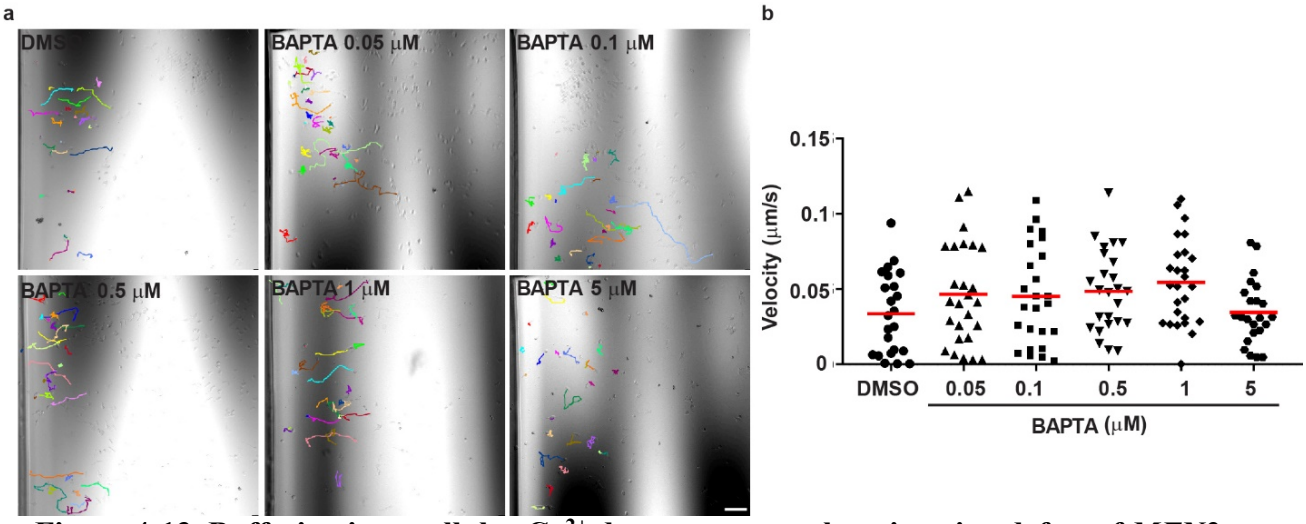

Figure 4-13. Buffering intracellular Ca^{2+} does not rescue the migration defect of *MFN2* knockdown dHL-60 cells.

a) Representative tracks and b) Quantification of MFN2 knockdown dHL-60 cells migrating toward fMLP in the presence of indicated concentrations of BAPTA. One representative result of three repeats is shown. Scale bar: 100 μm

MFN2 orchestrates the activation of CaMKII and TIAM2 to control neutrophil migration

Our data so far suggested that MFN2 regulates neutrophil adhesion to endothelium and adhesive migration, via suppressing Rac over-activation and possibly excessive levels of cytosolic Ca^{2+}. In the literature, several pathways have been identified to link cytosolic Ca^{2+} to focal adhesion dynamics and Rho GTPases. In fibroblasts, elevated Ca^{2+} facilitates focal adhesion disassembly by triggering the activation of Ca^{2+}/calmodulin-dependent protein kinase, CaMKII(Easley et al., 2008). CaMKIIγ is the predominant form of CaMKII in HL-60 cells which regulates differentiation of myeloid leukemia cells(Si et al., 2007). However CaMKII's role in neutrophil adhesion or migration is not characterized. We first visualized the active, phosphorylated CaMKII and focal complexes in polarized control and *MFN2* knock down dHL-60 cells. The number of PAXILLIN positive adhesion complexes was reduced in *MFN2*-depleted cells, especially at the cell front (Fig. 4-14a, b). Furthermore, the activated phosphorylated CaMKII colocalized with PAXILLIN and was significantly increased in *MFN2*-depleted cells (Fig. 4-14a, c). In addition, AIP, an inhibitor targeting the catalytic activity of CaMKII, was able to restore cell adhesive migration in *MFN2*-deficient cells, at least partially (Fig. 4-14e, f), indicating that MFN2 regulates the activation of CaMKII in neutrophils.

CaMKII phosphorylates Tiam1, a guanine nucleotide exchange factor of Rac, and enhances its nucleotide exchange activity, although the phosphorylation sites are unknown(Fleming et al., 1999a). Tiam1 promotes focal adhesion disassembly in fibroblasts(Rooney et al., 2010). In primary murine neutrophils, Tiam2 regulates cell motility also by triggering focal adhesion disassembly(Boespflug et al., 2014). We next assessed the function of TIAM2 in our system. TIAM2 formed puncta that colocalized with PAXILLIN which is distributed throughout the cell body including the leading edge of dHL-60 cells (Fig. 4-14d). Additionally, the TIAM inhibitor CAS1090893 restored adhesive migration in *MFN2*-depleted cells (Fig. 4-14e, f). Altogether, our data support a model that MFN2 suppresses the level of elevated cytosolic Ca^{2+} upon chemokine stimulation. Excessive Ca^{2+} in turn triggers over activation of CaMKII and its downstream target TIAM2, leading to RAC-mediated focal adhesion disassembly and impaired neutrophil adhesion (Fig. 4-14g).

Figure 4-14. MFN2 regulates adhesions through CaMKII and TIAM2 in dHL-60 cells.

a) Immunofluorescence of F-actin (phalloidin), PAXILLIN, p-CaMKII in indicated cell lines 3 min post fMLP stimulation. b) Quantification of PAXILLIN puncta at the leading edge of cells. c) Quantification of mean fluorescence intensity of p-CaMKII in the cell body. d) Immunofluorescence of F-actin (phalloidin) and TIAM2 in indicated dHL-60 cells treated with fMLP. Arrows: the direction of cell polarization; Arrow heads: the close proximity of PAXILLIN and pCAMKII or TIAM. e) Quantification of the velocity and f) representative tracks of dHL-60 cells migrating to fMLP in the presence of vehicle, the CaMK inhibitor AIP or the TIAM inhibitor CAS 1090893. Data were pooled from a total of 17 cells (in b) and 10 cells (in c) in three independent experiments in b and c. One representative result of three biological repeats is shown in e. *, $P<0.05$; **, $P<0.01$, unpaired *t*-test in b and c. *, $P<0.05$; ***, $P<0.001$, one-way ANOVA in e. Scale bar: 10 μm in a and d; 100 μm in f

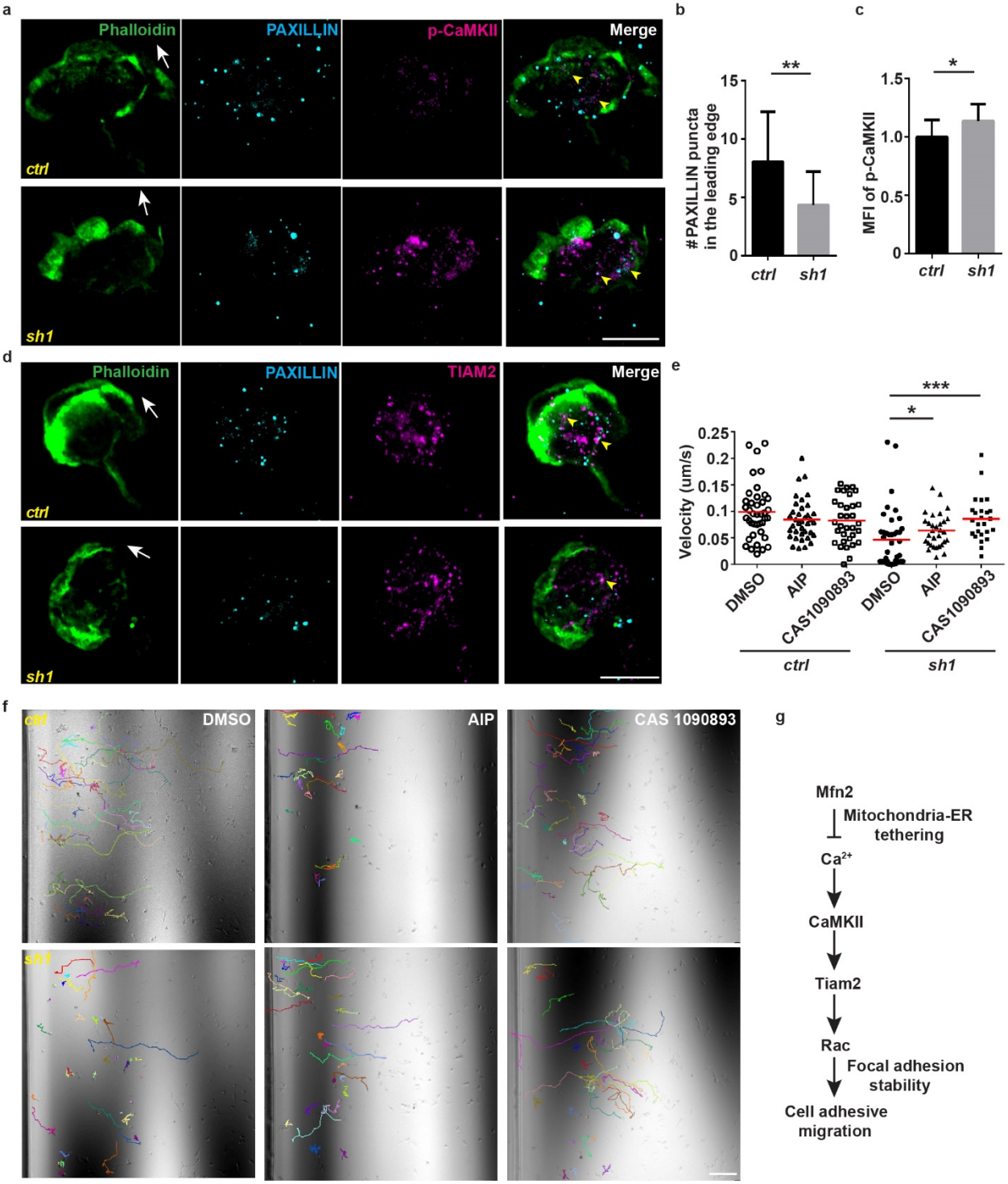
a
Phalloidin
PAXILLIN
p-CaMKII
Merge
ctrl
sh1
b
**
#PAXILLIN puncta in the leading edge
15
10
5
0
ctrl
sh1
c
*
MFI of p-CaMKII
1.5
1.0
0.5
0
ctrl
sh1
d
Phalloidin
PAXILLIN
TIAM2
Merge
ctrl
sh1
e
***
*
Velocity (um/s)
0.25
0.2
0.15
0.1
0.05
0
DMSO
AIP
CAS1090893
DMSO
AIP
CAS1090893
ctrl
sh1
f
ctrl
DMSO
AIP
CAS 1090893
sh1
g
Mfn2
Mitochondria-ER tethering
Ca2+
CaMKII
Tiam2
Rac
Focal adhesion stability
Cell adhesive migration

Discussion

Here we report that Mfn2 is crucial for neutrophil adhesion and adhesive migration, providing evidence that Mfn2 regulates the actin cytoskeleton and cell migration. By maintaining the tether between the mitochondria and ER, Mfn2 orchestrates intracellular Ca^{2+} signaling and regulates Rac activation. We also provide evidence that the Ca^{2+}-dependent kinase CaMKII and its substrate Tiam2 are downstream effectors of Mfn2, regulating the activation of Rac in neutrophils to modulate the stability of focal adhesion and cell migration. Therefore, we have identified the mechanism how Mfn2 regulates neutrophil adhesive migration, and highlighted the importance of mitochondria and their contact with the ER in neutrophils.

Studies using knockout mice and cell culture have concluded that Mfn1 and Mfn2 possess unique functions, although both mediate mitochondrial outer membrane fusion(Chen et al., 2003). Our data that only MFN2, but not MFN1, is required for neutrophil adhesive migration supports that mitochondrial fusion is not likely important for neutrophil migration. Our observation goes against a body of literature that mitochondrial fission promotes cell migration in other cell types(Campello et al., 2006; Zhao et al., 2013). Alternatively, we propose a model that, in neutrophils, the interaction of mitochondria with the ER is more critical than a fused network. Although MFN2 is not the only protein that can mediate the mitochondria-ER tether(Eisenberg-Bord et al., 2016), mitochondria and ER interaction was significantly reduced upon MFN2 deletion in dHL-60, suggesting that MFN2 is at least one of the critical tether proteins in neutrophils. The fused network of mitochondrial network in neutrophils is possibly a result of the abundant expression of the mitofusins. Mutations in human MFN2 cause Charcot-Marie-Tooth disease type 2A (CMT2A), a classical axonal peripheral sensorimotor neuropathy(Zuchner et al., 2004). MFN2 is also implicated in many other diseases such as cancer, cardiomyopathies, diabetes and Alzheimer's disease(Filadi et al., 2018). Currently, over 100 dominant mutations in the *MFN2* gene have been reported in CMT2A patients though how these mutations lead to disease is still largely unknown. The challenges in MFN2 research are that MFN2 regulates mitochondrial fusion and a plethora of cellular functions such as mitochondrial dynamics, transport, mtDNA stability, lipid metabolism and survival(Chandhok et al., 2018). In addition, gain-of-function and loss-of-function mutations are reported that affect different aspects of cellular functions(Chandhok et al., 2018). Our findings provide a new direction to understand the consequences of MFN2 deficiency in disease pathology, namely the actin cytoskeleton and Rac. Our findings also imply a possibility that the defect in

immune cell migration in humans may affect immunity or chronic inflammation and regulate the progression of the aforementioned diseases. Future work will be required to carefully evaluate the individual mutations of MFN2 identified in human diseases in immune cell migration. It is possible that mutations disrupting mitochondria-ER tethering, but not membrane fusion, result in defects in regulating cell adhesion and the cytoskeleton.

Our conclusions present a significant departure from the prevailing focus of bioenergy, in other word ATP, in cell migration. In many cell types, including neutrophils, the relevance of mitochondria-derived ATP in cell migration is emphasized(Bao et al., 2015; Bao et al., 2014). A recent report has confirmed the established literature that mitochondria do not provide ATP in neutrophils(Amini et al., 2018). Intriguingly, OPA1 deletion suppresses the production of neutrophil extracellular traps and alters the cellular ATP levels by indirectly suppressing glycolysis. In contrast, MFN2 deletion does not affect ATP levels (Fig. 4-12) or affect neutrophil extracellular trap formation(Amini et al., 2018), suggesting again distinct biological functions of OPA1 and MFN2, although both proteins regulate mitochondrial shapes. In vascular endothelial cells, mitochondria also serve as signaling rather than energy-producing moieties(Lugus et al., 2011). In our study, in addition to the altered Ca^{2+} level, mitochondrial membrane potential and ROS, both critical for neutrophil chemotaxis and migration(Fossati et al., 2003; Zhou et al., 2018), were reduced in stimulated *MFN2*-deficient dHL-60 cells. It remains to be determined whether the modest decreases in mitochondria membrane potential or ROS contribute to the defect of neutrophil migration upon MFN2 deletion.

Cell migration requires temporally and spatially regulated distribution of cytoskeleton networks, adhesion structures(Hind et al., 2016) and Rho family GTPases. During neutrophil migration, Rac is well appreciated to localize to the front of cells(Houk et al., 2012) where it nucleates branched actin to generate lamellipodia and membrane protrusion(Ridley, 2001). Recently, Fayngerts *et al* have developed a method to stain Rac-GTP and concluded that Rac-GTP enriches at the leading edge in both murine neutrophils and dHL-60 cells(Fayngerts et al., 2017a), without F-actin or other leading edge marker co-stained. In our current study, we observed a similar pattern of Rac-GTP staining, but noticed that active Rac does not necessarily localize to cell protrusions labeled with F-actin. This observation is also in line with live neutrophil imaging using Rac FRET reporter mice where Rac activation oscillates between cell front and rear(Johnsson et al., 2014). The

function of Rac in the cells is possibly related to its ability to trigger focal adhesion disassembly(Sander et al., 1999; Zhao et al., 2000). Nascent adhesions and focal complexes, prominent in highly motile cells like leukocytes (reviewed in(Huttenlocher and Horwitz, 2011)), may be required to generate an anchor for the polymerizing actin to overcome the membrane tension which allows cells to move forward. Integrin-mediated adhesions also dissemble at the rear to allow tail detachment. Conceptually, it makes sense that Rac is activated at both the front and rear to dissemble adhesion structures to regulate cell migration.

In neutrophils, there are four families of Rac-GEFs, including the Dbl-type P-Rex, Vav, Tiam and a structurally-unrelated DOCK family, with the Tiam2 least characterized(Pantarelli and Welch, 2018). Tiam1 localizes to focal adhesions via direct binding to Talin where it mediates Rac activation and promotes cell spreading and adhesion turnover(Wang et al., 2012). In our study, we observed fewer focal adhesions in *MFN2*-deficient neutrophils. The pharmacological inhibitor CAS1090893, which disrupts the interaction between Tiam and Rac, reversed the migration defect of *MFN2*-deficient neutrophils, indicating that Tiam is regulated by MFN2 in neutrophils. Indeed, blocking Tiam2 stimulated focal complex formation in murine neutrophils(Boespflug et al., 2014) and skin papilloma cells(Rooney et al., 2010). In addition, constitutively-active Tiam2 led to accumulation of adhesion structures around the cell periphery(Rooney et al., 2010), a phenotype also observed in *Mfn2-null* MEFs, further supporting that Tiam is over activated in cells lacking Mfn2.

Our result in leukocyte is consistent with previous work in murine fibroblasts(de Brito and Scorrano, 2008) that knocking out Mfn2 results in excessive cytosolic Ca^{2+} and defective mitochondrial calcium uptake. Intriguingly, blocking mitochondrial calcium import by inhibiting the mitochondria uniporter resulted in the reduction of the ER and cytosolic Ca^{2+} pools and a migration defect(Prudent et al., 2016), albeit with different mechanisms. It has been well-established that elevation of Ca^{2+} induces focal adhesion disassembly in multiple cell types(Conklin et al., 2005; Giannone et al., 2002), although the mechanism is less clear. In neutrophils, it was noted that cytosolic Ca^{2+} is required for neutrophils to detach from the substrates(Mandeville and Maxfield, 1997). Our results suggest that the CaMKII-Tiam2-Rac axis is a major pathway regulated by Mfn2 and cytosolic Ca^{2+} to regulate focal adhesion disassembly and neutrophil migration. Although cytosolic Ca^{2+} triggers the activation of Rac(Price et al.,

2003a), previous work in neutrophils suggests that Rac activation was independent of cytosolic Ca^{2+}(Geijsen et al., 1999; Price et al., 2003a). This discrepancy could be explained with the differences in assay conditions (suspension vs. adhesion) or Ca^{2+} levels (elevation vs. reduction). It remains to be determined which residues on Tiam2 are phosphorylated by CaMKII that lead to a conformational change and activation of Tiam family GEFs(Fleming et al., 1999b). Additional characterizations are also needed to determine whether other calcium sensitive molecules, such as Calcineurin, myosin light chain kinase, PKC/RhoGAP and Calpain(Franco et al., 2004; Hendey et al., 1996; Lee et al., 2005; Price et al., 2003a), are regulated by Mfn2 to regulate focal adhesion dynamics in neutrophils.

In summary, by suppression of Mfn2 in different models, we have discovered an essential role Mfn2 plays in neutrophil adhesion and migration, and determined the downstream mechanism, which may provide insights and potential therapeutic strategies for the treatment of inflammatory diseases and mitochondrial diseases

CHAPTER 5. MATERIALS AND METHODS

Animals

The zebrafish and mice experiments were conducted in accordance to the internationally accepted standards. The Animal Care and Use Protocols were approved by The Purdue Animal Care and Use Committee (PACUC), adhering to the Guidelines for Use of Zebrafish and Mice in the NIH Intramural Research Program (Protocol number: 1401001018 and 1803001702, respectively). To generate transgenic zebrafish lines, plasmids with the tol2 backbone were coinjected with Tol2 transposase mRNA into embryos of the AB strain at one-cell stage. All mice used in this study were purchased from Jackson Laboratories. Conditional *Mfn2* knockout mice (B6.129(Cg)-*Mfn2*^{tm3Dcc}/J) were crossed to S100A8-Cre (B6.Cg-Tg(S100A8-cre, -EGFP)1Ilw/J) transgenic mice to obtain a homozygous floxed *Mfn2* alleles with or without the Cre. All mice were used at age 6-12 weeks, and both male and female were used for experiments.

To generate a miR-223 deficient fish line, two individual single guide RNAs (sgRNAs) targeting *pre-mir-223* were designed: sgRNA1 binding site: 5'-TTAGAGTATTTGACAGACTG-3', and sgRNA2 binding site: 5'-TTTGTCAAATACCCCAAGAG-3'. The T7 promoter and the scaffold were added using overlapping PCR with the following primers listed from 5' to 3':
sgRNA1-P1:
GCGGCCTCTAATACGACTCACTATAGGGTTAGAGTATTTGACAGACTGGTTTTAGAG
CTA, sgRNA1-P2:
TGACAGACTGGTTTTAGAGCTAGAAATAGCAAGTTAAAATAAGGCTAGTCCGTTATC
AAC, sgRNA1-P3:
GATCCGCACCGACTCGGTGCCACTTTTTCAAGTTGATAACGGACTAGCCTTATTTTA
ACT; sgRNA2-P1:
GCGGCCTCTAATACGACTCACTATAGGGTTTGTCAAATACCCCAAGAGGTTTTAGAG
CTA, sgRNA2-P2:
ACCCCAAGAGGTTTTAGAGCTAGAAATAGCAAGTTAAAATAAGGCTAGTCCGTTAT
CAAC, sgRNA2-P3:
GATCCGCACCGACTCGGTGCCACTTTTTCAAGTTGATAACGGACTAGCCTTATTTTA
ACT.

Single guide RNAs were *in vitro* transcribed using MEGAshortscript T7 kit (Invitrogen) with the purified PCR products as templates. To make *Cas9* mRNA, the plasmid pT3TS-nCas9n (Addgene Plasmid #46757) (Jao et al., 2013) was linearized by XbaI and purified. *Cas9 mRNA* was generated using mMESSAGE mMACHINE T3 kit (Invitrogen). A mix of *sgRNA1* (100 ng/µl), *sgRNA2* (100 ng/µl) and *Cas9 mRNA* (150 ng/µl) was injected into one-cell stage embryos. The embryos were raised to sexual maturity and the F1s were screened by sequencing the *mir-223* locus. The homozygous mutant were obtained after several generations of backcross and incross.

To generate transgenic zebrafish lines, plasmids containing the tol2 backbone were coinjected with transposase mRNA into embryos at one-cell stage as described (Deng et al., 2011). The construct tol2-*lyzC*-Gal4-Vp16-*cyrs*-CFP was generated with Gateway Cloning (Thermo Fisher) using the tol2 kit (Kwan et al., 2007) to make *Tg(lyzc: Gal4-Vp16; crys: CFP)*^{pu8}. Founders were screened with green eyes.

To generate a miR-223 over expression line, *Tg(lyzC: RFP-miR-223)*^{pu9}, a 317 bp genomic DNA sequence containing miR-223 was PCR amplified using the following primers listed from 5' to 3': forward CTGGCAGTACGGGCTCAGGAGGAAGAGGGAGGAGTAAAATTGAAT, reverse TAACAGCAGTTGGCTAATGAATGTTGTCATCCTCCACATTTTGCA, and cloned into the BbsI site in the intron of the vector (De Rienzo et al., 2012). GFP was replaced by RFP and then inserted into a tol2 backbone with *lyzC* promoter. A transgenic line expressing the empty backbone, *Tg(lyzC: RFP)*^{pu10} was generated as the control.

To generate miR223 sponge line, *Tg(krt4: RFP-miR-223 sponge)*^{pu12}, a sequence containing six copies of bulged miR-223 binding sites was synthesized as a gBlocks Gene Fragment (Integrated DNA Technologies) and inserted downstream of RFP in a pME construct. The final construct was generated by Gateway Cloning. Founders were selected with red apical epithelial cells. A line with RFP *Tg(krt4: RFP)*^{pu13} was made as the control. The line *Tg(krt4: GFP)*^{pu11} was also generated for cell sorting. Multiple founders were obtained for each line and their offspring display similar phenotypes.

Cell Culture

HEK-293T cells, HBEC and H441 were obtained from American Type Culture Collection (ATCC), and maintained in their specific media in 37°C, 5% CO2 incubator. HEK-293T cells were cultured in 10%FBS 4.5g/glucose DMEM with sodium bicarbonate. HBEC cells were cultured in Keratinocyte Serum Free Media (KSFM), supplemented with 50µg/ml Bovine pituitary extract (BPE), 5ng/µl Epidermal growth factor (EGF) and 1X Penicillin-Streptomycin (PS). H441 cells were cultured in RPMI 1640 Medium supplemented with 10%FBS and 1XPS. Cells were checked monthly for mycoplasma using the e-Myco plus Mycoplasma PCR Detection Kit (Bulldog Bio 25234).

A clonal HL-60 line was a generous gift from Dr. Orion D. Weiner (UCSF). HEK293T, *wild-type*, *Mfn2-null* and *Mfn1-null* MEFs were purchased from American Type Culture Collection (ATCC). HUVEC was from Sigma-Aldrich (200P-05N). All cells were maintained in their specific media at 37°C with 5% CO_2. HL-60 cells were cultured in RPMI-1640 (Corning) with 10% FBS (Minipore), 25 mM HEPES, 1% sodium bicarbonate, and 1% sodium pyruvate. MEF cells were cultured in 10%FBS, 4.5g/glucose DMEM (Corning) with sodium bicarbonate. HUVEC was cultured in Endothelial cell Growth Media (R&D SYSTEMS, CCM027). HL-60 cells were differentiated with 1.5% DMSO for 5-6 days. Cells were checked monthly for mycoplasma using the e-Myco plus Mycoplasma PCR Detection Kit (Bulldog Bio 25234).
To generate knocking down lines in HL-60 cells, pLKO.1 lentiviral constructs with shRNA was obtained from Sigma-Aldrich (*MFN2-sh1*:TRCN0000082684, *MFN2-sh2*: TRCN0000082687, *MFN1-sh*: TRCN0000051837), and SHC 003 was used as a non-targeting control. MFN2 rescue construct was generated by replacing GFP with *sh1*-resistant *MFN2*. Primers MFN2r-F: CAAGTGTATTGTGAAGAGATGCGTGAAGAGCGGCAAG and MFN2r-R: TTCACAATACACTTGTTGCTCCCGAGCCGCCATG was used to make *sh1*-resistant *MFN2* with Mfn2-YFP (addgene #28010) as the template. Primers pLKO-F: AATTCTCGACCTCGAGACAAATGGC and pLKO-R: GGTGGCGACCGGGAGCGC were used to linearize the backbone of pLKO, and p-MFN2r-F: CTCCCGGTCGCCACCATGTCCCTGCTCTTCTCTCG and p-MFN2r-R: TCGAGGTCGAGAATTTTATCTGCTGGGCTGCAGGT were used to amplify *sh1*-resistant *MFN2* fragment. In-Fusion cloning (In-Fusion HD Cloning Plus kit, Clontech) was used to fuse the *sh1*-resistant *MFN2* fragment with the linearized backbone. pLKO.1 constructs together with

pCMV-dR8.2 dvpr (addgene #8455) and pCMV-VSV-G (addgene #8454) were co-transfected into HEK293T cells with Lipofectamin 3000 (Invitrogen L3000015) to produce lentivirus. Virus supernatant was collected at both 48 hpt and 72 hpt, and further concentrated with Lenti-X concentrator (Clotech 631232). HL-60 cells were infected with concentrated lentivirus in complete medium supplemented with 4 ug/ml polybrene (Sigma TR-1003-G) and then selected with 1 μg/ml puromycin (Gibco A1113803) to generate stable line.

Microinjection

For constructs, 1 nl of mixture containing 25 ng/ul DNA plasmid and 35 ng/μl Transposase mRNA was injected into the cytoplasm of one-cell stage embryos. For morpholinos, 3 nl of solution containing 200 μM *Pu.1* MO (5'-GATATACTGATACTCCATTGGTGGT-3') and 100 uM *Rac2* MO (5′-CCACCACACACTTTATTGCTTGCAT-3′) were injected into the yolk of one-cell stage embryos. For mRNAs, 500-600 pg *RFP* mRNAs, *TdTomato-CAAX* mRNAs or *RFP-miR-223 sponge* mRNAs were injected into the yolk of 4-cell stage embryos.

Tailfin wounding, Sudan black staining, Immunofluorescent staining, and TUNEL staining

Tailfin wounding, Sudan black staining, and immunofluorescent staining were carried out with 3 dpf embryos as described (Deng et al., 2011). Briefly, embryos were fixed in 4% paraformaldehyde in phosphate-buffered saline overnight at 4°C and stained with Sudan black, TUNEL label Mix (Roche), or double-immunostained for anti-GFP (abcam, ab13970) and anti-Tp63 (GeneTex, GTX124660) primary antibodies. Goat anti-Rabbit IgG (H+L), Alexa Fluor 568 (cat# A-11011) and Goat anti-Chicken IgY (H+L), Alexa Fluor 488 (cat# A-11039) (ThermoFisher) were used as the secondary antibodies, and DAPI (Sigma) stained nuclei. Neutrophils within 200 μm to the cut sites were quantified.

Isolation of RNA and quantitative PCR

Total RNA was purified with a mirVana miRNA purification Kit (ThermoFisher). For miRNA assays, miRNAs were reverse-transcribed using Universal cDNA Synthesis Kit II (Exiqon). miRNA qRT-PCR was performed with ExiLENT SYBR Green master mix (Exiqon). A LightCycler 96 Real-Time RCP system (Roche Life Science) was used for the assay. Results were normalized to U6 or miR-92a. Primers used in the assays are: miR-223-3p (205986), miR-142-3p

(204291), miR-92a (204258), dre-U6 (206999), and hsa-U6 (203907). For messenger RNAs, cDNAs were synthesized with Transcriptor First Strand cDNA Synthesis Kit (Roche). qRT-PCR was performed using FastStart Essential DNA Green Master (Roche). Results were normalized to *Rpl13a or Acta1b*. The efficiency of the primers were calculated using Real-time PCR Miner and corrected for the relative expression(Zhao and Fernald, 2005).

Primers used for qRT-PCR are listed from 5' to 3':
Cul1a: forward CAGTTCAAGAAGCACCTCACA, reverse GCTCAACACCTGAATGCTGA;
Cul1b: forward TCCTCCAACAAAACCCTGTT, reverse TGCTCCTCCAGCAATCGT;
Traf6: forward GCACTTTTGGATGTCGTGAA, reverse CATGTGCATCTGTGTAAACTCCT;
Tab1: forward CTAACGTAGGTGGTCAGAATCAGG, reverse AGTCTGGTCAGCTCGTCTTCA;
Cxcl8: forward GTCGCTGCATTGAAACAGAA, reverse CTTAACCCATGGAGCAGAGG;
Rpl13a: forward CTGAAACCCACACGCAAAT, reverse CAGCTTGGCCTTTTCCTTT;
Aimp1: forward ACGAGGCGAAAAAGATGAAA, reverse CACCTTCGCATCTTCCTGAG;
Cp: forward GCTCCGAGAACTCAAGAAACA, reverse GTGTCGGGACGAACCATT;
Acta1b: forward GCCTGAGGCAGTTTGTGAC, reverse GTCGTCACACATCTTGATGTATTCT.

Live imaging.

Time-lapse fluorescence images and NF-κB-GFP reporter images were acquired with AXIO Zoom V16 microscope (Zeiss). Embryos at 3 dpf were put on a glass-bottom dish. Images were analyzed using ImageJ. For GFP fluorescence intensity measurements, images within an experiment were collected using identical camera settings and background was subtracted with the rolling ball radius as 50. Mean fluorescence intensity of interested areas with identical size in one experiment was valued by Measurement in ImageJ and plotted in Prism (GraphPad) software. For confocal imaging, images were obtained using a laser-scanning confocal microscope (LSM 710, Zeiss) with a 1.0/20 x objective or a 2.0/40x water immersion objective lens.

Photoconversion assay

Photoconversion assays were performed as described (Yoo and Huttenlocher, 2011). Briefly, *Tg(miR-223$^{-/-}$, mpx-Dendra2)* embryos were wounded with a needle around the tailfin region at 3 dpf. At 1 hpw, neutrophils expressing Dendra2 at the wound were photoconverted into red by 405 nm laser using a laser-scanning confocal microscope (LSM 710, Zeiss) with a 1.0/20 x objective, and the number of photoconverted neutrophils was recorded. After 5 hours, the number of red neutrophils at the wound was counted. The percentage of neutrophils remaining at wound was calculated as the ratio of the number of red neutrophils at 6 hpw to the number of red neutrophils at 1 hpw.

Microarray

Embryos were collected before wounding and at 1 h and 6 h post wounding. Total RNAs were extracted with Trizol (Invitrogen) and further cleaned up with RNeasy MinElute kit (Qiagen). The quality and integrity of RNAs were confirmed using Agiloent Nano RNA QC chip (Sequencing Center of Purdue University). Transcriptomic microarray analysis was conducted using the one-color hybridization strategy to compare gene expression profiles among the different time points with a zebrafish V3 array (Agilent Technologies). Following hybridization, arrays were washed and scanned on an Agilent Technologies SureScan Microarray Scanner. Array image data was extracted using Agilent Feature Extraction Software and data was uploaded onto GeneSpring for statistical analysis. Microarray analysis was performed following MIAME guidelines. The data was deposited into Gene Expression Omnibus (GSE94996).

CRISPR screening

The high efficiency guides without off targeting were selected using CRISPRScan (Moreno-Mateos et al., 2015). Two individual sgRNAs were synthesized for each gene. 1 nl of solution containing 400 ng/µl sgRNAs and 400 ng/µl Cas9 protein (PNA, CP01) was injected into the cytoplasm of *miR-223$^{-/-}$* embryos at one-cell stage. When knock out two genes simultaneously, 200 ng/ul of sgRNAs for each gene were used. Tailfins were transected at 3 dpf, and embryos were fixed at 6 hpw. Neutrophil recruitment was measured and compared with embryos injected with *gfp* sgRNA. To determine the mutation efficiency of sgRNAs for *Myd88*, *Cul1a*, and *Cul1b,* injected embryos were collected at 3 dpf. The gene locus around the sgRNA binding sites of each

gene was PCR amplified and followed by library construction using Nextera and sequencing using an Illumina MiSeq 300 at the sequencing center of Purdue University.

Primers used to synthesize templates of sgRNAs are listed from 5' to 3':
gfp sgRNA forward:
TAATACGACTCACTATAGGCGAGGGCGATGCCACCTAGTTTTAGAGCTAGAAATAG
CAAG; *Myd88* sgRNA1 forward:
TAATACGACTCACTATAGGCGGCAGACTGGAGGACAGGTTTTAGAGCTAGAAATAG
CAAG; *Myd88* sgRNA2 forward:
TAATACGACTCACTATAGGAAAAGGTCTTGACGGACTGTTTTAGAGCTAGAAATAGC
AAG; *Caspa* sgRNA1forward:
TAATACGACTCACTATAGGGTACAGGTGGCTCCGGCTGTTTTAGAGCTAGAAATAGC
AAG; *Caspa* sgRNA2 forward:
TAATACGACTCACTATAGGCCGTGTTTGGGCCAGTGAGTTTTAGAGCTAGAAATAGC
AAG; *Il1b* sgRNA1 forward:
TAATACGACTCACTATAGGGATGTGGAGCGGAGCCTTGTTTTAGAGCTAGAAATAGC
AAG;
Il1b sgRNA2 forward:
TAATACGACTCACTATAGGGGCTGCAGGCCAGGTACGTTTTAGAGCTAGAAATAGC
AAG; *Crfb5* sgRNA1 forward:
TAATACGACTCACTATAGGAGTTCCGGTCACGGCGAGGTTTTAGAGCTAGAAATAGC
AAG; *Crfb5* sgRNA2 forward:
TAATACGACTCACTATAGGAGTGGCTGACGGTGTGTGGTTTTAGAGCTAGAAATAGC
AAG; *Crfb17* sgRNA1 forward:
TAATACGACTCACTATAGGGTGTGAGCTTCCAGGTGGGTTTTAGAGCTAGAAATAGC
AAG; *Crfb17* sgRNA2 forward:
TAATACGACTCACTATAGGGCATTATGGAACGAACATGTTTTAGAGCTAGAAATAGC
AAG; *Stat1a* sgRNA1 forward:
TAATACGACTCACTATAGGACCCCATGTGGCCGGTGGGTTTTAGAGCTAGAAATAGC
AAG; *Stat1a* sgRNA2 forward:
TAATACGACTCACTATAGGCCGAGGTGTTGAACCTGGGTTTTAGAGCTAGAAATAGC
AAG; *Stat1b* sgRNA1 forward:

TAATACGACTCACTATAGGTCTCCAGGTTCACGGTGGGTTTTAGAGCTAGAAATAGC
AAG; *Stat1b* sgRNA2 forward:
TAATACGACTCACTATAGGAGGATGTGTTGGCATACAGTTTTAGAGCTAGAAATAGC
AAG; *Jak2a* sgRNA1 forward:
TAATACGACTCACTATAGGGATGGAGTTCCTCCCGTTGTTTTAGAGCTAGAAATAGC
AAG; *Jak2a* sgRNA2 forward:
TAATACGACTCACTATAGGCGGCGGCGCCGGAGCCAGGTTTTAGAGCTAGAAATAG
CAAG; *Ifng1* sgRNA1 forward:
TAATACGACTCACTATAGGGCCCGATAATACACCTTCGTTTTAGAGCTAGAAATAGC
AAG; *Ifng1* sgRNA2 forward:
TAATACGACTCACTATAGGACACGCTTGCAAAGGATTGTTTTAGAGCTAGAAATAGC
AAG; *Ifng2* sgRNA1 forward:
TAATACGACTCACTATAGGGATGAAGCTACAAAGGAGGTTTTAGAGCTAGAAATAG
CAAG; *Ifng2* sgRNA2 forward:
TAATACGACTCACTATAGGTGCTCTTGTCTAGGTTCTGTTTTAGAGCTAGAAATAGC
AAG; *Irf3* sgRNA1 forward:
TAATACGACTCACTATAGGAGGTGCTGTCGGTGGTTTGTTTTAGAGCTAGAAATAGC
AAG;
Irf3 sgRNA2 forward:
TAATACGACTCACTATAGGATCCTGCTGGACCCCCAAGTTTTAGAGCTAGAAATAGC
AAG; *Irf7* sgRNA1 forward:
TAATACGACTCACTATAGGGGAAAGTGGGCAGTACGAGTTTTAGAGCTAGAAATAG
CAAG; *Irf7* sgRNA2 forward:
TAATACGACTCACTATAGGTGGAATTGCTCAACTTGGGTTTTAGAGCTAGAAATAGC
AAG; *Cul1a* sgRNA1 forward:
TAATACGACTCACTATAGGGTGTGACGAGGGCCGCAAGTTTTAGAGCTAGAAATAG
CAAG; *Cul1a* sgRNA2 forward:
TAATACGACTCACTATAGGGGAGGAGCTCAGTTTGTGGTTTTAGAGCTAGAAATAGC
AAG; *Cul1b* sgRNA1 forward:
TAATACGACTCACTATAGGGGGTGTTCTGGCCCCTGGGTTTTAGAGCTAGAAATAGC
AAG; *Cul1b* sgRNA2 forward:
TAATACGACTCACTATAGGGCGTCGGGAGTGTGATGAGTTTTAGAGCTAGAAATAG

CAAG. The reverse primer for all sgRNA templates is 5'-AAAAGCACCGACTCGGTGCCACTTTTTCAAGTTGATAACGGACTAGCCTTATTTTAACTTGCTATTTCTAGCTCTAAAAC-3'.

Dual luciferase reporter assays

The dual luciferase reporter assay was performed as described (Gonzalez-Martin et al., 2016). Briefly, *miR-223* was cloned into human expression vector pCDNA. The 3'UTR fragments of zebrafish *Cul1a*, *Cul1b*, *Traf6*, *Tab1*, and human *CUL1*, *TAB2* were cloned into the psiCHECK-2 vector (Promega). The pCDNA and psiCHECK-2 constructs were co-transfected into HEK293T cells using Lipofectamine 3000 (Invitrogen). After 48h, cells were lysed and luciferase activity was measured using the Dual Glo-Luciferase assay system (Promega, PF-E2920) on Synergy 2(Biotek). The renilla luciferase activity was normalized to the firefly luciferase activity. Three independent repeats were performed for each 3'UTR. The ratio of renilla luciferase activity to firefly luciferase activity of each 3' UTR for the control pCDNA vector was set as 1.

Primers used for amplifying 3'UTR are listed from 5' to 3':

dre-Cul1a: forward TAGGCGATCGCTCGAGACATTTCTTTGCTCCTCCAT, reverse TTGCGGCCAGCGGCCGCTACATACAGAAACTTTTAATCC;

dre-Cul1b: forward TAGGCGATCGCTCGAGAAACAACATCCTCTGGAGTT, reverse TTGCGGCCAGCGGCCGCTCAATATGTCAGTTTCCCAAA;

dre-Traf6: forward TAGGCGATCGCTCGAGGCAATTTTTTGTTTTCAGTCTTAAGTTCTC, reverse TTGCGGCCAGCGGCCGCACATTAAAACATTATTATTTATAGGACATGAG;

dre-Tab1: forward TAGGCGATCGCTCGAGCATCTGTGAGCACAGTCCGTCGTC, reverse TTGCGGCCAGCGGCCGCGTACTGCAGTAAACTGGTGTATTGTG;

hsa-CUL1: forward TAGGCGATCGCTCGAG CCCTTCTGGAAGGGTCTGACTGTG, reverse TTGCGGCCAGCGGCCGCTTGTACAGAAATCCTTTAATTTTCTTTATTTTCACAC;

hsa-TAB2: forward TAGGCGATCGCTCGAGGCCAAATGGCCCTGTATCTTCTC, reverse TTGCGGCCAGCGGCCGCTCCACATTAGAATATAAGTTTTTTAATTTTTAT.

NF-κB reporter assay

To generate a NF-κB reporter plasmid, five copies of NF-κB binding sites were cloned into psiCHECK2 (Promega) to control the expression of firefly luciferase (*hluc*+). HEK293T cells

were seeded in 12 well plates and transfected with 1 μg of the reporter plasmids and 250 ng of miR-223 over-expression plasmid or the vector control using Lipofectamine 3000 (Invitrogen). HBEC cells were seeded in 12 well plates and transfected with 500 ng of the NF-κB reporter, together with 250 ng of miR-223 over-expressing construct, 500 ng of the miR-223 sponge or corresponding control plasmids using FuGENE HD (Promega). After 48h, cells were stimulated with PBS or heat-killed *P. aeruginosa* for 6 hours. The cells were then lysed and luciferase activity was measured using the Dual Glo-Luciferase assay system (Promega, PF-E2920) on Synergy 2 (Biotek). The firefly luciferase activity was normalized to the renilla luciferase activity and further normalized with the PBS-treated vector control. Three independent repeats were performed.

Fluorescence activated cell sorting

Trypsin dissociated cells of *Tg(lyzC: GFP)(Vincent et al., 2016)*, *Tg(mpeg: Dendra2)(Vincent et al., 2016)*, *Tg(krt4: GFP)*^{pu11} and embryos injected with Tol2-*tp63*-AcGFP plasmid (a generous gift from Dr. Sandra Rieger, MDI Biological Laboratory) were sorted by FACS as described(Deng et al., 2011). The quality of sorting was demonstrated by RT-PCR amplifying different cell type markers using QIAGEN OneStep Ahead RT-PCR kit (Qiagen).

Primers are listed from 5' to 3':
mpeg: forward CTTTAATTCAGAGCCACGGAGGAGC, reverse GTAGACAACCCTAAGAAACCACAGG;
mpx: forward ACCAGTGAGCCTGAGACACGCA, reverse TGCAGACACCGCTGGCAGTT;
tp63: forward GGGATAAAAGGAAGAAAACTAGGG, reverse GCCCCAGGCTTGTATACTGA;
krt4: forward CTATGGAAGTGGTCTTGGTGGAGG, reverse CCTGAAGAGCATCAACCTTGGC;
myoD: forward CCTTGCTTCAACACCAACGACATG, reverse GTCATAGCTGTTCCGTCTTCTCGTC;
ef1a: forward TACGCCTGGGTGTTGGACAAA, reverse TCTTCTTGATGTATCCGCTGA.
3 dpf embryos of *Tg(lyzC:nls-cas9-2A-mCherry/U6a/c:control sgRNA)*^{pu15} or *Tg(lyzC:nls-cas9-2A-mCherry/U6a:polg sgRNA)*^{pu16} were digested with trypsin to prepare cell suspensions and sorted by FACS.

Translating ribosome affinity purification (TRAP)

Tissue-specific TRAP was performed as described (Heiman et al., 2014). Briefly, 25 µl/sample Dynabeads Protein G (Invitrogen; 100-07D) were collected on a magnetic rack and incubated with 10 µl anti-GFP antibody (Invitrogen A11122) for 2 hours at room temperature and then washed. More than 100 WT or *miR-223*$^{-/-}$ embryos injected with Tol2-*tp63*-GFP-L10a plasmid were collected at 1 hpw and homogenized by a prechilled Dounce homogenizer containing cell-lysis buffer on ice. Cell lysate supernatant was incubated with coated beads at 4˚C for 16-18h with end-over-end mixing on a tube rotator. After incubation, the beads were collected with a magnet and washed for four times with high-salt buffer. RNAs were eluted from beads and further purified by RNeasy MinElute kit (Qiagen). The quality of tissue-specific TRAP was identified by RT-PCR amplifying different cell type markers using OneStep Ahead RT-PCR kit (Qiagen). The quantification of the target genes was performed by one-step quantitative RT-PCR with SuperScript III Platinum one-step qRT-PCR kit (Invitrogen).

Plasmids

All constructs were generated by gateway cloning using LR Clonase II Plus enzyme (Invitrogen). The p5E-lyzC entry vector was generated by replacing the ubiquitin promoter with the *lyzC* promoter in pENTR5'_ubi (addgene #27320). pENTR5'_ubi was digested by Xho I and BamH I, and *lyzC* promoter was amplified with primers p5E-lyzC-F/R. In-Fusion cloning (In-Fusion HD Cloning Plus kit, Clontech) was used to fuse the *lyzC* fragment with the linearized backbone. To make pME-Cas9-2A-mCherry, Cas9 was amplified using pME-Cas9-T2A-GFP (addgene #63155) as the template with primers pME-Cas9-F/R. Primers 2A-mCherry-F/R were used to amplify 2A-mCherry. Both Cas9 and 2A-mCherry were fused into pME backbone linearized by Sal I and BamH I with In-Fusion cloning. For p3E-U6a plasmid, U6a was amplified by primers p3E-U6a-F/R using pU6a:sgRNA#2 (Addgene #64246) as the template and inserted into a p3E backbone with polyA. Similarly, both U6a and U6c (using pU6c:sgRNA#4 (Addgene #64248) as the template) were amplified and fused into the p3E backbone with polyA to generate p3E-U6a-U6c using primers p3E-U6ac-F/R and p3E-U6c-F/R, respectively.

A detailed protocol for cloning one or two sgRNAs into the backbones is included in the supplementary information. *rac2* (ENSDARG00000038010), *ndufs2* (ENSDARG00000007526), *uqcrc1* (ENSDARG00000052304*)*, *sod1* (ENSDARG00000043848) or *sod2* (ENSDARG00000042644) were cloned into p3E-U6a-U6c. The final constructs were assembled

using the gateway reactions with the destination vector (pDestTol2pA2) from the Tol2Kit (Kwan et al., 2007).

To generate p5E-DsRed-biUAS, DsRed-biUAS was amplified from pT2-pA-DsRed-T4-E1b-UAS-E1b-Htau40-p301L-PA-2 (a gift from Dr. Bettina Schmid) using primers DsRed-biUAS-F/R, and inserted into p5E backbone. For pME-Sod2-2A-Catalase construct, Sod2-2A-Catalase was amplified with primers Sod2-2A-Catalase-F/R using CMV-Sod2-2A-Catalase (addgene # 67635) as the template and fused into pME backbone. The destination vector pDestR4R2pA (Lawson Lab #465) was used to generate the final expression plasmids. Primers used were listed below (guide RNA sequences were indicated with underscores):

p5E-lyzC-F: GCCCTTAAAACTCGAGAGTTTGACTTGGGTTGATTAT

p5E-lyzC-R: CGCCCTTTTTGGATCCCTTTATCAAGACCAGTGGAG

pME-Cas9-F: CCCCCTCGAGGTCGACTCGCCACCATGGATAAGAAGTATAGCATC

pME-Cas9-R: CGTGGCTCCGGATCCCACCTTTCTCTTCTTCTTAG

2A-mcherry-F: GGATCCGGAGCCACGAAC

2A-mcherry-R: TAGAACTAGTGGATCCTTACTTGTACAGCTCGTCC

p3E-U6a-F: ATGATCCTCTAGATCGAGGTCTCTGACTAAAAAAGCACCGACTC

p3E-U6a-R: TTGCCTAGGGTCGACTTTCTCCAGCCTCGGTCATTCAG

p3E-U6ac-F: GAGGTCTCTGACTAAAAAAGCACCGACTC

p3E-U6ac-R: GTTGCCTAGGGTCGATTTCTCCAGCCTCGGTCATTCAG

p3E-U6c-F: ATGATCCTCTAGATCCCTTGGGTAGCAGCGAAGTC

p3E-U6c-R: TTAGTCAGAGACCTCGGGCCCGGTCTCTCCAATC

Polg guide-F: ATGGTGGTGTGGCTACGCAGTTTAAGAGCTATGCTGG

Polg guide-R: TAGCCACACCACCATCGAACCAAGAGCTGGAGGGAG

Rac2 guide-1-F:
GGCTGTATCCCAGAGTCCCGTTTAAGAGCTATGCTGGAAACAGCATAGC

Rac2 guide-1-R: ACAGGGTCTCGCATTGGCCCGAACTAGGAGCCTGGAGAACTGC

Rac2 guide-2-F: AATGCGAGACCCTGTGTTTAAGAGCTATGCTGGAAACAGCATAGC

Rac2 guide-2-R: CTCTGGGATACAGCCCGAACCAAGAGCTGGAGGGAGA

Ndufs2 guide-1-F:
GTGCATATGTCAGACCCGGGTTTAAGAGCTATGCTGGAAACAGCATAGCAAG

Ndufs2 guide-1-R:
CCTCAGCGCCAATGACACCCGAACTAGGAGCCTGGAGAACTGCTATATAAAC

Ndufs2 guide-2-F:
TCATTGGCGCTGAGGGTTTAAGAGCTATGCTGGAAACAGCATAGCAAGTTTAAATA
AG
Ndufs2 guide-2-R:
GTCTGACATATGCACCGAACCAAGAGCTGGAGGGAGAGCTATATATACCAG
Uqcrc1 guide-1-F:
GTAGTGGTGGTGCACACTGGTTTAAGAGCTATGCTGGAAACAGCATAG
Uqcrc1 guide-1-R:
CTCGGGAACATACTGCTTCCGAACTAGGAGCCTGGAGAACTGCTATATAAAC
Uqcrc1 guide-2-F:
CAGTATGTTCCCGAGGTTTAAGAGCTATGCTGGAAACAGCATAGCAAGTTTAAATAA
G
Uqcrc1 guide-2-R:
GTGCACCACCACTACCGAACCAAGAGCTGGAGGGAGAGCTATATATAC
Sod1 guide-1-F:
GTGGTGGTCGTCTGGCCTGGTTTAAGAGCTATGCTGGAAACAGCATAGCAAG
Sod1 guide-1-R:
GTGAAGTGACCGGCACCGCCGAACTAGGAGCCTGGAGAACTGCTATATAAAC
Sod1 guide-2-F:
TGCCGGTCACTTCACGTTTAAGAGCTATGCTGGAAACAGCATAGCAAGTTTAAATAA
G
Sod1 guide-2-R:
CCAGACGACCACCACCGAACCAAGAGCTGGAGGGAGAGCTATATATAC
Sod2 guide-1-F:
GCAGGCTGAAGGGAGACTTGTTTAAGAGCTATGCTGGAAACAGCATAGCAAG
Sod2 guide-1-R:
CCGTGGCTGTTCAGGGCTCCGAACTAGGAGCCTGGAGAACTGCTATATAAAC
Sod2 guide-2-F:
CCTGAACAGCCACGGGTTTAAGAGCTATGCTGGAAACAGCATAGCAAGTTTAAATA
AG
Sod2 guide-2-R:
CTCCCTTCAGCCTGCCGAACCAAGAGCTGGAGGGAGAGCTATATATAC

DsRed-biuas-F: GCCCTTAAAACTCGAGCCCAATGCATTGGCGCCG
DsRed-biuas-R: CGCCCTTTTTGGATCCGGTGGCGGCAAGCTCCTT
Sod2-2A-catalase-F: CCCCCTCGAGGTCGACTCGCCACCATGGTTGGGATAAGGCTGG
Sod2-2A-catalase-R: TAGAACTAGTGGATCCTTAGGCCTGCGTGTAGGT
mfn2 guide1-F1:
GTGGATGAGCTGCGGGTGGGTTTAAGAGCTATGCTGGAAACAGCATAGC
mfn2 guide1-R1: CGCACCTCCGCCACCTGCCCGAACTAGGAGCCTGGAGAACTGC
mfn2 guide1-F2: GGTGGCGGAGGTGCGGTTTAAGAGCTATGCTGGAAACAGCATAGC
mfn2 guide1-R2: CCGCAGCTCATCCACCGAACCAAGAGCTGGAGGGAGA
mfn2 guide2-F1:
GGGGGATACCTGTCCAAAGGTTTAAGAGCTATGCTGGAAACAGCATAGCAAG
mfn2 guide2-R1:
AGACCTTCCTCTATGTGCCCGAACTAGGAGCCTGGAGAACTGCTATATAAAC
mfn2 guide2-F2:
CATAGAGGAAGGTCTGTTTAAGAGCTATGCTGGAAACAGCATAGCAAGTTTAAATA
AG
mfn2 guide2-R2:
GGACAGGTATCCCCCCGAACCAAGAGCTGGAGGGAGAGCTATATATAC
opa1 guide-F1:
GTAGTTGGGGACCAGAGTGGTTTAAGAGCTATGCTGGAAACAGCATAGC
opa1 guide-R1: CCTCACTGCTCAGCTGCCCGAACTAGGAGCCTGGAGAACTGC
opa1 guide-F2: AGCTGAGCAGTGAGGGTTTAAGAGCTATGCTGGAAACAGCATAGC
opa1 guide-R2: CTGGTCCCCAACTACCGAACCAAGAGCTGGAGGGAGA

Live imaging

Time-lapse spinning disk confocal microscopy (SDCM) was performed with a Yokogawa scanning unit (CSU-X1-A1) mounted on an Olympus IX-83 microscope, equipped with a 100X 1.45–numerical aperture (NA) UPlanSApo oil objective (Olympus) and an Andor iXon Ultra 897BV EMCCD camera (Andor Technology). GFP and mCherry were excited with 488 nm and 561 nm and fluorescence emission collected through 525/30-nm and 607/36-nm filters, respectively, to determine the localization of mitochondria in migrating neutrophils in vivo. Images were captured using MetaMorph version 7.8.8.0 software at 10 s interval of 5 min. Time-

lapse fluorescence images for neutrophil motility were obtained by a laser scanning confocal microscope (LSM 710, Zeiss) with a 1.0/20 x objective at 1 min interval of 30 min. The velocity of neutrophils was quantified using ImageJ with MTrackJ plugin and plotted in Prism 6.0 (GraphPad).

Time-lapse images for zebrafish circulation, LTB_4 bath, flow adhesion assay were obtained with AXIO Zoom V16 microscope (Zeiss) at no interval or 30 s interval (LTB_4 bath). Time-lapse fluorescence images for zebrafish neutrophil motility were acquired by a laser scanning confocal microscope (LSM 710, Zeiss) with a 1.0/20 x objective lens at 1 min interval of 30 min. Neutrophils were tracked using ImageJ with MTrackJ plugin and the velocity was plotted in Prism 6.0 (GraphPad).

For confocal imaging, images were obtained using a laser-scanning confocal microscope (LSM 800, Zeiss) with a 1.4/63x oil immersion objective lens. Images were analysis with ImageJ.
For fluorescence intensity measurement, images within an experiment were acquired using identical camera settings and background was subtracted by ImageJ with the rolling ball radius as 50. Mean fluorescence intensity of interested areas was measured by Measurement in ImageJ and plotted in Prism (GraphPad) software. For colocalization analysis, background was subtracted in both channels using ImageJ with the rolling ball radius as 50. Images were then processed by Coloc 2 of ImageJ to calculate the colocalization. Interaction between channels was quantified by Manders' colocalization coefficient.

mRNA rescue

To make *sod1* mRNA, the cDNA of *sod1* was amplified from zebrafish total RNA with the following primers using SuperScript III one-step RT-PCR system with Platinum *Taq* High Fidelity kit (Invitrogen): pcs2-sod1-F: TCTTTTTGCAGGATCCTCGCCACCATGGTGAACAAGGCCGTTT, pcs2-sod1-R: GTTCTAGAGGCTCGAGTCACTGAGTGATGCCGATC. The purified PCR products were then inserted into PCS2 backbone using In-Fusion cloning (Clontech). To generate mRNA, the final PCS-sod1 construct was linearized by Not I and used for in vitro transcription with mMESSAGE mMACHINE Sp6 kit (Life technologies). 1 nl of mixture containing 25 ng/µl *sod1* knocking out construct, 35 ng/µl Tol2 transposase mRNA, and 300 ng/µl *sod1* mRNA was injected into the

cytoplasm of embryos at one-cell stage. *GFP* mRNA was used as the control. Neutrophil motility was measured at 3 dpf using confocal microscopy.

Chemicals

Embryos at 3 dpf were treated with 1% DMSO, 0.1 μM Rotenone (Sigma), 0.1 μM Antimycin (Sigma), 200 μM Diphenyleneiodonium chloride (DPI, Sigma), 10 μM Celastrol (Sigma), or 200 μM N-acetylcysteine (NAC, Sigma) for 30-60 mins, followed by time-lapse fluorescence imaging for neutrophil motility with confocal microscope. For chemical rescue, embryos injected with *sod1* or *sod2* knockout construct were treated with 200 μM NAC or 50 μM mitoTEMPO (Cayman Chemical) at 1 dpf for 48 hours. Neutrophil motility was measured at 3 dpf using confocal microscope.

Isolation of DNA and quantitative PCR

Genomic DNA was purified by QIAamp DNA Mini Kit (Qiagen) from sorted cells. 10 μg of poly(dA: dT) (Invivogen) were used as the carrier DNA. Quantitative PCR was performed using FastStart Essential DNA Green Master (Roche) to determine the relative abundance of mitochondrial DNA. Results were normalized to nucleic DNA. Primers for zebrafish mtDNA (forward: CAAACACAAGCCTCGCCTGTTTAC; reverse: CACTGACTTGATGGGGGAGACAGT) and nucDNA (forward: ATGGGCTGGGCGATA AAATTGG; reverse: ACATGTGCATGTCGCTCCCAA A) were used (Rooney et al, 2015). The efficiency of the primers were calculated using Real-time PCR Miner and corrected for the relative abundance (Zhao and Fernald, 2005).

T7 endonuclease I assay

T7 endonuclease I (NEB) was used to detect mutations caused by CRISPR/Cas. Genomic DNA containing sgRNA recognition site was amplified by PCR from sorted cells. PCR products were purified with PCR purification kit (Clontech) and reannealed in a thermocycler using the following conditions: 95°C for 5 min, 95-85°C with ramp rate as -0.3°C/second; 85-25°C with ramp rate as -0.1°C/second. Reannealed PCR products were incubated with T7 endonuclease I at 37°C for 1 hour, followed by agarose gel electrophoresis. Primers used for this assay were Polg-F/R as described above.

Adhesion assay

Adhesion assay was performed as described(Liu et al., 2012). Differentiated HL-60 cells were resuspended in mHBSS (HBSS with 0.5% FBS and 20 mM HEPES) and plated in 96-well plate (greiner bio-one 655069) coated with 10 μg/ml fibrinogen (sigma F3879) for 1 h with 20,000 cells /well. Cells were incubated at 37^{o}C for 15 min. PBS or fMLP (sigma F3506) at a final concentration of 100 nM was added to each well, and cells were incubated for another 15 min. Then cells were gently agitated and wash with mHBSS twice to remove unattached cells, and stained with 0.5% crystal violet with 4% paraformaldehyde for 30 min at room temperature. Adhesion of cells was assessed by measurement of absorbance at 570 nm.

μ-slide Chemotaxis

Differentiated HL-60 cells were resuspended in mHBSS at 4x10^{6}/ml and loaded into μ-slides (ibidi, 80322) following manufacturer's instructions. fMLP was added to the right reservoir at a concentration of 1 μM. Chemotaxis was recorded every 1 min for 2 h using a laser scanning confocal microscope (LSM 710, Zeiss) with a 1.0/10 x objective. The velocity of neutrophils was measured using ImageJ with MTrackJ plugin and plotted in Prism 6.0 (GraphPad). For inhibitor treatments, dHL-cells were pre-treated with DMSO, NSC23766 (200 μM, Sigma SML0952), AIP (50 μM, R&D SYSTEMS 5959/1) or CAS 1090893 (50 μM, Millipore 553511) for 30 min before loading into μ-slides.

Flow adhesion

Neutrophil flow adhesion assay was performed as described(Zhou et al., 2014). Briefly, 5x10^{5} HUVEC cells in 2 ml were plated onto 10 ug/ml fibrinogen-coated 35 mm plate (Corning 430165), and incubated at 37^{o}C. Then the HUVEC monolayer was primed by 20 ng/ml human TNF-a (Life technologies PHC3015) for 4-6 h. dHL-60 cells were harvested and resuspended at a cell density of 5x10^{5} cells/ml in complete medium. dHL-60 cells were flowed on top of HUVEC monolayer at a speed of 350 μl/min using a syringe pump. Cells adhering to the monolayer were recorded using AXIO Zoom V16 microscope (Zeiss) with camera streaming for 5 min. The total number of adherent neutrophils were quantified at 5 min.

Rac-GTP pulldown assay

PAK-GST-coated beads (Cytoskeleton BK035) was used to isolate active Rac from whole-cell lysate as described(Graziano et al., 2017). Briefly, dHL-60 cells were serum starved with RPMI medium lacking FBS for 1 h in the incubator at a density of $2x10^6$ cells/ml. After starvation, cells were pelleted and suspended in mHBSS, and plated on fibrinogen-coated 100 mm tissue culture dish to attach for 30 min. fMLP was then added to the cells at a final concentration of 100 nM, then cells were lysed with ice-cold lysis buffer at indicated time points and collected by scrapples. 10 µg PAK-GST beads were mixed with each sample and incubated at 4°C for 1h. Protein beads were washed and processed for western blot.

Western Blot

Protein samples were separated using SDS-PAGE and transferred onto nitrocellulose membranes (LI-COR NC9680617). Membranes were blocked for ~30 min in PBST (PBS and 0.1% Tween 20) with 5% BSA. After blocking, membranes were incubated with primary antibodies diluted 1:1,000 in PBST at 4°C for overnight and secondary antibodies diluted 1:10,000 in PBST at room temperature for 1 h. Odyssey (LI-Cor) was used to image membranes. Primary antibodies anti-Mfn2 (Cell Signaling 9482S), anti-Mfn1 (Cell Signaling 14793S), anti-beta-Tubulin (DSHB, E7), anti-Rac1/2/3 (Cell Signaling 2465S) and secondary antibody anti-rabbit (ThermoFisher SA5-35571), anti-mouse (Invitrogen 35518) were used. For active Rac pull down assays, images were analyzed by ImageJ. The ratio of active Rac to total Rac was calculated and normalized to the value of vector control.

Bone Marrow Neutrophil isolation

Femurs and Tibias from mice 8-12 weeks of age were isolated and whole bone marrow was isolated, and passed through a 70 µm filter followed by RBC lysis (Qiagen 158904). Bone marrow neutrophils were isolated using a negative selection column (MACS 130-097-658). Neutrophils viability was determined by trypan blue staining showing >99% viability. Cells were allowed to rest in RPMI for 1h prior to downstream experiments. $2x10^6$ neutrophils were used for western blot to assess *Mfn2* KO (anti-Mfn2, Invitrogen-PA5-42171) efficiency where Vinculin (anti-Vinculin, Sigma V9131) was used as a loading control.

Peritonitis model

1ml of 4% thioglycollate (Sigma B2551) was injected directly into the peritoneal cavity of mice 6-8 weeks of age. After 3 hours of incubation, peritoneal ascites were collected by introducing 8 ml of PBS into the cavity and collecting the ascites immediately afterwards. Cells were subjected to RBC lysis and viability was determined via trypan blue staining. Total cells were stained with CD11b (BD 557686) and Ly6G (BD 566453) on ice for 30 minutes and washed 3 times with staining buffer. Cells profiles were collected with a BD fortessa analyzer and analyzed with Beckman kaluza software. Neutrophil population was defined as FCS/SSC high and CD11b+Ly6G^{high}.

Immunostaining

dHL-60 cells were resuspended in mHBSS and attached to fibrinogen-coated slides for 30 min. Then cells were stimulated with 100 nM fMLP for 3 min and fixed with 3% paraformaldehyde in PBS for 15 min at 37^{o}C. The immunostaining of fixed cells were performed as described(Fayngerts et al., 2017b). Briefly, after fixation, cells were permeabilized in PBS with 0.1% Triton X-100 and 3% BSA for 1 h at room temperature. dHL-60 cells were incubated with phalloidin -AlexaFluor 488 (Invitrogen A12379) or primary antibodies diluted 1:100 in 3% BSA overnight at 4 ^{o}C. The cells were then stained with secondary antibodies diluted 1:500 in 3% BSA and DAPI (Invitrogen D3571) for 1 h at room temperature. Images were acquired using LSM 800 (Zeiss) and processed with ImageJ. For MEF cells staining, cells were plated onto fibrinogen-coated slides and incubated for ~4 h at 37 ^{o}C, followed with fixation with 3% paraformaldehyde in PBS. Primary antibodies anti-Mfn2 (Cell Signaling 9482S), anti-TOMM20 (Santa Cruz sc-17764), anti-Calnexin (ThermoFisher MA3-027), anti-Tubulin (Sigma T5168), anti-Paxillin (Invitrogen AHO0492), anti-RAC-GTP (NewEast Biosciences 26903), anti-p-CaMKII (Cell Signaling 12716S), anti-Tiam2 (Abcam ab199426), and secondary antibody anti-rabbbit AlexaFluor 568 (Invitrogen A-11011), anti-mouse AlexaFluor 647 (Invitrogen A21236) were used.

Electron microscopy

Transmission Electron Microscopy was performed at Purdue Life Science Microscopy Facility. dHL-60 cells were pelleted and fixed in 2.5% glutaraldehyde in 0.1 M sodium cacodylate buffer, post-fixed in buffered 1% osmium tetroxide containing 0.8% potassium ferricyanide, and en bloc

stained in 1% aqueous uranyl acetate. They were then dehydrated with a graded series of acetonitrile and embedded in EMbed-812 resin. Thin sections (80nm) were cut on a Leica EM UC6 ultramicrotome and stained with 2% uranyl acetate and lead citrate. Images were acquired using a Gatan US1000 2K CCD camera on a FEI Tecnai G2 20 electron microscope equipped with a LaB6 source and operating at 100 kV or 200kV.

Ca^{2+} measurement

Fluo-4 Calcium Imaging Kit (Invitrogen F10489) was used for cytosolic Ca^{2+} measurement. dHL-60 cells were resuspended in mHBSS and incubated with PowerLoad solution and Fluo-4 dye at 37 ^{o}C for 15 min and then at room temperature for 15 min. After incubation, cells were washed with mHBSS and loaded into fibrinogen-coated 96-well plates (greiner bio-one 655069) with 20,000 cells in 150 ul for each well, followed by incubation at 37 ^{o}C for 30 min. Green fluorescence images were recorded by BioTek Lionheart FX Automated Microscope with 20x phase lens at 1s interval of 10s. Then 15 ul of 1 uM fMLP was injected into cells using the injector of BioTek Lionheart FX Automated Microscope. Images were recorded for another 2 min with 1s interval. The fluorescence intensity of basal Ca^{2+} level was set to 0.

For mitochondrial Ca^{2+} measurement, Rhod-2 (Invitrogen R1245MP) was used. dHL-60 cells were incubated in mHBSS with Rhod-2 at 37 ^{o}C for 30 min, and then washed and added into fibrinogen-coated 96-well plates with 150 µl/well. After 30 min incubation, time-lapse red fluorescence images were acquired by BioTek Lionheart FX Automated Microscope with 1s interval of 10s and followed by fMLP injection and image recording for another 2 min with 1s interval. The fluorescence intensity of basal Ca^{2+} was normalized to 0.

Cell spreading

MEF cell spreading assay was performed as described(Jovic et al., 2007). Briefly, cells were trypsinized and replated onto fibrinogen-coated µ-slide 8 well plates (ibidi 80826) with complete medium. Time-lapse images were acquired using BioTek Lionheart FX Automated Microscope with 20x phase lens at 2 min interval of ~3 h at 37°C with 5% CO_2.

Wound closure

MEF cells in complete medium were seeded onto 96-well plates (FALCON 353075) and incubated at 37 ºC overnight. A wound was induced by automated 96-well WoundScratcher (BioTek) for each well. Cells were washed twice with mHBSS and time-lapse images were acquired using BioTek Lionheart FX Automated Microscope with 4x phase lens at 20 min interval of ~12 h at 37°C with 5% CO_2.

Flow cytometry analysis

dHL-60 cells were harvested and resuspended into ice-cold FACS buffer (PBS with 1% BSA) at a concentration of $1x10^6$ cells/ml. 5 ul of Annexin V (BD 563973) solution were added into 100 ul cell suspension and incubated at room temperature for 30 min. Cells were washed for three times with ice-cold FACS buffer, and followed by flow cytometry analysis.

Mitochondrial membrane potential, ROS, and ATP measurement

Mitochondrial membrane potential was measured using TMRM. dHL-60 cells were resuspended in mHBSS and incubated with 150 nM MitoTracker (Invitrogen M22426), 20 nM TMRM (Invitrogen T668), and 0.2 μg/ml Hoechst (Invitrogen H3570) for 30 min at 37 ºC. Then cells were washed and plated onto fibrinogen-coated μ-slide 8 well plates. After 30 min incubation, cells were stimulated with or without fMLP at a concentration of 100 nM. The fluorescent images were acquired using BioTek Lionheart FX Automated Microscope with 20x phase lens, and processed using ImageJ. Mitochondrial membrane potential was measured using the fluorescence intensity of TMRM normalized to the intensity of MitoTracker of each cell. For mitochondrial ROS measurement, MitoSOX (M36008) was used. 5 μM of mitoROX was added to the cell suspension and incubated for 30 min at 37 ºC. Cellular ATP level was measured by ATP Assay Kit (abcam #ab83355) according to the assay procedure. Briefly, dHL-60 cells treated with or without fMLP were harvested, washed with PBS, and resuspended in ATP Assay Buffer. Samples with ATP reaction mix were loaded into 96-well plate (greiner bio-one 655069) and incubate at room temperature for 30 min protected from light. Results were measured by microplate reader (BioTek) at Ex/Em = 535/587. All results were normalized to control cell lines without fMLP treatment.

Mutational Efficiency Quantification

To determine the mutation efficiency in *Tg(lyzC:nls-cas9-2A-mCherry/U6a:polg sgRNA)*^{pu16}, the *polg*, *mfn2*, and *opa1* locus around the sgRNA binding site was amplified by PCR using primers (Polg-F: CAGCCAACGTATGCGGCTAC, Polg-R: CAGCTCTGCGGGTGACTGTTC, mfn2-F1: GGCGATGATAAACATGGCAGTTTG, mfn2-R1: GTACCACAGGTGCACAGTGTC, mfn2-F2: CTGGGACGCATCGGCCAATG, mfn2-R2: CTACCTGCTTCAGGCATTCCCTG, mfn2#2-F1: GTCGGGCTTCTCCTAAGTTATTC, mfn2#2-R1: CAGTGTCCATAGCCTAGAGTCTGC, mfn2#2-F2: GTGGTCTCATATAATTTTGCTTGCTG, mfn2#2-R2: CACACGCGAATCGATAAGAGGAAT, opa1-F1: CAAGCTCATTAAAGGTTTGAAACCACTTG, opa1-R1: CTCCACAAATCACATAGGTGAC, opa1-F2: GTGCCTGAATGCTCTACACTTTC, opa1-R: CATGATAACAATACCATGCACATGC), followed by library construction using Nextera library prep kit and sequencing using an Illumina MiSeq 300 at the sequencing center of Purdue University. Raw reads have been deposited to the Sequence Read Archive (Accession number SRP132222, https://www.ncbi.nlm.nih.gov/Traces/study/?acc=SRP132222). Mutational efficiency was calculated using the CrispRVariants R package (Lindsay et al., 2016), with the specific code below to compare aligned reads and count read frequencies:

```
crispr_set <- readsToTarget(c("./crisprVariants/2018-01-05_Data/001664pr.bam",
"./crisprVariants/2018-01-05_Data/001675pr.bam"), target = sgRNA40_target,
reference = sgRNA40_RevComp_Reference, names=c("polg #1","polg #2"),
target.loc=sgRNA40.revC.loc, orientation="target", chimera.to.target=25)
```

The mutational efficiency was calculated using the following command built into CrispRVariants:

```
mutationEfficiency(crispr_set)
```

Mutation types where calculated by using the following command built into CrispRvariants that provides consensus sequences of the different mutations found in the 2 deep sequencing paired-end samples:

```
consensusSeqs(crispr_set)
```

The consensus sequences are labeled using the CIGAR string format and mutational frequencies where determined from that labeling.

Statistical analysis

Statistical analysis was performed with Prism 6 (GraphPad). An unpaired two-tailed student's *t* test, or ANOVA was used to determine the statistical significance of differences between groups. A *P* value of less than 0.05 indicated in the figures by asterisks was considered as statistically significant

REFERENCES

Abdallah, D.S.A., Egan, C.E., Butcher, B.A., and Denkers, E.Y. (2011). Mouse neutrophils are professional antigen-presenting cells programmed to instruct T(h)1 and T(h)17 T-cell differentiation. Int Immunol *23*, 317-326.

Ablain, J., Durand, E.M., Yang, S., Zhou, Y., and Zon, L.I. (2015). A CRISPR/Cas9 vector system for tissue-specific gene disruption in zebrafish. Developmental cell *32*, 756-764.

Abram, C.L., Roberge, G.L., Pao, L.I., Neel, B.G., and Lowell, C.A. (2013). Distinct roles for neutrophils and dendritic cells in inflammation and autoimmunity in motheaten mice. Immunity *38*, 489-501.

Aggad, D., Stein, C., Sieger, D., Mazel, M., Boudinot, P., Herbomel, P., Levraud, J.P., Lutfalla, G., and Leptin, M. (2010). In vivo analysis of Ifn-gamma1 and Ifn-gamma2 signaling in zebrafish. Journal of immunology *185*, 6774-6782.

Allingham, M.J., van Buul, J.D., and Burridge, K. (2007). ICAM-1-mediated, Src- and Pyk2-dependent vascular endothelial cadherin tyrosine phosphorylation is required for leukocyte transendothelial migration. J Immunol *179*, 4053-4064.

Amini, P., Stojkov, D., Felser, A., Jackson, C.B., Courage, C., Schaller, A., Gelman, L., Soriano, M.E., Nuoffer, J.M., Scorrano, L.*, et al.* (2018). Neutrophil extracellular trap formation requires OPA1-dependent glycolytic ATP production. Nature communications *9*, 2958.

Amulic, B., Cazalet, C., Hayes, G.L., Metzler, K.D., and Zychlinsky, A. (2012). Neutrophil function: from mechanisms to disease. Annu Rev Immunol *30*, 459-489.

Anderson, S., Bankier, A.T., Barrell, B.G., de Bruijn, M.H., Coulson, A.R., Drouin, J., Eperon, I.C., Nierlich, D.P., Roe, B.A., Sanger, F.*, et al.* (1981). Sequence and organization of the human mitochondrial genome. Nature *290*, 457-465.

Baek, D., Villen, J., Shin, C., Camargo, F.D., Gygi, S.P., and Bartel, D.P. (2008). The impact of microRNAs on protein output. Nature *455*, 64-71.

Bao, Y., Ledderose, C., Graf, A.F., Brix, B., Birsak, T., Lee, A., Zhang, J., and Junger, W.G. (2015). mTOR and differential activation of mitochondria orchestrate neutrophil chemotaxis. J Cell Biol *210*, 1153-1164.

Bao, Y., Ledderose, C., Seier, T., Graf, A.F., Brix, B., Chong, E., and Junger, W.G. (2014). Mitochondria regulate neutrophil activation by generating ATP for autocrine purinergic signaling. J Biol Chem *289*, 26794-26803.

Bauernfeind, F., Rieger, A., Schildberg, F.A., Knolle, P.A., Schmid-Burgk, J.L., and Hornung, V. (2012). NLRP3 inflammasome activity is negatively controlled by miR-223. Journal of immunology *189*, 4175-4181.

Bi, D., Lopez, J.H., Schwarz, J.M., and Manning, M.L. (2014). Energy barriers and cell migration in densely packed tissues. Soft matter *10*, 1885-1890.

Boespflug, N.D., Kumar, S., McAlees, J.W., Phelan, J.D., Grimes, H.L., Hoebe, K., Hai, T., Filippi, M.D., and Karp, C.L. (2014). ATF3 is a novel regulator of mouse neutrophil migration. Blood *123*, 2084-2093.

Borregaard, N. (2010). Neutrophils, from marrow to microbes. Immunity *33*, 657-670.

Borregaard, N., and Herlin, T. (1982). Energy metabolism of human neutrophils during phagocytosis. J Clin Invest *70*, 550-557.

Brantley, D.M., Chen, C.L., Muraoka, R.S., Bushdid, P.B., Bradberry, J.L., Kittrell, F., Medina, D., Matrisian, L.M., Kerr, L.D., and Yull, F.E. (2001). Nuclear factor-kappaB (NF-kappaB) regulates proliferation and branching in mouse mammary epithelium. Molecular biology of the cell *12*, 1445-1455.

Brinkmann, V., Reichard, U., Goosmann, C., Fauler, B., Uhlemann, Y., Weiss, D.S., Weinrauch, Y., and Zychlinsky, A. (2004). Neutrophil extracellular traps kill bacteria. Science *303*, 1532-1535.

Bruehl, R.E., Moore, K.L., Lorant, D.E., Borregaard, N., Zimmerman, G.A., McEver, R.P., and Bainton, D.F. (1997). Leukocyte activation induces surface redistribution of P-selectin glycoprotein ligand-1. J Leukoc Biol *61*, 489-499.

Bunting, M., Harris, E.S., McIntyre, T.M., Prescott, S.M., and Zimmerman, G.A. (2002). Leukocyte adhesion deficiency syndromes: adhesion and tethering defects involving beta 2 integrins and selectin ligands. Curr Opin Hematol *9*, 30-35.

Campello, S., Lacalle, R.A., Bettella, M., Manes, S., Scorrano, L., and Viola, A. (2006). Orchestration of lymphocyte chemotaxis by mitochondrial dynamics. Journal of Experimental Medicine *203*, 2879-2886.

Campello, S., and Scorrano, L. (2010). Mitochondrial shape changes: orchestrating cell pathophysiology. EMBO Rep *11*, 678-684.

Casanova-Acebes, M., Pitaval, C., Weiss, L.A., Nombela-Arrieta, C., Chevre, R., N, A.G., Kunisaki, Y., Zhang, D., van Rooijen, N., Silberstein, L.E*., et al.* (2013). Rhythmic modulation of the hematopoietic niche through neutrophil clearance. Cell *153*, 1025-1035.

Chandhok, G., Lazarou, M., and Neumann, B. (2018). Structure, function, and regulation of mitofusin-2 in health and disease. Biol Rev Camb Philos Soc *93*, 933-949.

Chen, C., Li, L., Lodish, H., and Bartel, D. (2004). MicroRNAs Modulate Hematopoietic lineage differentiation.pdf>. Science *303*, 83-85.

Chen, H., Detmer, S.A., Ewald, A.J., Griffin, E.E., Fraser, S.E., and Chan, D.C. (2003). Mitofusins Mfn1 and Mfn2 coordinately regulate mitochondrial fusion and are essential for embryonic development. The Journal of cell biology *160*, 189-200.

Chen, H., McCaffery, J.M., and Chan, D.C. (2007). Mitochondrial fusion protects against neurodegeneration in the cerebellum. Cell *130*, 548-562.

Chen, Q., Wang, H., Liu, Y., Song, Y., Lai, L., Han, Q., Cao, X., and Wang, Q. (2012). Inducible microRNA-223 down-regulation promotes TLR-triggered IL-6 and IL-1beta production in macrophages by targeting STAT3. PloS one *7*, e42971.

Chiaretti, S., Messina, M., Tavolaro, S., Zardo, G., Elia, L., Vitale, A., Fatica, A., Gorello, P., Piciocchi, A., Scappucci, G.*, et al.* (2010). Gene expression profiling identifies a subset of adult T-cell acute lymphoblastic leukemia with myeloid-like gene features and over-expression of miR-223. Haematologica *95*, 1114-1121.

Cipolla, G.A. (2014). A non-canonical landscape of the microRNA system. Frontiers in genetics *5*, 337.

Conklin, M.W., Lin, M.S., and Spitzer, N.C. (2005). Local calcium transients contribute to disappearance of pFAK, focal complex removal and deadhesion of neuronal growth cones and fibroblasts. Developmental biology *287*, 201-212.

Dancey, J.T., Deubelbeiss, K.A., Harker, L.A., and Finch, C.A. (1976). Neutrophil kinetics in man. J Clin Invest *58*, 705-715.

Davis, R.E., Sharma, S., Chen, Y., Sundar, S., and Wilson, M.E. (2017). Inhibitory Ligand Pd-L1 on Mhc Class Ii-Expressing Neutrophils and Murine Leishmaniasis in Human. Am J Trop Med Hyg *97*, 241-241.

de Brito, O.M., and Scorrano, L. (2008). Mitofusin 2 tethers endoplasmic reticulum to mitochondria. Nature *456*, 605-610.

de Oliveira, S., Rosowski, E.E., and Huttenlocher, A. (2016). Neutrophil migration in infection and wound repair: going forward in reverse. Nat Rev Immunol *16*, 378-391.

De Rienzo, G., Gutzman, J.H., and Sive, H. (2012). Efficient shRNA-mediated inhibition of gene expression in zebrafish. Zebrafish *9*, 97-107.

Deng, Q., and Huttenlocher, A. (2012). Leukocyte migration from a fish eye's view. Journal of cell science *125*, 3949-3956.

Deng, Q., Yoo, S.K., Cavnar, P.J., Green, J.M., and Huttenlocher, A. (2011). Dual roles for Rac2 in neutrophil motility and active retention in zebrafish hematopoietic tissue. Developmental cell *21*, 735-745.

Desai, S.P., Bhatia, S.N., Toner, M., and Irimia, D. (2013). Mitochondrial Localization and the Persistent Migration of Epithelial Cancer cells. Biophys J *104*, 2077-2088.

Doench, J.G., Hartenian, E., Graham, D.B., Tothova, Z., Hegde, M., Smith, I., Sullender, M., Ebert, B.L., Xavier, R.J., and Root, D.E. (2014). Rational design of highly active sgRNAs for CRISPR-Cas9-mediated gene inactivation. Nature biotechnology *32*, 1262-1267.

Dorhoi, A., Iannaccone, M., Farinacci, M., Fae, K., and Schreiber, J. (2013). MicroRNA-223 controls susceptibility to tuberculosis by regulating lung neutrophil recruitment. The Journal of clinical investigation *123*, 4836-4848.

Easley, C.A.t., Brown, C.M., Horwitz, A.F., and Tombes, R.M. (2008). CaMK-II promotes focal adhesion turnover and cell motility by inducing tyrosine dephosphorylation of FAK and paxillin. Cell Motil Cytoskeleton *65*, 662-674.

Eisenberg-Bord, M., Shai, N., Schuldiner, M., and Bohnert, M. (2016). A Tether Is a Tether Is a Tether: Tethering at Membrane Contact Sites. Developmental cell *39*, 395-409.

Enyedi, B., Jelcic, M., and Niethammer, P. (2016). The Cell Nucleus Serves as a Mechanotransducer of Tissue Damage-Induced Inflammation. Cell *165*, 1160-1170.

Erle, D.J., and Sheppard, D. (2014). The cell biology of asthma. The Journal of cell biology *205*, 621-631.

Faurschou, M., and Borregaard, N. (2003). Neutrophil granules and secretory vesicles in inflammation. Microbes Infect *5*, 1317-1327.

Fayngerts, S.A., Wang, Z., Zamani, A., Sun, H., Boggs, A.E., Porturas, T.P., Xie, W., Lin, M., Cathopoulis, T., Goldsmith, J.R.*, et al.* (2017a). Direction of leukocyte polarization and migration by the phosphoinositide-transfer protein TIPE2. Nat Immunol *18*, 1353-1360.

Fayngerts, S.A., Wang, Z.J., Zamani, A., Sun, H.H., Boggs, A.E., Porturas, T.P., Xie, W.D., Lin, M., Cathopoulis, T., Goldsmith, J.R.*, et al.* (2017b). Direction of leukocyte polarization and migration by the phosphoinositide-transfer protein TIPE2. Nature immunology *18*, 1353-+.

Fazi, F., Rosa, A., Fatica, A., Gelmetti, V., De Marchis, M.L., Nervi, C., and Bozzoni, I. (2005). A minicircuitry comprised of microRNA-223 and transcription factors NFI-A and C/EBPalpha regulates human granulopoiesis. Cell *123*, 819-831.

Filadi, R., Pendin, D., and Pizzo, P. (2018). Mitofusin 2: from functions to disease. Cell death & disease *9*, 330.

Fleming, I.N., Elliott, C.M., Buchanan, F.G., Downes, C.P., and Exton, J.H. (1999a). Ca2+/calmodulin-dependent protein kinase II regulates Tiam1 by reversible protein phosphorylation. J Biol Chem *274*, 12753-12758.

Fleming, I.N., Elliott, C.M., Buchanan, F.G., Downes, C.P., and Exton, J.H. (1999b). Ca2+/calmodulin-dependent protein kinase II regulates Tiam1 by reversible protein phosphorylation. Journal of Biological Chemistry *274*, 12753-12758.

Formichi, P., Radi, E., Branca, C., Battisti, C., Brunetti, J., Da Pozzo, P., Giannini, F., Dotti, M.T., Bracci, L., and Federico, A. (2016). Oxidative stress-induced apoptosis in peripheral blood lymphocytes from patients with POLG-related disorders. Journal of the neurological sciences *368*, 359-368.

Fossati, G., Moulding, D.A., Spiller, D.G., Moots, R.J., White, M.R., and Edwards, S.W. (2003). The mitochondrial network of human neutrophils: role in chemotaxis, phagocytosis, respiratory burst activation, and commitment to apoptosis. J Immunol *170*, 1964-1972.

Franco, S.J., Rodgers, M.A., Perrin, B.J., Han, J., Bennin, D.A., Critchley, D.R., and Huttenlocher, A. (2004). Calpain-mediated proteolysis of talin regulates adhesion dynamics. Nat Cell Biol *6*, 977-983.

Frezza, C., Pollard, P.J., and Gottlieb, E. (2011). Inborn and acquired metabolic defects in cancer. J Mol Med-Jmm *89*, 213-220.

Fuchs, T.A., Abed, U., Goosmann, C., Hurwitz, R., Schulze, I., Wahn, V., Weinrauch, Y., Brinkmann, V., and Zychlinsky, A. (2007). Novel cell death program leads to neutrophil extracellular traps. J Cell Biol *176*, 231-241.

Furze, R.C., and Rankin, S.M. (2008). The role of the bone marrow in neutrophil clearance under homeostatic conditions in the mouse. FASEB J *22*, 3111-3119.

Futosi, K., Fodor, S., and Mocsai, A. (2013). Neutrophil cell surface receptors and their intracellular signal transduction pathways. Int Immunopharmacol *17*, 638-650.

Gambardella, L., and Vermeren, S. (2013). Molecular players in neutrophil chemotaxis--focus on PI3K and small GTPases. J Leukoc Biol *94*, 603-612.

Gault, W.J., Enyedi, B., and Niethammer, P. (2014). Osmotic surveillance mediates rapid wound closure through nucleotide release. The Journal of cell biology *207*, 767-782.

Geijsen, N., van Delft, S., Raaijmakers, J.A.M., Lammers, J.W.J., Collard, J.G., Koenderman, L., and Coffer, P.J. (1999). Regulation of p21rac activation in human neutrophils. Blood *94*, 1121-1130.

Giannone, G., Ronde, P., Gaire, M., Haiech, J., and Takeda, K. (2002). Calcium oscillations trigger focal adhesion disassembly in human U87 astrocytoma cells. Journal of Biological Chemistry *277*, 26364-26371.

Glancy, B., Willis, W.T., Chess, D.J., and Balaban, R.S. (2013). Effect of calcium on the oxidative phosphorylation cascade in skeletal muscle mitochondria. Biochemistry-Us *52*, 2793-2809.

Gomes, L.C., Di Benedetto, G., and Scorrano, L. (2011). During autophagy mitochondria elongate, are spared from degradation and sustain cell viability. Nature cell biology *13*, 589-598.

Gonzalez-Martin, A., Adams, B.D., Lai, M., Shepherd, J., Salvador-Bernaldez, M., Salvador, J.M., Lu, J., Nemazee, D., and Xiao, C. (2016). The microRNA miR-148a functions as a critical regulator of B cell tolerance and autoimmunity. Nature immunology *17*, 433-440.

Gottardo, F., Liu, C.G., Ferracin, M., Calin, G.A., Fassan, M., Bassi, P., Sevignani, C., Byrne, D., Negrini, M., Pagano, F.*, et al.* (2007). Micro-RNA profiling in kidney and bladder cancers. Urologic oncology *25*, 387-392.

Graziano, B.R., Gong, D., Anderson, K.E., Pipathsouk, A., Goldberg, A.R., and Weiner, O.D. (2017). A module for Rac temporal signal integration revealed with optogenetics. Journal of Cell Biology *216*, 2515-2531.

Grimson, A., Farh, K.K., Johnston, W.K., Garrett-Engele, P., Lim, L.P., and Bartel, D.P. (2007). MicroRNA targeting specificity in mammals: determinants beyond seed pairing. Molecular cell *27*, 91-105.

Guan, X., Gao, Y., Zhou, J., Wang, J., Zheng, F., Guo, F., Chang, A., Li, X., and Wang, B. (2015). miR-223 Regulates Adipogenic and Osteogenic Differentiation of Mesenchymal Stem Cells Through a C/EBPs/miR-223/FGFR2 Regulatory Feedback Loop. Stem cells *33*, 1589-1600.

Gurol, T., Zhou, W., and Deng, Q. (2016). MicroRNAs in neutrophils: potential next generation therapeutics for inflammatory ailments. Immunological reviews *273*, 29-47.

Ha, M., and Kim, V.N. (2014). Regulation of microRNA biogenesis. Nature reviews. Molecular cell biology *15*, 509-524.

Hall, A. (1998). Rho GTPases and the actin cytoskeleton. Science *279*, 509-514.

Hall, C., Flores, M.V., Storm, T., Crosier, K., and Crosier, P. (2007). The zebrafish lysozyme C promoter drives myeloid-specific expression in transgenic fish. BMC developmental biology *7*, 42.

Hall, C.J., Boyle, R.H., Sun, X., Wicker, S.M., Misa, J.P., Krissansen, G.W., Print, C.G., Crosier, K.E., and Crosier, P.S. (2014). Epidermal cells help coordinate leukocyte migration during inflammation through fatty acid-fuelled matrix metalloproteinase production. Nature communications *5*, 3880.

Haneklaus, M., Gerlic, M., O'Neill, L.A., and Masters, S.L. (2013). miR-223: infection, inflammation and cancer. J Intern Med *274*, 215-226.

Harraz, M., Eacker, S., Wang, X., Dawson TM, and Dawson, V. (2012). MicroRNA-223 is neuroprotective by targeting glutamate receptors. Proceedings of the National Academy of Sciences of the United States of America *109*, 18962-18967.

Harvie, E.A., and Huttenlocher, A. (2015). Neutrophils in host defense: new insights from zebrafish. J Leukoc Biol *98*, 523-537.

Heggeness, M.H., Simon, M., and Singer, S.J. (1978). Association of Mitochondria with Microtubules in Cultured-Cells. Proceedings of the National Academy of Sciences of the United States of America *75*, 3863-3866.

Heiman, M., Kulicke, R., Fenster, R.J., Greengard, P., and Heintz, N. (2014). Cell type-specific mRNA purification by translating ribosome affinity purification (TRAP). Nature protocols *9*, 1282-1291.

Hendey, B., Lawson, M., Marcantonio, E.E., and Maxfield, F.R. (1996). Intracellular calcium and calcineurin regulate neutrophil motility on vitronectin through a receptor identified by antibodies to integrins alpha v and beta 3. Blood *87*, 2038-2048.

Henry, K.M., Loynes, C.A., Whyte, M.K., and Renshaw, S.A. (2013). Zebrafish as a model for the study of neutrophil biology. J Leukoc Biol *94*, 633-642.

Hidalgo, A., Peired, A.J., Wild, M., Vestweber, D., and Frenette, P.S. (2007). Complete identification of E-selectin ligands on neutrophils reveals distinct functions of PSGL-1, ESL-1, and CD44. Immunity *26*, 477-489.

Hind, L.E., Vincent, W.J., and Huttenlocher, A. (2016). Leading from the Back: The Role of the Uropod in Neutrophil Polarization and Migration. Dev Cell *38*, 161-169.

Hoesel, B., and Schmid, J.A. (2013). The complexity of NF-κB signaling in inflammation and cancer. Mol Cancer *12*.

Hong, C., Kidani, Y., N, A.G., Phung, T., Ito, A., Rong, X., Ericson, K., Mikkola, H., Beaven, S.W., Miller, L.S.*, et al.* (2012). Coordinate regulation of neutrophil homeostasis by liver X receptors in mice. J Clin Invest *122*, 337-347.

Houk, A.R., Jilkine, A., Mejean, C.O., Boltyanskiy, R., Dufresne, E.R., Angenent, S.B., Altschuler, S.J., Wu, L.F., and Weiner, O.D. (2012). Membrane tension maintains cell polarity by confining signals to the leading edge during neutrophil migration. Cell *148*, 175-188.

Huttenlocher, A., and Horwitz, A.R. (2011). Integrins in cell migration. Cold Spring Harbor perspectives in biology *3*, a005074.

Ismail, N., Wang, Y., Dakhlallah, D., Moldovan, L., Agarwal, K., Batte, K., Shah, P., Wisler, J., Eubank, T.D., Tridandapani, S.*, et al.* (2013). Macrophage microvesicles induce macrophage differentiation and miR-223 transfer. Blood *121*, 984-995.

Jao, L.E., Wente, S.R., and Chen, W. (2013). Efficient multiplex biallelic zebrafish genome editing using a CRISPR nuclease system. Proceedings of the National Academy of Sciences of the United States of America *110*, 13904-13909.

John, B., Enright, A.J., Aravin, A., Tuschl, T., Sander, C., and Marks, D.S. (2004). Human MicroRNA targets. PLoS biology *2*, e363.

Johnnidis, J.B., Harris, M.H., Wheeler, R.T., Stehling-Sun, S., Lam, M.H., Kirak, O., Brummelkamp, T.R., Fleming, M.D., and Camargo, F.D. (2008). Regulation of progenitor cell proliferation and granulocyte function by microRNA-223. Nature *451*, 1125-1129.

Johnsson, A.E., Dai, Y., Nobis, M., Baker, M.J., McGhee, E.J., Walker, S., Schwarz, J.P., Kadir, S., Morton, J.P., Myant, K.B.*, et al.* (2014). The Rac-FRET mouse reveals tight spatiotemporal control of Rac activity in primary cells and tissues. Cell reports *6*, 1153-1164.

Jonas, S., and Izaurralde, E. (2015). Towards a molecular understanding of microRNA-mediated gene silencing. Nature reviews. Genetics *16*, 421-433.

Jovic, M., Naslavsky, N., Rapaport, D., Horowitz, M., and Caplan, S. (2007). EHD1 regulates beta 1 integrin endosomal transport: effects on focal adhesions, cell spreading and migration. J Cell Sci *120*, 802-814.

Kang, T., Yi, J., Guo, A., Wang, X., Overall, C.M., Jiang, W., Elde, R., Borregaard, N., and Pei, D. (2001). Subcellular distribution and cytokine- and chemokine-regulated secretion of leukolysin/MT6-MMP/MMP-25 in neutrophils. J Biol Chem *276*, 21960-21968.

Kanther, M., Sun, X., Muhlbauer, M., Mackey, L.C., Flynn, E.J., 3rd, Bagnat, M., Jobin, C., and Rawls, J.F. (2011). Microbial colonization induces dynamic temporal and spatial patterns of NF-kappaB activation in the zebrafish digestive tract. Gastroenterology *141*, 197-207.

Kasper, D.M., Moro, A., Ristori, E., Narayanan, A., Hill-Teran, G., Fleming, E., Moreno-Mateos, M., Vejnar, C.E., Zhang, J., Lee, D.*, et al.* (2017). MicroRNAs Establish Uniform Traits during the Architecture of Vertebrate Embryos. Developmental cell *40*, 552-565 e555.

Kawakami, K. (2005). Transposon tools and methods in zebrafish. Dev Dynam *234*, 244-254.

Kennedy, A.D., and DeLeo, F.R. (2009). Neutrophil apoptosis and the resolution of infection. Immunol Res *43*, 25-61.

Kim, N.D., and Luster, A.D. (2015). The role of tissue resident cells in neutrophil recruitment. Trends in immunology *36*, 547-555.

Kohler, A., De Filippo, K., Hasenberg, M., van den Brandt, C., Nye, E., Hosking, M.P., Lane, T.E., Mann, L., Ransohoff, R.M., Hauser, A.E.*, et al.* (2011). G-CSF-mediated thrombopoietin release triggers neutrophil motility and mobilization from bone marrow via induction of Cxcr2 ligands. Blood *117*, 4349-4357.

Kolaczkowska, E., and Kubes, P. (2013). Neutrophil recruitment and function in health and inflammation. Nat Rev Immunol *13*, 159-175.

Krek, A., Grun, D., Poy, M.N., Wolf, R., Rosenberg, L., Epstein, E.J., MacMenamin, P., da Piedade, I., Gunsalus, K.C., Stoffel, M., and Rajewsky, N. (2005). Combinatorial microRNA target predictions. Nature genetics *37*, 495-500.

Kuwano, Y., Spelten, O., Zhang, H., Ley, K., and Zarbock, A. (2010). Rolling on E- or P-selectin induces the extended but not high-affinity conformation of LFA-1 in neutrophils. Blood *116*, 617-624.

Kwan, K.M., Fujimoto, E., Grabher, C., Mangum, B.D., Hardy, M.E., Campbell, D.S., Parant, J.M., Yost, H.J., Kanki, J.P., and Chien, C.B. (2007). The Tol2kit: a multisite gateway-based construction kit for Tol2 transposon transgenesis constructs. Developmental dynamics : an official publication of the American Association of Anatomists *236*, 3088-3099.

Lacy, P. (2005). The role of Rho GTPases and SNAREs in mediator release from granulocytes. Pharmacol Ther *107*, 358-376.

Lam, P.Y., Fischer, R.S., Shin, W.D., Waterman, C.M., and Huttenlocher, A. (2014). Spinning disk confocal imaging of neutrophil migration in zebrafish. Methods in molecular biology *1124*, 219-233.

Lammermann, T., Afonso, P.V., Angermann, B.R., Wang, J.M., Kastenmuller, W., Parent, C.A., and Germain, R.N. (2013). Neutrophil swarms require LTB4 and integrins at sites of cell death in vivo. Nature *498*, 371-375.

Lammermann, T., Bader, B.L., Monkley, S.J., Worbs, T., Wedlich-Soldner, R., Hirsch, K., Keller, M., Forster, R., Critchley, D.R., Fassler, R., and Sixt, M. (2008). Rapid leukocyte migration by integrin-independent flowing and squeezing. Nature *453*, 51-55.

Lawrence, T. (2009). The nuclear factor NF-kappaB pathway in inflammation. Cold Spring Harbor perspectives in biology *1*, a001651.

LeBert, D.C., Squirrell, J.M., Rindy, J., Broadbridge, E., Lui, Y., Zakrzewska, A., Eliceiri, K.W., Meijer, A.H., and Huttenlocher, A. (2015). Matrix metalloproteinase 9 modulates collagen matrices and wound repair. Development *142*, 2136-2146.

Lee, H., and Kimelman, D. (2002). A dominant-negative form of p63 is required for epidermal proliferation in zebrafish. Developmental cell *2*, 607-616.

Lee, S.Y., Voronov, S., Letinic, K., Nairn, A.C., Di Paolo, G., and De Camilli, P. (2005). Regulation of the interaction between PIPKI gamma and talin by proline-directed protein kinases. J Cell Biol *168*, 789-799.

Lewis, S.C., Uchiyama, L.F., and Nunnari, J. (2016). ER-mitochondria contacts couple mtDNA synthesis with mitochondrial division in human cells. Science *353*, aaf5549.

Li, S., Li, Z., Guo, F., and Qin, X. (2011a). miR-223 regulates migration and invasion by targeting Artemin in human esophageal carcinoma. Journal of Biomedical Science *18*.

Li, T., Morgan, M.J., Choksi, S., Zhang, Y., Kim, Y.S., and Liu, Z.G. (2010). MicroRNAs modulate the noncanonical transcription factor NF-kappaB pathway by regulating expression of the kinase IKKalpha during macrophage differentiation. Nature immunology *11*, 799-805.

Li, X., Zhang, Y., Zhang, H., Liu, X., Gong, T., Li, M., Sun, L., Ji, G., Shi, Y., Han, Z.*, et al.* (2011b). miRNA-223 promotes gastric cancer invasion and metastasis by targeting tumor suppressor EPB41L3. Mol Cancer Res *9*, 824-833.

Li, X.O., Kondo, Y., Bao, Y.I., Staudenmaier, L., Lee, A., Zhang, J.P., Ledderose, C., Wen, F.Q., and Junger, W. (2016). Removal of extracellular ATP improves fMLP-induced neutrophil chemotaxis. Eur Respir J *48*.

Li, Y., Li, Y., Cao, X., Jin, X., and Jin, T. (2017). Pattern recognition receptors in zebrafish provide functional and evolutionary insight into innate immune signaling pathways. Cellular & molecular immunology *14*, 80-89.

Lindsay, M.A. (2008). microRNAs and the immune response. Trends in immunology *29*, 343-351.

Lisse, T.S., Middleton, L.J., Pellegrini, A.D., Martin, P.B., Spaulding, E.L., Lopes, O., Brochu, E.A., Carter, E.V., Waldron, A., and Rieger, S. (2016). Paclitaxel-induced epithelial damage and ectopic MMP-13 expression promotes neurotoxicity in zebrafish. Proceedings of the National Academy of Sciences of the United States of America *113*, E2189-2198.

Liu, L.H., Aerbajinai, W., Ahmed, S.M., Rodgers, G.P., Angers, S., and Parent, C.A. (2012). Radil controls neutrophil adhesion and motility through beta 2-integrin activation. Mol Biol Cell *23*, 4751-4765.

Lu, J., and Clark, A.G. (2012). Impact of microRNA regulation on variation in human gene expression. Genome research *22*, 1243-1254.

Lu, L.F., and Liston, A. (2009). MicroRNA in the immune system, microRNA as an immune system. Immunology *127*, 291-298.

Luchsinger, L.L., de Almeida, M.J., Corrigan, D.J., Mumau, M., and Snoeck, H.W. (2016). Mitofusin 2 maintains haematopoietic stem cells with extensive lymphoid potential. Nature *529*, 528-531.

Lugus, J.J., Ngoh, G.A., Bachschmid, M.M., and Walsh, K. (2011). Mitofusins are required for angiogenic function and modulate different signaling pathways in cultured endothelial cells. J Mol Cell Cardiol *51*, 885-893.

Maes, T., Cobos, F.A., Schleich, F., Sorbello, V., Henket, M., De Preter, K., Bracke, K.R., Conickx, G., Mesnil, C., Vandesompele, J.*, et al.* (2016). Asthma inflammatory phenotypes show differential microRNA expression in sputum. The Journal of allergy and clinical immunology *137*, 1433-1446.

Maianski, N.A., Geissler, J., Srinivasula, S.M., Alnemri, E.S., Roos, D., and Kuijpers, T.W. (2004). Functional characterization of mitochondria in neutrophils: a role restricted to apoptosis. Cell Death Differ *11*, 143-153.

Maianski, N.A., Mul, F.P., van Buul, J.D., Roos, D., and Kuijpers, T.W. (2002). Granulocyte colony-stimulating factor inhibits the mitochondria-dependent activation of caspase-3 in neutrophils. Blood *99*, 672-679.

Majumdar, R., Tavakoli Tameh, A., and Parent, C.A. (2016). Exosomes Mediate LTB4 Release during Neutrophil Chemotaxis. PLoS biology *14*, e1002336.

Mandeville, J.T.H., and Maxfield, F.R. (1997). Effects of buffering intracellular free calcium on neutrophil migration through three-dimensional matrices. Journal of cellular physiology *171*, 168-178.

Marks, P.W., and Maxfield, F.R. (1990). Transient Increases in Cytosolic Free Calcium Appear to Be Required for the Migration of Adherent Human-Neutrophils. Journal of Cell Biology *110*, 43-52.

Martin, C., Burdon, P.C., Bridger, G., Gutierrez-Ramos, J.C., Williams, T.J., and Rankin, S.M. (2003). Chemokines acting via CXCR2 and CXCR4 control the release of neutrophils from the bone marrow and their return following senescence. Immunity *19*, 583-593.

Mathias, J.R., Perrin, B.J., Liu, T.X., Kanki, J., Look, A.T., and Huttenlocher, A. (2006). Resolution of inflammation by retrograde chemotaxis of neutrophils in transgenic zebrafish. J Leukoc Biol *80*, 1281-1288.

McDonald, B., Pittman, K., Menezes, G.B., Hirota, S.A., Slaba, I., Waterhouse, C.C.M., Beck, P.L., Muruve, D.A., and Kubes, P. (2010). Intravascular danger signals guide neutrophils to sites of sterile inflammation. Science *330*, 362-366.

Milani, P., Gagliardi, S., Cova, E., and Cereda, C. (2011). SOD1 Transcriptional and Posttranscriptional Regulation and Its Potential Implications in ALS. Neurology research international *2011*, 458427.

Mimaki, M., Wang, X., McKenzie, M., Thorburn, D.R., and Ryan, M.T. (2012). Understanding mitochondrial complex I assembly in health and disease. Biochimica et biophysica acta *1817*, 851-862.

Mocsai, A., Walzog, B., and Lowell, C.A. (2015). Intracellular signalling during neutrophil recruitment. Cardiovasc Res *107*, 373-385.

Moreno-Mateos, M.A., Vejnar, C.E., Beaudoin, J.D., Fernandez, J.P., Mis, E.K., Khokha, M.K., and Giraldez, A.J. (2015). CRISPRscan: designing highly efficient sgRNAs for CRISPR-Cas9 targeting in vivo. Nature methods *12*, 982-988.

N, A.G., Bensinger, S.J., Hong, C., Beceiro, S., Bradley, M.N., Zelcer, N., Deniz, J., Ramirez, C., Diaz, M., Gallardo, G.*, et al.* (2009). Apoptotic cells promote their own clearance and immune tolerance through activation of the nuclear receptor LXR. Immunity *31*, 245-258.

Naon, D., Zaninello, M., Giacomello, M., Varanita, T., Grespi, F., Lakshminaranayan, S., Serafini, A., Semenzato, M., Herkenne, S., Hernandez-Alvarez, M.I.*, et al.* (2016). Critical reappraisal confirms that Mitofusin 2 is an endoplasmic reticulum-mitochondria tether. Proc Natl Acad Sci U S A *113*, 11249-11254.

Nathan, C. (2006). Neutrophils and immunity: challenges and opportunities. Nature reviews. Immunology *6*, 173-182.

Neudecker, V., Brodsky, K.S., Clambey, E.T., Schmidt, E.P., Packard, T.A., Davenport, B., Standiford, T.J., Weng, T., Fletcher, A.A., Barthel, L.*, et al.* (2017). Neutrophil transfer of miR-223 to lung epithelial cells dampens acute lung injury in mice. Science translational medicine *9*.

Niethammer, P., Grabher, C., Look, A.T., and Mitchison, T.J. (2009). A tissue-scale gradient of hydrogen peroxide mediates rapid wound detection in zebrafish. Nature *459*, 996-999.

Nusse, O., and Lindau, M. (1988). The dynamics of exocytosis in human neutrophils. J Cell Biol *107*, 2117-2123.

Orellana, E.A., and Kasinski, A.L. (2015). MicroRNAs in Cancer: A Historical Perspective on the Path from Discovery to Therapy. Cancers *7*, 1388-1405.

Pantarelli, C., and Welch, H.C.E. (2018). Rac-GTPases and Rac-GEFs in neutrophil adhesion, migration and recruitment. Eur J Clin Invest *48 Suppl 2*, e12939.

Peachman, K.K., Lyles, D.S., and Bass, D.A. (2001). Mitochondria in eosinophils: functional role in apoptosis but not respiration. Proc Natl Acad Sci U S A *98*, 1717-1722.

Pedruzzi, E., Fay, M., Elbim, C., Gaudry, M., and Gougerot-Pocidalo, M.A. (2002). Differentiation of PLB-985 myeloid cells into mature neutrophils, shown by degranulation of terminally differentiated compartments in response to N-formyl peptide and priming of superoxide anion production by granulocyte-macrophage colony-stimulating factor. Br J Haematol *117*, 719-726.

Perry, J.J., Shin, D.S., Getzoff, E.D., and Tainer, J.A. (2010). The structural biochemistry of the superoxide dismutases. Biochimica et biophysica acta *1804*, 245-262.

Peterman, E.M., Sullivan, C., Goody, M.F., Rodriguez-Nunez, I., Yoder, J.A., and Kim, C.H. (2015). Neutralization of Mitochondrial Superoxide by Superoxide Dismutase 2 Promotes Bacterial Clearance and Regulates Phagocyte Numbers in Zebrafish. Infect Immun *83*, 430-440.

Peters, N.C., Egen, J.G., Secundino, N., Debrabant, A., Kimblin, N., Kamhawi, S., Lawyer, P., Fay, M.P., Germain, R.N., and Sacks, D. (2008). In vivo imaging reveals an essential role for neutrophils in leishmaniasis transmitted by sand flies. Science *321*, 970-974.

Phillipson, M., Heit, B., Colarusso, P., Liu, L., Ballantyne, C.M., and Kubes, P. (2006). Intraluminal crawling of neutrophils to emigration sites: a molecularly distinct process from adhesion in the recruitment cascade. J Exp Med *203*, 2569-2575.

Phillipson, M., Kaur, J., Colarusso, P., Ballantyne, C.M., and Kubes, P. (2008). Endothelial domes encapsulate adherent neutrophils and minimize increases in vascular permeability in paracellular and transcellular emigration. PLoS One *3*, e1649.

Porporato, P.E., Payen, V.L., Perez-Escuredo, J., De Saedeleer, C.J., Danhier, P., Copetti, T., Dhup, S., Tardy, M., Vazeille, T., Bouzin, C.*, et al.* (2014). A mitochondrial switch promotes tumor metastasis. Cell reports *8*, 754-766.

Pospieszalska, M.K., and Ley, K. (2009). Dynamics of Microvillus Extension and Tether Formation in Rolling Leukocytes. Cell Mol Bioeng *2*, 207-217.

Price, L.S., Langeslag, M., ten Klooster, J.P., Hordijk, P.L., Jalink, K., and Collard, J.G. (2003a). Calcium signaling regulates translocation and activation of Rac. Journal of Biological Chemistry *278*, 39413-39421.

Price, L.S., Langeslag, M., ten Klooster, J.P., Hordijk, P.L., Jalink, K., and Collard, J.G. (2003b). Calcium signaling regulates translocation and activation of Rac. J Biol Chem *278*, 39413-39421.

Prudent, J., Popgeorgiev, N., Gadet, R., Deygas, M., Rimokh, R., and Gillet, G. (2016). Mitochondrial Ca(2+) uptake controls actin cytoskeleton dynamics during cell migration. Scientific reports *6*, 36570.

Rambold, A.S., Cohen, S., and Lippincott-Schwartz, J. (2015). Fatty acid trafficking in starved cells: regulation by lipid droplet lipolysis, autophagy, and mitochondrial fusion dynamics. Developmental cell *32*, 678-692.

Reichel, C.A., Rehberg, M., Lerchenberger, M., Berberich, N., Bihari, P., Khandoga, A.G., Zahler, S., and Krombach, F. (2009). Ccl2 and Ccl3 mediate neutrophil recruitment via induction of protein synthesis and generation of lipid mediators. Arteriosclerosis, thrombosis, and vascular biology *29*, 1787-1793.

Reichenbach, J., Schubert, R., Horvath, R., Petersen, J., Futterer, N., Malle, E., Stumpf, A., Gebhardt, B.R., Koehl, U., Schraven, B., and Zielen, S. (2006). Fatal neonatal-onset mitochondrial respiratory chain disease with T cell immunodeficiency. Pediatric research *60*, 321-326.

Renshaw, S.A., and Trede, N.S. (2012). A model 450 million years in the making: zebrafish and vertebrate immunity. Dis Model Mech *5*, 38-47.

Rhodes, J., Hagen, A., Hsu, K., Deng, M., Liu, T.X., Look, A.T., and Kanki, J.P. (2005). Interplay of pu.1 and gata1 determines myelo-erythroid progenitor cell fate in zebrafish. Developmental cell *8*, 97-108.

Ridley, A.J. (2001). Rho GTPases and cell migration. J Cell Sci *114*, 2713-2722.

Roberto, V.P., Tiago, D.M., Gautvik, K., and Cancela, M.L. (2015). Evidence for the conservation of miR-223 in zebrafish (Danio rerio): Implications for function. Gene *566*, 54-62.

Romani, L., Mencacci, A., Cenci, E., Spaccapelo, R., Del Sero, G., Nicoletti, I., Trinchieri, G., Bistoni, F., and Puccetti, P. (1997). Neutrophil production of IL-12 and IL-10 in candidiasis and efficacy of IL-12 therapy in neutropenic mice. J Immunol *158*, 5349-5356.

Rooney, C., White, G., Nazgiewicz, A., Woodcock, S.A., Anderson, K.I., Ballestrem, C., and Malliri, A. (2010). The Rac activator STEF (Tiam2) regulates cell migration by microtubule-mediated focal adhesion disassembly. EMBO Rep *11*, 292-298.

Rosowski, E.E., Deng, Q., Keller, N.P., and Huttenlocher, A. (2016a). Rac2 Functions in Both Neutrophils and Macrophages To Mediate Motility and Host Defense in Larval Zebrafish. Journal of immunology.

Rosowski, E.E., Deng, Q., Keller, N.P., and Huttenlocher, A. (2016b). Rac2 Functions in Both Neutrophils and Macrophages To Mediate Motility and Host Defense in Larval Zebrafish. Journal of immunology *197*, 4780-4790.

Sander, E.E., ten Klooster, J.P., van Delft, S., van der Kammen, R.A., and Collard, J.G. (1999). Rac downregulates Rho activity: reciprocal balance between both GTPases determines cellular morphology and migratory behavior. J Cell Biol *147*, 1009-1022.

Scapini, P., Lapinet-Vera, J.A., Gasperini, S., Calzetti, F., Bazzoni, F., and Cassatella, M.A. (2000). The neutrophil as a cellular source of chemokines. Immunol Rev *177*, 195-203.

Scapini, P., Laudanna, C., Pinardi, C., Allavena, P., Mantovani, A., Sozzani, S., and Cassatella, M.A. (2001). Neutrophils produce biologically active macrophage inflammatory protein-3alpha (MIP-3alpha)/CCL20 and MIP-3beta/CCL19. Eur J Immunol *31*, 1981-1988.

Schuler, M.H., Lewandowska, A., Caprio, G.D., Skillern, W., Upadhyayula, S., Kirchhausen, T., Shaw, J.M., and Cunniff, B. (2017). Miro1-mediated mitochondrial positioning shapes intracellular energy gradients required for cell migration. Molecular biology of the cell *28*, 2159-2169.

Semerad, C.L., Liu, F., Gregory, A.D., Stumpf, K., and Link, D.C. (2002). G-CSF is an essential regulator of neutrophil trafficking from the bone marrow to the blood. Immunity *17*, 413-423.

Sepulcre, M.P., Alcaraz-Perez, F., Lopez-Munoz, A., Roca, F.J., Meseguer, J., Cayuela, M.L., and Mulero, V. (2009). Evolution of lipopolysaccharide (LPS) recognition and signaling: fish TLR4 does not recognize LPS and negatively regulates NF-kappaB activation. Journal of immunology *182*, 1836-1845.

Si, J., Mueller, L., and Collins, S.J. (2007). CaMKII regulates retinoic acid receptor transcriptional activity and the differentiation of myeloid leukemia cells. The Journal of clinical investigation *117*, 1412-1421.

Sica, A., Matsushima, K., Van Damme, J., Wang, J.M., Polentarutti, N., Dejana, E., Colotta, F., and Mantovani, A. (1990). IL-1 transcriptionally activates the neutrophil chemotactic factor/IL-8 gene in endothelial cells. Immunology *69*, 548-553.

Smith, P.M., Fox, J.L., and Winge, D.R. (2012). Biogenesis of the cytochrome bc(1) complex and role of assembly factors. Biochimica et biophysica acta *1817*, 276-286.

Song, Z., Chen, H., Fiket, M., Alexander, C., and Chan, D.C. (2007). OPA1 processing controls mitochondrial fusion and is regulated by mRNA splicing, membrane potential, and Yme1L. The Journal of cell biology *178*, 749-755.

Stamatopoulos, B., Meuleman, N., Haibe-Kains, B., Saussoy, P., Neste, E., and Michaux, L. (2009). microRNA-29c and microRNA-223 down-regulation has in vivo significance in chronic lymphocytic leukemia and improved disease risk stratification. Blood *113*, 5237-5245.

Steegmaier, M., Borges, E., Berger, J., Schwarz, H., and Vestweber, D. (1997). The E-selectin-ligand ESL-1 is located in the Golgi as well as on microvilli on the cell surface. J Cell Sci *110 (Pt 6)*, 687-694.

Stumpf, J.D., Saneto, R.P., and Copeland, W.C. (2013). Clinical and molecular features of POLG-related mitochondrial disease. Cold Spring Harbor perspectives in biology *5*, a011395.

Sugatani, T., and Hruska, K.A. (2007). MicroRNA-223 is a key factor in osteoclast differentiation. J Cell Biochem *101*, 996-999.

Tabet, F., Vickers, K.C., Cuesta Torres, L.F., Wiese, C.B., Shoucri, B.M., Lambert, G., Catherinet, C., Prado-Lourenco, L., Levin, M.G., Thacker, S.*, et al.* (2014). HDL-transferred microRNA-223 regulates ICAM-1 expression in endothelial cells. Nature communications *5*, 3292.

Tang, Y., Y., W., Chen, Q., and Qiu, N. (2015). MiR-223 inhibited cell metastasis of human cervical cancer by modulating epithelial-mesenchymal transition. Int J Clin Exp Pathol *8*, 11224-11229.

Tsai, F.C., Kuo, G.H., Chang, S.W., and Tsai, P.J. (2015). Ca2+ signaling in cytoskeletal reorganization, cell migration, and cancer metastasis. Biomed Res Int *2015*, 409245.

Tucker, K.A., Lilly, M.B., Heck, L., Jr., and Rado, T.A. (1987). Characterization of a new human diploid myeloid leukemia cell line (PLB-985) with granulocytic and monocytic differentiating capacity. Blood *70*, 372-378.

Urban, C.F., Ermert, D., Schmid, M., Abu-Abed, U., Goosmann, C., Nacken, W., Brinkmann, V., Jungblut, P.R., and Zychlinsky, A. (2009). Neutrophil extracellular traps contain calprotectin, a cytosolic protein complex involved in host defense against Candida albicans. PLoS Pathog *5*, e1000639.

van Buul, J.D., Anthony, E.C., Fernandez-Borja, M., Burridge, K., and Hordijk, P.L. (2005). Proline-rich tyrosine kinase 2 (Pyk2) mediates vascular endothelial-cadherin-based cell-cell adhesion by regulating beta-catenin tyrosine phosphorylation. J Biol Chem *280*, 21129-21136.

van der Vaart, M., Spaink, H.P., and Meijer, A.H. (2012). Pathogen recognition and activation of the innate immune response in zebrafish. Adv Hematol *2012*, 159807.

Villeneuve, N.F., Lau, A., and Zhang, D.D. (2010). Regulation of the Nrf2-Keap1 antioxidant response by the ubiquitin proteasome system: an insight into Cullin-Ring ubiquitin ligases. Antioxidants & Redox Signaling *13*.

Vincent, W.J., Freisinger, C.M., Lam, P.Y., Huttenlocher, A., and Sauer, J.D. (2016). Macrophages mediate flagellin induced inflammasome activation and host defense in zebrafish. Cellular microbiology *18*, 591-604.

Walker, M.A., Slate, N., Alejos, A., Volpi, S., Iyengar, R.S., Sweetser, D., Sims, K.B., and Walter, J.E. (2014). Predisposition to infection and SIRS in mitochondrial disorders: 8 years' experience in an academic center. J Aller Cl Imm-Pract *2*, 465-U173.

Wang, S., Watanabe, T., Matsuzawa, K., Katsumi, A., Kakeno, M., Matsui, T., Ye, F., Sato, K., Murase, K., Sugiyama, I.*, et al.* (2012). Tiam1 interaction with the PAR complex promotes talin-mediated Rac1 activation during polarized cell migration. J Cell Biol *199*, 331-345.

Warburg, O. (1956). On respiratory impairment in cancer cells. Science *124*, 269-270.

Williams, M.R., Azcutia, V., Newton, G., Alcaide, P., and Luscinskas, F.W. (2011). Emerging mechanisms of neutrophil recruitment across endothelium. Trends Immunol *32*, 461-469.

Wong, Q.W., Lung, R.W., Law, P.T., Lai, P.B., Chan, K.Y., To, K.F., and Wong, N. (2008). MicroRNA-223 is commonly repressed in hepatocellular carcinoma and potentiates expression of Stathmin1. Gastroenterology *135*, 257-269.

Woodfin, A., Voisin, M.B., Beyrau, M., Colom, B., Caille, D., Diapouli, F.M., Nash, G.B., Chavakis, T., Albelda, S.M., Rainger, G.E.*, et al.* (2011). The junctional adhesion molecule JAM-C regulates polarized transendothelial migration of neutrophils in vivo. Nat Immunol *12*, 761-769.

Woodfin, A., Voisin, M.B., Imhof, B.A., Dejana, E., Engelhardt, B., and Nourshargh, S. (2009). Endothelial cell activation leads to neutrophil transmigration as supported by the sequential roles of ICAM-2, JAM-A, and PECAM-1. Blood *113*, 6246-6257.

Yamahashi, Y., Cavnar, P.J., Hind, L.E., Berthier, E., Bennin, D.A., Beebe, D., and Huttenlocher, A. (2015). Integrin associated proteins differentially regulate neutrophil polarity and directed migration in 2D and 3D. Biomedical microdevices *17*, 100.

Yin, L.L., Maddison, L.A., Li, M.Y., Kara, N., LaFave, M.C., Varshney, G.K., Burgess, S.M., Patton, J.G., and Chen, W.B. (2015). Multiplex Conditional Mutagenesis Using Transgenic Expression of Cas9 and sgRNAs. Genetics *200*, 431-+.

Ying, W., Tseng, A., Chang, R.C., Morin, A., and Brehm, T. (2015). MicroRNA-223 is a crucial mediator of PPARr-regulated alternative macrophage activation. The Journal of clinical investigation *125*, 4149-4159.

Yoo, S.K., and Huttenlocher, A. (2011). Spatiotemporal photolabeling of neutrophil trafficking during inflammation in live zebrafish. J Leukoc Biol *89*, 661-667.

Yoshimura, T., and Takahashi, M. (2007). IFN-gamma-mediated survival enables human neutrophils to produce MCP-1/CCL2 in response to activation by TLR ligands. J Immunol *179*, 1942-1949.

Zanotelli, M.R., Goldblatt, Z.E., Miller, J.P., Bordeleau, F., Li, J., VanderBurgh, J.A., Lampi, M.C., King, M.R., and Reinhart-King, C.A. (2018). Regulation of ATP utilization during metastatic cell migration by collagen architecture. Molecular biology of the cell *29*, 1-9.

Zarbock, A., Deem, T.L., Burcin, T.L., and Ley, K. (2007). Galphai2 is required for chemokine-induced neutrophil arrest. Blood *110*, 3773-3779.

Zeytun, A., Chaudhary, A., Pardington, P., Cary, R., and Gupta, G. (2010). Induction of cytokines and chemokines by Toll-like receptor signaling: strategies for control of inflammation. Crit Rev Immunol *30*, 53-67.

Zhao, J., Zhang, J., Yu, M., Xie, Y., Huang, Y., Wolff, D.W., Abel, P.W., and Tu, Y. (2013). Mitochondrial dynamics regulates migration and invasion of breast cancer cells. Oncogene *32*, 4814-4824.

Zhao, S., and Fernald, R.D. (2005). Comprehensive algorithm for quantitative real-time polymerase chain reaction. Journal of computational biology : a journal of computational molecular cell biology *12*, 1047-1064.

Zhao, Z.S., Manser, E., Loo, T.H., and Lim, L. (2000). Coupling of PAK-interacting exchange factor PIX to GIT1 promotes focal complex disassembly. Mol Cell Biol *20*, 6354-6363.

Zhou, W., Cao, L., Jeffries, J., Zhu, X., Staiger, C.J., and Deng, Q. (2018). Neutrophil-specific knockout demonstrates a role for mitochondria in regulating neutrophil motility in zebrafish. Dis Model Mech *11*.

Zhou, Y.B., Kucik, D.F., Szalais, A.J., and Edberg, J.C. (2014). Human Neutrophil Flow Chamber Adhesion Assay. Jove-J Vis Exp.

Zhuang, G., Meng, C., Guo, X., Cheruku, P.S., Shi, L., Xu, H., Li, H., Wang, G., Evans, A.R., Safe, S.*, et al.* (2012). A novel regulator of macrophage activation: miR-223 in obesity-associated adipose tissue inflammation. Circulation *125*, 2892-2903.

Zmijewski, J.W., Lorne, E., Zhao, X., Tsuruta, Y., Sha, Y.G., Liu, G., Siegal, G.P., and Abraham, E. (2008). Mitochondrial respiratory complex I regulates neutrophil activation and severity of lung injury. American journal of respiratory and critical care medicine *178*, 168-179.

Zuchner, S., Mersiyanova, I.V., Muglia, M., Bissar-Tadmouri, N., Rochelle, J., Dadali, E.L., Zappia, M., Nelis, E., Patitucci, A., Senderek, J.*, et al.* (2004). Mutations in the mitochondrial GTPase mitofusin 2 cause Charcot-Marie-Tooth neuropathy type 2A. Nat Genet *36*, 449-451.

PUBLICATIONS

1. **Wenqing Zhou**, Arpita S. Pal, Alan Yi-Hui Hsu, Theodore Gurol, Xiaoguang Zhu, Sarah E. Wirbisky, Jennifer Freeman, Andrea Kasinski, Qing Deng. MicroRNA-223 suppresses the canonical NF-kB pathway in basal keratinocytes to dampen neutrophilic inflammation. 2018. *Cell Reports*. 22: 1810-1823.

2. **Wenqing Zhou**, Lingyan Cao, Jacob Jeffries, Xiaoguang Zhu, Christopher J Staiger, Qing Deng. Neutrophil-specific knockout demonstrates a role for mitochondria in regulating neutrophil motility in zebrafish. 2018. *Disease Models & Mechanism*. 11:dmm033027. *Doi: 10.1242/dmm.033027.*

3. **Wenqing Zhou**, Alan Hsu, Tianqi Wang, Jacob Jefferies, Haroon Mohammad, Xu Wang, David Umulis, Mohamed N. Seleem, Qing Deng. Mitofusin 2 regulates neutrophil adhesive migration via suppressing Rac activation. 2019. *BioRxiv*. *Doi: https://doi.org/10.1101/608091*

4. Jacob Jeffries, **Wenqing Zhou**, Alan Y Hsu, Qing Deng. MicroRNA-223 at the crossroads of inflammation and cancer. 2019. *Cancer Lett.* 451: 136-141

5. Alan Yi-Hui Hsu, Decheng Wang, Theodore Gurol, **Wenqing Zhou**, Xiaoguang Zhu, Hsiu-Yi Lu, Qing Deng. Overexpression of microRNA-722 fine-tunes neutrophilic inflammation by inhibiting *Rac2* in zebrafish. 2017. *Disease Models & Mechanisms*. 10:1323-1332.

6. Theodore Gurol, **Wenqing Zhou**, Qing Deng. MicroRNAs in neutrophils: potential next generation therapeutics for inflammatory ailments. 2016. *Immunological Reviews*. 273(1): 29-47.

7. **Wenqing Zhou**, Kaihu Yao, Gang Zhang, Yonghong Yang, Yun Li, Yuan Lv, Jie Feng. Mechanism for transfer of transposon Tn*2010* carrying macrolide resistance genes in *Streptococcus pneumoniae* and its effects on genome evolution. 2014. *J Antimicrob Chemother.* 69(6): 1470-3.

8. Zhihai Sui*, **Wenqing Zhou***, Kaihu Yao*, Li Liu, Gang Zhang, Yonghong Yang, Jie Feng. Complete genome sequence of *Streptococcus pneumoniae* strain A026, a clinical multidrug-resistant isolate carrying Tn*2010*. 2013. *Genome Announc.* 1(6):e01034-13. doi:10.1128/genomeA.01034-13. *Contribute equally to this work.